CHAPTER 8

Basin stratigraphy

Earth and Ocean seem
To sleep in one another's arms and dream
Of waves, flowers, clouds, woods, rocks and all that we
Read in their smiles, and call reality.

(PERCY BYSSHE SHELLEY, *EPIPSYCHIDION* (1821))

SUMMARY

The stratigraphy in a sedimentary basin is the result of the interplay of the generation of space or accommodation and the influx of sediment. Stratigraphic geometries and gross depositional environments are therefore determined by the tectonic mechanisms causing subsidence, local patterns of faulting, the nature of sediment routing systems, and sea-level change.

Stratigraphic cycles can be modeled from first principles using expressions for accommodation and sediment supply. A fundamental parameter is the magnitude of the eustatic change compared to the subsidence rate. Increasing importance of tectonic subsidence causes stratigraphic cycles to become asymmetrical and retrogradational. Typical glacio-eustatic cycles have a high enough frequency and amplitude to generate unconformities, even at high tectonic subsidence rates. Lower frequency/amplitude "nonglacial" cycles are easily overwhelmed by tectonic subsidence to produce monotonically rising relative sea levels. Key stratigraphic surfaces are commonly diachronous, with a phase shift of up to one-quarter of a eustatic period. The evolution of water depth through a set of stratigraphic cycles depends on relative sea level and sediment supply. The magnitude of the sediment supply determines whether accommodation is underfilled or overfilled. In the case of the latter, sediment is bypassed *via* a nondepositional surface. Even small variations in sediment supply can have major impact on depositional facies, water depth, and movement of the coast. Stratigraphy may be either accommodation-limited, where cycles and facies are determined by accommodation and sediment supply is always adequate: or sediment supply-limited, where depositional space is always great enough to accommodate the sediment supply.

Stratigraphy is packaged into large and small genetic units, from megasequences (or supersequences) to depositional sequences and then parasequences (or higher order genetic units). Depositional sequences are bounded by unconformities or lateral conformities, but may be better recognized by their maximum flooding surfaces.

The widely used Vail–Haq curve of "global" sea-level change relies on a global correlation of synchronous stratigraphic boundaries. However, it is unlikely that sequence boundaries are truly synchronous, partly because of the variations of tectonic subsidence rate in co-existing sedimentary basins, and partly because the different response times of sediment routing systems to base level change produces different sediment inputs in coeval basins. The search for perfect synchrony is therefore futile.

Depositional sequences can be subdivided into *systems tracts* deposited at particular intervals on the relative sea level curve. *Lowstand systems tracts* consist of basin-floor fans, slope fans, and wedges accreting onto the continental slope, at the shelf edge or as a series of regressive wedges on continental ramps. During relative sea-level lowstands, the continental shelf may become exposed, karstified, or incised by river drainage networks. During rapid relative sea-level rise, *transgressive systems tracts* backstep onto the basin margin. After the period of maximum flooding of the basin margin, *highstand systems tracts* prograde into the basin producing marked clinoform geometries over basal downlap surfaces. Smaller genetic stratigraphic units or parasequences are recognized ubiquitously in core, electric logs, and at outcrop. The boundaries of shallow marine, shallowing-up

parasequences are commonly marked by a flooding surface accompanied by a marked facies dislocation. In both carbonate and siliciclastic systems, parasequences may be driven by orbital mechanisms in the Milankovitch band or may be unforced (autocyclic).

The driving mechanisms for stratigraphic patterns fall into two major categories: tectonic and eustatic. Tectonic mechanisms include flexure under sediment loads during phases of thermal subsidence in failed rift and passive margin basins, flexure by moving tectonic loads in foreland basins, and accommodation generation during the evolution of fault arrays in extensional and contractional settings. Changes in regional in-plane stress fields caused by major plate boundary reorganizations can also cause vertical movements that are large enough to have an impact on basin stratigraphy.

Absolute changes in sea level (*eustatic* changes) may be caused by changes in the volume of ocean water or changes in the volume of ocean basins. Additions of juvenile water from the continuing differentiation of the lithosphere are probably compensated by losses due to hydrothermal alteration of new ocean crust. Sediment influx to ocean basins is potentially able to cause slow sea-level rises but the process is counteracted by sediment removal at subduction zones. Volume changes in the ocean ridge system caused by variations in spreading rate are thought to be responsible for long-term changes in global sea level, involving a maximum sea level during the Late Cretaceous and falling with varying severity through the Cenozoic to the present. Thermal expansion and contraction of the oceanic reservoir causes small changes in absolute sea level. Glaciations and deglaciations are very rapid processes changing the volume of water in the ocean system and are responsible for the familiar sea level variations of the Quaternary. Climate change also affects the functioning of sedimentary systems, principally through the effect on vegetation, weathering and erosion, and far-field sediment transport to basins.

The last decade has seen the growth of numerical approaches to the simulation of stratigraphy. Numerical models for carbonates rely on a carbonate productivity versus depth function combined with rules for the surface transport of sediment. Siliciclastic models require a linkage between catchment processes, fluvial transport, and sediment distribution in the basin. Numerical schemes are successful at simulating the geometries observed in stratigraphy and in furthering our understanding of the complexity of catchment–basin systems.

The depositional systems of sedimentary basins are highly variable. Continental systems include fluvial, desert, lacustrine, and glacial systems. Coastal and nearshore systems include siliciclastic shorelines and carbonate–evaporite shorelines. Continental shelf systems include siliciclastic systems as well as carbonate shelves and reefs. Deep sea depositional systems include slope aprons, submarine fans, deep-water sediment drifts and basins plains, and the predominantly biochemical sediments of the pelagic realm.

Basins of different type have different assemblages of depositional styles. The sedimentary systems of *intracratonic* sags are commonly continental and endorheic. Whereas the Chad Basin, Africa is predominantly composed of siliciclastic fluviatile, lacustrine and aeolian deposits, the Michigan Basin, USA is dominated by shallow marine carbonates and evaporites. *Continental rift basins* have tectonically controlled syn–rift fills that are commonly lacustrine and fluviatile in the early stages and may become shallow marine and even deep marine in later stages. Vulcanism accompanies rift sedimentation. The nature of the sedimentary fill depends on its climatic zone – the East African Rift system illustrates this phenomenon, with alkaline shallow lakes in the semi-arid north and deep, freshwater lakes in the wetter south. Supply of clastics to rift lakes is determined by the geometry of tilted fault blocks producing half-graben. *Failed rifts* such as the Benue Trough, Africa or North Sea pass from the syn–rift stage into a period of thermal subsidence characterized by marginal and open marine, commonly deltaic, sedimentation. Continued stretching leads to *proto-oceanic troughs* with evaporites, sapropels, and pelagic sediments. *Passive margins* are characterized by sediment derived from the continent, building thick seaward-prograding, principally shallow marine clastic wedges. Other margins are typified by thick carbonate banks. Deeply buried evaporites are commonly remobilized during the passive margin phase.

In convergent settings, sediment accumulates in foredeep and thrust-sheet-top basins in the flexural downwarp (*foreland basin*) ahead of orogenic wedges. Early deposits are commonly turbiditic and the basin underfilled. Later deposits are shallow marine or continental as the basin reaches steady-state or overfilled status. Retroarc foreland basins differ in having a composition of the sedimentary fill that reflects the large amounts of plutonic and volcanic rocks in the orogenic belt.

Ocean trenches, *accretionary basins*, and *forearc basins* are found at convergent ocean–ocean or ocean–continent boundaries. The sedimentary fills are typically strongly

tectonized and their compositions are dominated by detritus from adjacent ocean crust and arc. Sediments are generally deep water and commonly turbiditic, although some accretionary complexes are above sea level, as in the Makran of Pakistan. *Backarc basins* on oceanic crust are dominated by deep marine sedimentation of pelagic oozes with marginal shallow water or alluvial fringes. There are some examples of backarc spreading on continental crust, such as the Pannonian Basin of central Europe.

Strike–slip basins have complex sedimentary fills indicating rapid subsidence, and major lateral facies changes from active fault scarps with breccias and conglomerates to centrally located finer grained zones. The Ridge Basin California and the Dead Sea are classic examples on land whereas the California Borderland basins represent deep marine equivalents.

The previous chapters have provided some insights into the possible physical causes of the main classes of sedimentary basin. The long-term response of the depositional surface in sedimentary basins is prolonged subsidence, but the detailed interplay of subsidence and sediment supply in time and place gives rise to the stratigraphy of a basin. In this chapter we examine how large scale factors and their interaction give rise to distinct basin stratigraphies.

8.1 A PRIMER ON PROCESS STRATIGRAPHY

8.1.1 Introduction

In this book, we define *Process Stratigraphy* as the science of the recognition and interpretation of the genetic structure of stratigraphy. *Genetic Stratigraphy* (Galloway 1989; Homewood et al. 1992) and *Dynamic Stratigraphy* (Matthews 1974; Cross 1990) are equally appropriate terms, and *Time Stratigraphy* (Wheeler 1964) is an allied concept. However, we avoid the term *Sequence Stratigraphy* since this implies a restriction of concern to the level of the depositional sequence. Process stratigraphy makes use of systematic branches of stratigraphy (biostratigraphy, magnetostratigraphy, chemostratigraphy, lithostratigraphy) but is not itself a taxonomic exercise. The fundamental aim of process stratigraphy is to understand the driving mechanisms for the range of stratigraphic architectures found in sedimentary basins. The science of process stratigraphy has revolutionized sedimentary geology by replacing simple but potentially erroneous lithological correlations with the beginnings of a process understanding of the distribution of stratigraphic elements within time–space. In common with other rapidly developing enterprises, process stratigraphy has become heavily jargonized and vulnerable to overgeneralized, totalitarian world views (see discussion in Miall and Miall 2001). However, it represents an extremely valuable methodological and interpretational tool for the dynamic understanding of the stratigraphy of sedimentary basins.

A number of texts provide a modern understanding of process stratigraphy, often from the utilitarian point of view of a hydrocarbon industry explorationist, such as Emery and Meyers (1996) and Homewood et al. (1992, 2000). Many texts provide sections on process stratigraphy as part of a wider mission, such as Reading (1996), Leeder (1999), and Miall (2000). High resolution sequence stratigraphy, which focuses on the structure of stratigraphy below the level of the depositional sequence, is colorfully examined by van Wagoner et al. (1990). The application of sequence stratigraphy to carbonate reefs and platforms is treated by Schlager (1992) and Sarg (1988).

The history of process stratigraphy dates back to the mid-1900s when stratigraphy was recognized to be divisible into packages of sedimentary rock separated by unconformities of inter-regional extent (Sloss 1950, 1963). A major breakthrough, however, was the use of seismic reflection surveys in the 1960s and 1970s carried out for hydrocarbon exploration (Payton 1977). An analysis of the geometry of stratigraphic units deduced from their seismic reflection character led industry Earth scientists to believe that eustatic changes of sea level were the primary control on the development of stratigraphic packages. In 1987 a "global" sea-level chart was published (Haq et al. 1987) on the basis of the apparent recognition of distinctive stratigraphic boundaries (unconformities and correlative conformities) in widely separated locations. The volume edited by Wilgus et al. (1988) represented a second wave of sequence stratigraphic thinking by introducing ideas on accommodation (see below) in sedimentary basins and on the relationship between stratigraphic packaging and cycles of relative sea level. Since the late 1980s there has been substantial criticism of some of the new stratigraphic terminology, of its reliance on eustasy as its overwhelming driving mechanism and on the presumed global synchroneity of key stratigraphic surfaces such as sequence boundaries (see Miall 1991, 1992 for a trenchant view).

More recently, numerical modeling (Harbaugh et al. 1999; Burgess et al. 2002) has been directed at examining in detail some of the controls and feedbacks involved in the generation of stratigraphic packages.

The key idea of process stratigraphy is that space is made available for sediment to accumulate, termed *accommodation*. Sediment fluxes cause an underfilling, filling, or overfilling of this available space. Accommodation generation and sediment supply vary strongly in space and in time, causing a complex 4-D packaging of stratigraphic units.

8.1.2 Relative sea-level change and accommodation: definitions

Eustasy is global sea level measured from the sea surface to a fixed datum, such as the center of the Earth. The controls on eustatic sea level are discussed in §8.3.

Relative sea level is sea level measured relative to a moving datum, often a distinctive horizon such as a horizon within a sediment pile, or the lower contact with basement. Relative sea level is therefore affected by processes such as tectonic uplift and subsidence, compaction and eustasy.

Water depth is of course the vertical distance between the sea surface and the seabed. Although water depth commonly changes during a relative sea-level change, it may also be influenced by the sediment input into a sedimentary basin with no relative sea-level change. Eustasy, relative sea level, and water depth are all distinctive concepts (Fig. 8.1).

Accommodation – the space made available for sediment to accumulate – is controlled by *base level*, since sediment can only accumulate long term up to base level. Base level may be a graded stream profile on land, or a graded shelf profile on the continental shelf.

We can write a change in accommodation ΔA as

$$\Delta A = \Delta E + \Delta S + \Delta C \tag{8.1}$$

where A is accommodation, E is eustasy, S is subsidence, and C is compaction. A change in water depth ΔW can also be written

$$\Delta W = \Delta A - \Delta D = (\Delta E + \Delta S + \Delta C) - \Delta D \tag{8.2}$$

where ΔD is the amount of sediment deposited.

8.1.3 Forward modeling of stratigraphic cycles from first principles

Sloss (1962) argued some time ago that transgressions and regressions of the shoreline were controlled (at least in part) by the relative magnitudes of the rate of sea-level change and rate of subsidence. Pitman (1978) developed an early model of a slowly subsiding continental margin with a more rapidly changing sea level and by treating the problem quantitatively was able to create a synthetic stratigraphy that could be compared with seismic reflection results. The papers by Read et al. (1986) and Grotzinger (1986a, b) were early attempts to forward

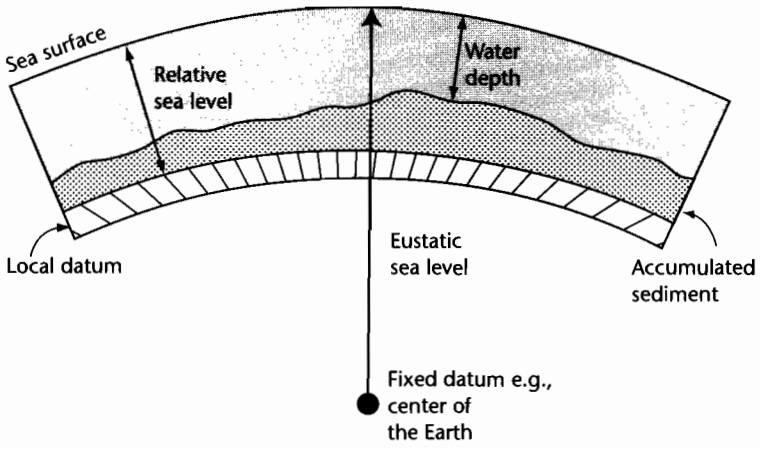

Fig. 8.1 Definitions of terms used in process stratigraphy (after Jervey 1988; Emery and Meyers 1996): eustatic sea level, relative sea level, and water depth.

model cyclical, high-resolution, shallow marine carbonate platform stratigraphy.

Any forward model must make use of the relationship among the key parameters in equation (8.2). For example, Turcotte and Willeman (1983), Turcotte and Kenyon (1984), and Turcotte and Bernthal (1984) modeled eustatic sea level in terms of two end-member types: (i) a rapid rise followed by a slow fall, and (ii) slow rise in sea level followed by a rapid fall. In initial forward modeling studies and conceptual exercises such as the early offerings of the Exxon group (Vail et al. 1977a, b) sediment supply was considered to be constant through the cycle of relative sea-level change.

In the discussion that follows, we build an analytical method for considering the stratigraphic cycles generated under a sinusoidal eustatic variation in a basin with a background tectonic subsidence rate and with a sediment supply coupled to the relative sea-level variation. We ignore compaction and the isostatic response to water and sediment loads. Although the assumptions and algorithms are undoubtedly a crude simplification of the complexities of nature, a simple 1-D forward model is the prerequisite for all process stratigraphic thinking. A Matlab program is provided at www.erdw.ethz.ch/Allen.

We therefore initially consider the variation of relative sea level through a cycle of eustatic change with wavelength λ and amplitude h_0 in a basin with a linear tectonic subsidence rate a (Fig. 8.2). The elevation in sea level caused by a sinusoidal eustatic fluctuation is

$$h = h_0 \sin\left(\frac{2\pi t}{\lambda}\right) \tag{8.3}$$

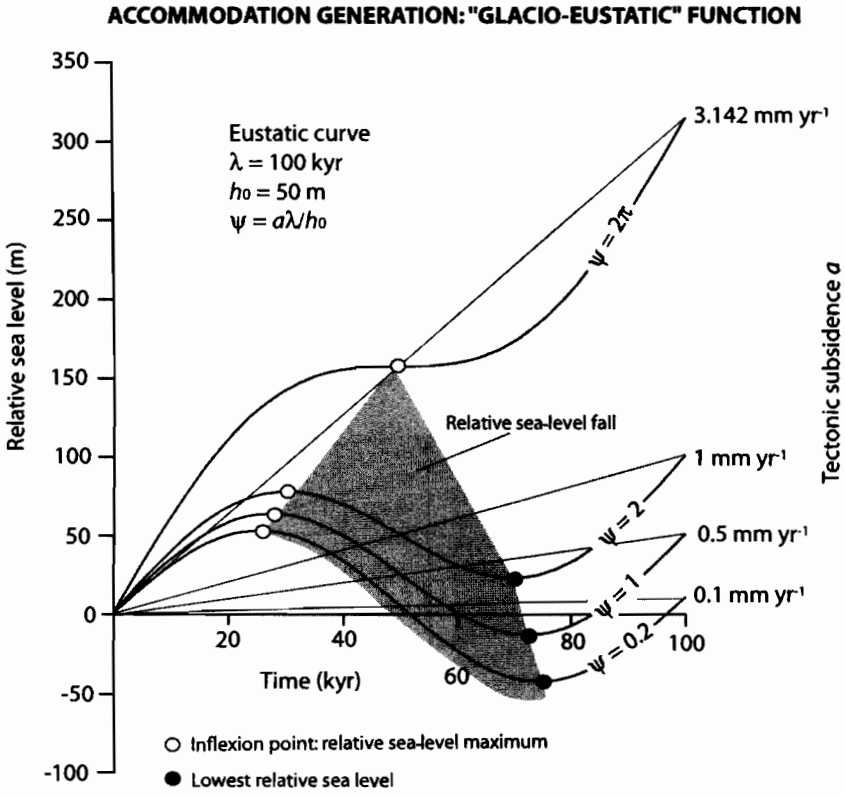

Fig. 8.2 Variation in relative sea level through a cycle of eustatic change with wavelength λ and amplitude h_0 in a basin with a linear tectonic subsidence rate a. The dimensionless parameter Ψ varies from 0.2 to 2π, corresponding to tectonic subsidence rates from 0.1 to πmm yr^{-1} (grey area). Increasing values of Ψ cause the relative sea-level maximum (open circle) to be delayed in the cycle. For the "glacial" eustatic parameters used, tectonic subsidence must be > πmm yr^{-1} in order for the relative sea-level fall to disappear.

Adding the tectonic subsidence rate, assumed linear, to obtain the relative sea level h_{rel}, we have

$$h_{rel} = h_0 \sin\left(\frac{2\pi t}{\lambda}\right) + at \tag{8.4}$$

where t is time. A number of different relative sea-level scenarios result from the magnitude of the eustatic change compared to the subsidence rate. This can be expressed in terms of the dimensionless parameter $\Psi = a\lambda/h_0$. If the amplitude of the sinusoidal eustatic change far exceeds the change in tectonic subsidence (Ψ is small), the relative sea-level variation is also near-sinusoidal and the maximum relative sea level is very close to the eustatic peak (Fig. 8.2). As the tectonic subsidence rate increases relative to the amplitude of eustatic change (Ψ increases), the relative sea-level curve becomes more asymmetrical and the peak of relative sea level becomes delayed in the eustatic cycle. At a critical tectonic subsidence rate (Ψ is large), there is no relative sea-level fall, but instead an inflexion point in relative sea level significantly following the eustatic peak. In Figure 8.2, relative sea level is equivalent to accommodation since the curves begin at zero water depth rather than at some point on a graded profile.

The point at which the inflexion point in relative sea level occurs is at $dh_{rel}/dt = 0$. Differentiating (8.4) gives

$$\frac{dh_{rel}}{dt} = h_0 \frac{2\pi}{\lambda} \cos\left(\frac{2\pi t}{\lambda}\right) + a \tag{8.5}$$

Setting $dh_{rel}/dt = 0$ gives the solution

$$t = \frac{\lambda}{2\pi} \cos^{-1}\left(-\frac{\lambda}{2\pi}\frac{a}{h_0}\right) \tag{8.6}$$

Equation (8.6) shows that for a given eustatic period λ, the time period to the relative sea-level inflexion point decreases with increasing values of the dimensionless parameter $\Psi = a\lambda/h_0$.

At what critical value of a does relative sea level increase monotonically, that is, dh_{rel}/dt is always positive? This is when

$$a > h_0 \frac{2\pi}{\lambda} \cos\left(\frac{2\pi t}{\lambda}\right) \tag{8.7}$$

for all t, which is when $\lambda a/2\pi h_0 > 1$, or $\Psi/2\pi > 1$.

Eustatic sea-level change takes place at a wide range of periods and amplitudes. The dominant signal for the glacial–interglacial variations of the Pleistocene is a period of 100 kyr and amplitude of 50 m (variation in height of 100 m). Let us call this a typical "glacio-eustatic cycle." On the other hand, cycles of eustatic change inferred from stratigraphy (e.g., mid–late Eocene cycles in the Nummulitic Limestone of Switzerland, Allen et al. (2001), and from the Oligocene stratigraphy of the New Jersey coastal plain, Kominz and Pekar 2001) imply cycles of longer duration (*c.* 0.5–2 Myr) and lower amplitude (10–20 m). The fact that these cycles exist in stratigraphy deposited during climatic conditions when there was limited ice suggests that mechanisms other than glacio-eustasy were responsible. Let us call these variations "nonglacial cycles." In unforced cycles (§8.3.6) no eustatic change is required and the facies and water depth changes are produced by internal dynamics driving variations in sediment transport.

Substitution of parameter values in equation (8.7) shows that the critical tectonic subsidence rate for a monotonic rise in relative sea-level ($h_0 = 50$ m, $\lambda = 100$ kyr) is 3.14 mm yr^{-1}. Such rates of tectonic subsidence are rare, which implies that eustatic cycles of this type are likely to always produce relative sea-level falls. If relative sea-level falls are accompanied by erosion, we should expect to find erosional unconformities in stratigraphy formed under the influence of "glacio-eustatic" cycles. If, however, the eustatic variation is 20 m amplitude with a wavelength of 400 kyr, the critical tectonic subsidence rate becomes 0.3 mm yr^{-1}, and if the amplitude and wavelength are 10 m and 1 Myr, the critical tectonic subsidence rate becomes 0.06 mm yr^{-1}. These values are similar to or below the rate of subsidence experienced in most sedimentary basins. In situations of slow "nonglacial" eustatic change, relative sea level may monotonically rise under a background tectonic subsidence.

It can also be seen from Figure 8.2 that the triangular field of relative sea-level fall narrows to a point at $t =$ 50,000 yr on the curve $a_{crit} = 3.14$ mm yr^{-1}. Clearly, when correlating different locations in a basin with spatially variable tectonic subsidence rate, we should expect significant diachroneity of the onset of erosion due to relative sea-level fall and of flooding during relative sea-level rise. The delay in the onset of erosion is a quarter of a eustatic wavelength or $\lambda/4$. The difference in the timing of flooding is also $\lambda/4$. Since diachroneity of key stratigraphic surfaces is to be expected from a globally synchronous eustatic change, it is curious that the inference of stratigraphic synchroneity is seen as an acid test for a eustatic control (see also Miall 1991, 1994).

We now add the effects of sediment supply. Sediment supply controls how much of the accommodation is filled (Fig. 8.3). In the simplest scenario, the sediment supply rate s could be considered a constant velocity, in which case water depth as a function of time $w(t)$ is given by

$$w(t) = h_0 \sin\left(\frac{2\pi t}{\lambda}\right) + at - st \tag{8.8}$$

However, it is reasonable to assume that sediment supply rate is coupled in some way to the rate of change of relative sea level. If sediment supply rate $s(t)$ peaks at the maximum rate of relative sea-level fall, and is zero at the maximum rate of relative sea-level rise, we can write

$$s(t) = \frac{1}{2} s_0 \{1 + \sin(2\pi t/\lambda)\} \tag{8.9}$$

It would also be simple to formulate sediment supply as coupled to the rate of relative sea-level variation but with a certain time lag to account for the response time of sediment delivery systems to any base level change (§7.5). However, to obtain the sediment accumulated S at any point within a relative sea-level cycle simply using eqn (8.9), we integrate it to give

$$S(t) = \frac{1}{2} s_0 \left\{ t - \frac{\lambda}{2\pi} \cos\left(\frac{2\pi t}{\lambda}\right) \right\} + c \tag{8.10}$$

Since the total accumulated sediment is zero at $t = 0$, c must be $\frac{1}{2} s_0 \frac{\lambda}{2\pi}$. The thickness of *potential* accumulated sediment is

$$S(t) = \frac{1}{2} s_0 \frac{\lambda}{2\pi} \left\{ \frac{2\pi t}{\lambda} - \cos\left(\frac{2\pi t}{\lambda}\right) + 1 \right\} \tag{8.11}$$

and the water depth is therefore

$$w(t) = h_0 \sin\left(\frac{2\pi t}{\lambda}\right) + at - \frac{1}{2} s_0 \frac{\lambda}{2\pi} \left\{ \frac{2\pi t}{\lambda} - \cos\left(\frac{2\pi t}{\lambda}\right) + 1 \right\} \tag{8.12}$$

where the first term is the eustatic effect, the second the tectonic subsidence effect and the third the sediment supply effect. The evolution of water depth through a relative sea-level cycle with different rates of sediment supply and tectonic subsidence rate is sketched in Figure 8.3.

For high rates of sediment supply relative to the rate of relative sea-level change, water depths initially increase, then decrease as sediment fills the available accommodation. Shortly after the peak of relative sea level, sediment supply exceeds accommodation, causing bypassing of excess sediment and the cutting of a disconformity or unconformity as relative sea level continues to fall. At intermediate sediment supply rates, water depths increase for a significant part of the relative sea-level cycle, then gradually decrease until accommodation is filled. The onset of bypassing and erosion is delayed in the cycle of relative sea-level change compared to the high sediment supply case. As relative sea-level rises, sediment again starts to accumulate in unfilled accommodation under initially increasing water depths. In the case of low sediment supply rates, water depth increases initially, and decreases during relative sea-level fall, but accommodation is never completely filled during a cycle of relative sea-level change. Clearly, the variation in water depth through a stratigraphic cycle, the thickness of sediment preserved, the nature of flooding surfaces and disconformities and their time span, are all related to the interplay of eustatic variation, tectonic subsidence rate and sediment supply rate. This is a fundamental reason why stratigraphic cycles are so variable. Synthetic stratigraphic cycles are shown in Figure 8.4 to illustrate the variations in thickness and water depth in "glacio-eustatic" cycles with varying sediment supply rates.

Some selective conclusions from this quantitative analysis of cycle development are as follows:

8.1.3.1 Cycle thickness

If previously deposited sediment is easily eroded during a relative sea level fall, stratigraphic cycle thicknesses depend on two factors: (i) where sediment supply rates are high, cycle thickness depends on the tectonic subsidence over the period of time between the onset of the cycle and the time of relative sea level lowstand. (ii) where sediment supply rates are low compared to the tectonic subsidence rate, cycle thickness depends only on the sediment accumulated over the duration of the eustatic cycle. We can therefore get similar stratigraphic cycle thicknesses under two contrasting scenarios – by erosion during a relative sea-level fall, and by underfilling of the available accommodation. The first is obviously a case of *accommodation-limited* stratigraphy. The latter is a case of *sediment supply-limited* stratigraphy.

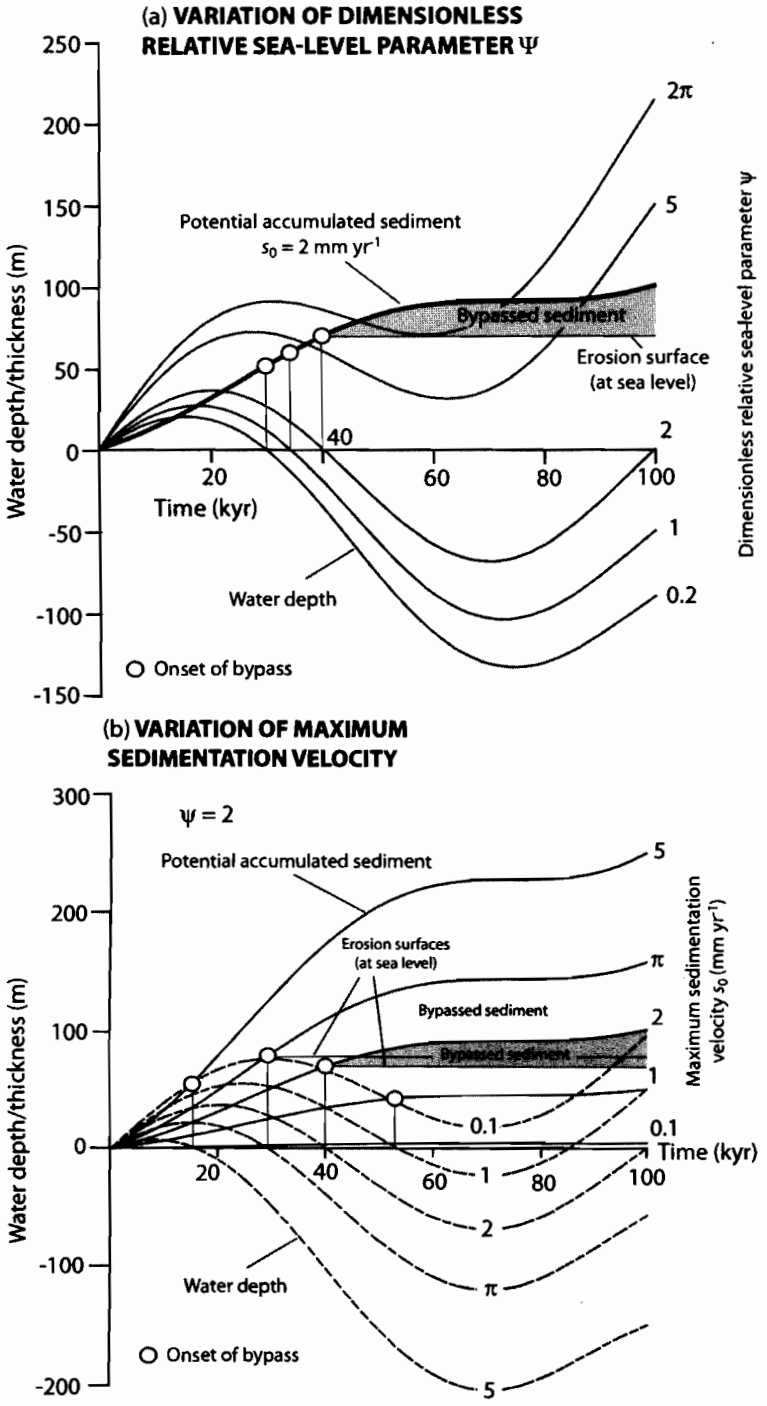

Fig. 8.3 Water depth and potential sediment accumulation during a cycle of relative sea-level change with variable tectonic subsidence rate and sediment supply, using the glacio-eustatic function. (a) Variation in water depth as a function of the dimensionless relative sea-level parameter ψ with a constant maximum sedimentation parameter $s_0 = 2\,\text{mm yr}^{-1}$. When accommodation is filled, sediment starts to bypass the depositional site (illustrated for the case of $\psi = 2$). The onset of bypass occurs progressively later as tectonic subsidence increases (ψ increases). At $\psi = 2$, the basin remains water-filled until 40 kyr, after which erosion and sediment bypass take place until the beginning of the next glacio-eustatic cycle. (b) Variation in water depth and potential accumulated sediment as a function of the sedimentation velocity s_0, with a constant dimensionless relative sea-level parameter ψ of 2, corresponding to a tectonic subsidence rate a of 1 mm yr^{-1}. High sediment supply rates cause the available accommodation to be filled early during the cycle of relative sea-level change, after which sediment is bypassed and eroded (two illustrations at $s_0 = 2$ and $\pi\,\text{mm yr}^{-1}$), whereas at low supply rates ($s_0 = 0.1\,\text{mm yr}^{-1}$), the accommodation remains unfilled. The evolution of water depth during a cycle of relative sea level, sedimentary facies, and the occurrence of erosional bypass surfaces are all critically dependent on the sediment supply.

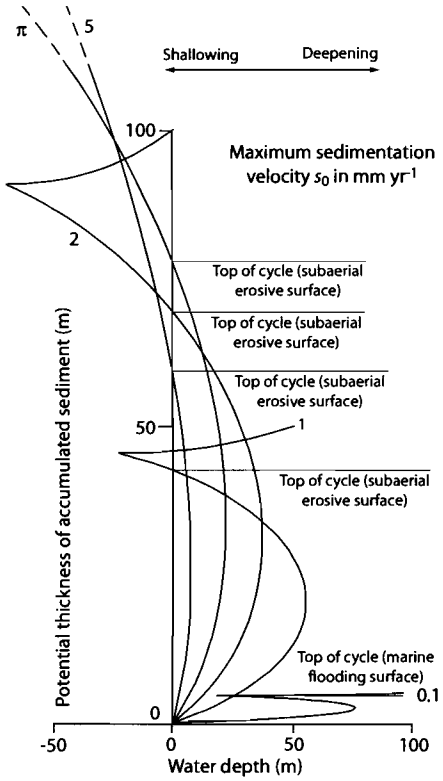

Fig. 8.4 Stratigraphic cycles generated using the algorithms in the text for a glacio-eustatic cycle ($\Psi = 2$) using different values of the maximum sedimentation velocity s_0, from 0.1 to 5 mm yr^{-1}. Cycle thicknesses and water depth trends vary strongly from the thin, sediment starved, deep water case ($s_0 = 0.1$ mm yr^{-1}) with a nonerosional flooding surface as an upper boundary, to the thicker, top-truncated shallow-water cycles at higher values of s_0.

8.1.3.2 Sedimentary facies and water depth variation

For simplicity, we assume that sedimentary facies are dependent on water depth. A common feature of model output is that stratigraphic cycles have thick deepening-up portions. This is because in the case of high sediment supply, relative sea-level fall causes erosion and therefore the removal of the upper, shallow-water part of the stratigraphic cycle. In the case of low sediment supply, accommodation generation outstrips sediment accumulation, causing a temporal increase in water depth. How then do we generate the common *shallowing-up* cycles of the stratigraphic record?

If we believe that eustatic change is important, the most straightforward answer is that the preservation of the shallow-water upper portion of a stratigraphic cycle must be due to the predominance of relative sea-level cycles possessing inflexion points, but insignificant relative sea-level falls. We know from equation (8.7) that inflexion points in the relative sea-level curve occur at $a/h_0 = 2\pi/\lambda$. If $\Psi = a\lambda/h_0$ falls below 2π there is an increasing risk of erosion of the upper part of the stratigraphic cycle as long as the sediment supply is adequate to fill the accommodation space. As base-level, or the graded profile is reached, excess sediment is bypassed into deeper water. In many continental and shallow marine environments, sediment supply is easily capable of filling accommodation. The generation of shallowing-upward cycles therefore depends critically on the value of Ψ, rather than on the sediment supply rate.

Alternatively, if there is no eustatic change, and the cycles are unforced, the common pattern of shallowing-up cyclicity may be due to variations in flooding and progradation driven by internal dynamics of the sedimentary system under a background tectonic subsidence.

Sediment cannot accumulate for long periods of time above the graded profile. Consequently, within a relative sea-level cycle, sediment may be bypassed downstream or into deeper water. High sediment supply in a basin with adequate accommodation will cause sedimentary facies belts to *aggrade*. If sediment supply is less than the accommodation, facies belts will *retrograde*. If sediment supply exceeds accommodation, facies belts will *prograde*. We illustrate the effects of a variable sediment supply on progradation and retrogradation as follows. Consider a sedimentary basin undergoing a uniform and steady rate of tectonic subsidence a with a sinusoidal sediment supply expressed as a vertical velocity of sedimentation as given in equation (8.9).

Choosing realistic parameter values, it is simple to produce (mathematically) stratigraphic cycles involving shallowing and deepening of water depth. Since "negative" water depths may result in erosion, and deepening may be associated with *transgressive ravinement*, some cycles will be bounded by unconformities and flooding surfaces. The balance between the rate of accommodation generation by tectonic subsidence and the long-term sediment accumulation rate determines whether a succession of cycles is retrogradational or progradational. These markedly different stratigraphic styles are very sensitive to this balance (Fig. 8.5). Cycles are retrogradational with

$s_0 = 2\,\text{mm yr}^{-1}$ and $\psi = 2.2$ ($a = 1.1\,\text{mm yr}^{-1}$), but become aggradational if the tectonic subsidence rate is reduced to $a = 1.0\,\text{mm yr}^{-1}$ ($\psi = 2.0$) and progradational at $a = 0.9\,\text{mm yr}^{-1}$ ($\psi = 1.8$). A 20% change in tectonic subsidence rate can therefore cause major changes in cycle stacking patterns. Consequently, sediment supply variations, caused by climate change or internal dynamics, are potentially extremely important in influencing stratigraphic packaging, without recourse to eustatic change.

Consider Figure 8.3b where the low sediment supply causes a low sediment accumulation rate compared to relative sea level. Sediment accumulation can be said to be *sediment supply-limited*. In this case, new water depth is generated with every cycle of relative sea level. After several cycles of relative sea level, marine shorelines will be strongly retrogradational or transgressive, and basinal locations should be dominated by deep-water shale deposition. Where sediment supply is moderate, an initially marine basin is filled to sea level, coastal plain sediments accumulated up to the graded stream profile (base level), followed by erosion and incision as relative sea level falls. Excess sediment is bypassed and delivered to other places in the basin where accommodation may be higher. If sediment supply is high, the shoreline regresses immediately, causing the progradation of deltaic and coastal plain sediments. In this case, sediment accumulation is *accommodation-limited*.

The depositional architecture is therefore very sensitive to the interplay between sediment supply and accommodation generation. We can envisage a continuum of geometrical possibilities where the sediment supply rate varies in relation to the accommodation. For example, for a morphology involving low gradient topsets and steeper gradient clinoforms (Fig. 8.6), the increase in topset accommodate ΔV_{ta} (as a volume) is the product of the relative sea-level change and the topset area. If the sediment supply is greater than ΔV_{ta}, the clinoforms will prograde, the *offlap break* migrating strongly offshore. However, if the sediment supply is progressively reduced, the offlap break first climbs, then becomes near-vertical, and then migrates landward when sediment supply is less than ΔV_{ta}.

8.2 STRATIGRAPHIC CYCLES: DEFINITION AND RECOGNITION

Although the cyclical nature of stratigraphy at a range of scales has been recognized for many decades, a significant advance was made by the recognition of the packaging of stratigraphic units from seismic reflection data. Vail et al. (1977a) claimed to recognize a hierarchy of cycles of relative sea-level change largely on the basis of the depositional limits of onlap and toplap within the coastal facies of marine sediments.

8.2.1 Supersequences and megasequences

Sloss (1988) traced the history of ideas on sequence stratigraphy over the second half of the last century. The importance of rock-stratigraphic units traceable over wide areas of the North American continent and bounded by unconformities of "interregional scope" has long been recognized (Sloss 1950, 1963). Six such *supersequences* (termed "sequences" by Sloss) occupying the Phanerozoic were defined, with a duration of 50–120 Myr (Fig. 8.7). Each supersequence is thinner and represents a shorter period of deposition at the center of the craton compared to its margin, so that the bounding unconformities increase in duration from the craton edge (10 Myr gap) to the craton center (150 Myr gap). Burgess and Gurnis (1995) and Burgess et al. (1997) interpreted the supersequences as due to the effects of cycles of subduction around the edges of the North American Plate (Chapter 5).

Hubbard et al. (1985), using primarily a subsurface seismic reflection database, introduced a similar concept of *megasequences*, representing the stratigraphic packages deposited during distinct phases of plate motion. Consequently, a megasequence may correspond to a period of continental extension with synrift and postrift components, or to a period of convergent plate motion characterized by flexure of the continental lithosphere. Megasequences are also bounded by extensive but not global major unconformities. Since sedimentary basins are deformations of the lithosphere under a set of plate-scale driving forces, the concept of the megasequence is of primary importance in basin analysis.

8.2.2 Depositional sequences

The primary meso-scale units of stratigraphy are termed *depositional sequences*. They are coherent packets of strata that are genetically related and which can be traced for considerable distances across a basin. Depositional

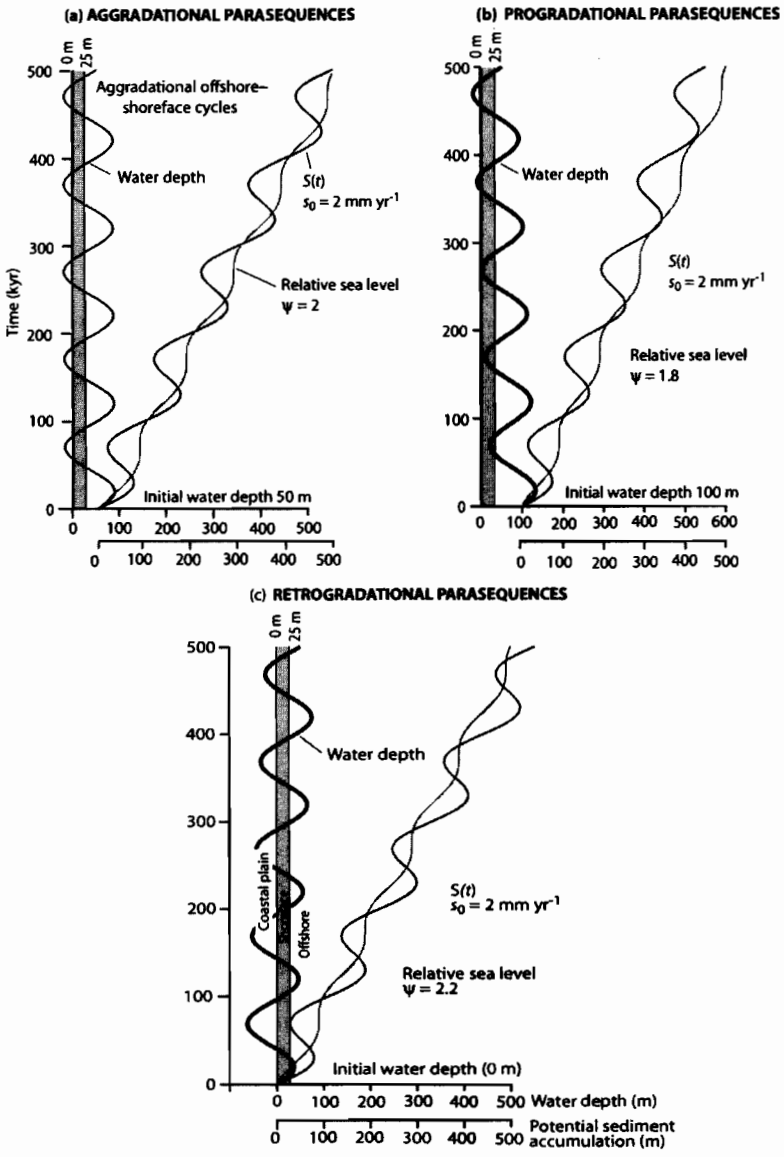

Fig. 8.5 Sensitivity of retrogradational *versus* progradational cycles resulting from variations in tectonic subsidence rate a, with a constant maximum sedimentation velocity of $s_0 = 2\,\text{mm yr}^{-1}$. (a) Aggradational cycles (parasequences) containing offshore, shoreface (0–25 m) and potentially thin coastal plain deposits are produced at $\psi = 2$ ($a = 1\,\text{mm yr}^{-1}$), using an initial water depth of 50 m. Relative sea level and sediment supply are in balance. (b) Progradational cycles produced by a small decrease in ψ to 1.8 ($a = 0.9\,\text{mm yr}^{-1}$), with an initial water depth of 100 m, showing that younger cycles contain progressively lesser amounts of offshore deposits and more shoreface deposits. (c) Retrogradational cycles produced by a small increase in ψ to 2.2 ($a = 1.1\,\text{mm yr}^{-1}$), with an initial water depth of zero, showing that coastal plain–shoreface cycles are progressively replaced by shoreface–offshore cycles with time. Small variations in tectonic subsidence rate (relative to the sediment supply) therefore cause major variations in the stacking patterns of cycles.

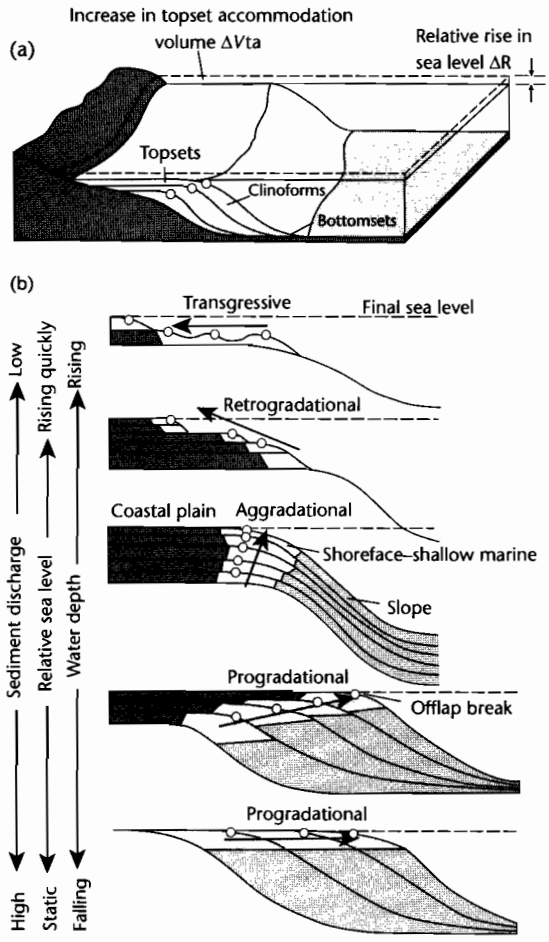

Fig. 8.6 Large scale architecture of depositional units in relation to accommodation and sediment supply (after Galloway 1989). (a) A rise in relative sea level causes an increase in topset accommodation volume ΔV_{ta}, equal to the product of the relative sea-level rise and the topset area; (b) Stratigraphic patterns change from transgressive to retrogradational, aggradational, and progradational as the sediment supply increases relative to the topset accommodation. White circles approximate position of beach (or offlap break).

sequences can be recognized in the subsurface using seismic stratigraphic methods, the tops and bases being marked by bounding unconformities or laterally correlatable conformities (Mitchum et al. 1977) (Fig. 8.8). Within a depositional sequence, individual strata can exhibit a variety of geometrical relationships to the depositional boundary (Dunbar and Rogers 1957) (Fig. 8.9). Widespread recognition of these geometric relationships was only possible with the availability of high-quality seismic reflection data. As well as helping to define a depositional sequence boundary, these types of discordant relationship also furnish clues as to the origin of the unconformity. Onlap, downlap, and toplap indicate nondepositional hiatuses, whereas truncation indicates an erosional hiatus or it may be the result of structural disruption (Vail et al. 1977a).

The minimum stratigraphic unit that can be called a depositional sequence must have a significance in the basin either in terms of thickness or in terms of geological time. Depositional sequences have a chronostratigraphic significance because they were deposited during a time interval limited by the ages of the sequence boundaries where they are conformities. Where unconformities mark the boundaries, the age range is reduced. The total time interval during which a sequence is deposited is called a *sechron*.

It has been claimed that many genetic depositional sequences are better recognized not by their erosional sequence boundaries, but by their *maximum flooding surfaces* (Frazier 1974; Galloway 1989) (Fig. 8.10). Maximum flooding surfaces represent the period of greatest inundation of the basin margin. Although the depositional sequence boundary (Mitchum et al. 1977) can be easily recognized on seismic reflection sections by a downward shift in the position of coastal onlap (see below), it is commonly difficult to recognize in log, core, and outcrops. The maximum flooding surface, which is also easily recognized on seismic reflection sections as the reflector with most landward penetration, is also easily recognized in electrical logs, cores, and outcrop, since it is commonly associated with the deepest water or condensed sedimentary facies (Loutit et al. 1988). The position of the maximum flooding surface within depositional sequences is strongly determined by the minima in sediment supply. The use of maximum flooding surfaces as a tool in subsurface mapping is well illustrated by the case study of Partington et al. (1993) in the North Sea basin.

The algebra expressing the variation between eustasy, tectonic subsidence, and sediment supply in §8.1 demonstrates that the period of greatest increase in new space available is at the *inflection point* of the *rising limb* of the curve of rate of relative sea-level change, and the period of greatest decrease in new space available is at the inflection point of the *falling limb* of the curve of rate of relative sea level. Since the inflection points on the falling

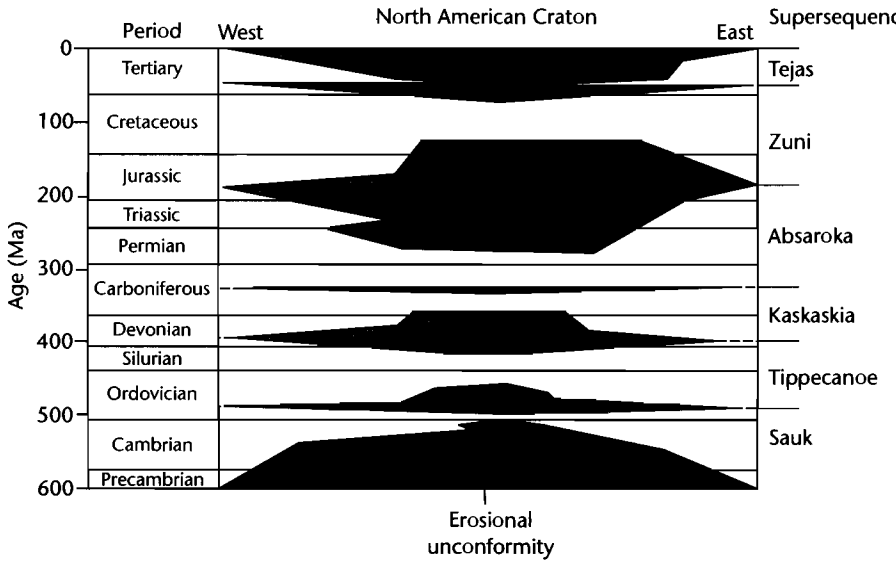

Fig. 8.7 The supersequences of the North American craton of Sloss (1963).

limb of the rate of relative sea-level curve mark times of least available new space, sedimentation commonly shifts to the basin plain and the shelf is subjected to erosion. An unconformity is produced and is accompanied by a basinward shift in coastal onlap and a cessation of fluvial deposition. If the rate of relative sea-level fall is rapid, streams are rejuvenated and incise into the former shelf giving *Type 1 unconformities* (Fig. 8.11). However, if the rate of relative sea-level lowering is slow, there is a gradual but widespread denudation without substantial river incision, giving *Type 2 unconformities*.

Using seismic reflection results, a team of geologists and biostratigraphers from Exxon constructed a chart of relative sea level through time (Vail et al. 1977b), updated and improved by Haq et al. (1987, 1988). These charts, colloquially known as the Vail and Haq curves, are based on the concept of depositional sequences and the kinds of baselap and toplap at sequence boundaries. The Vail–Haq curves are composed of *cycles of relative change of sea level*. In essence, the Haq et al. (1987) curve is presented as having two components: (i) a *long-term* eustatic curve defining "first order cycles" or "megacycles" of period >100 Myr; it is probably equivalent to the sea-level change resulting from changes in mid-ocean ridge volumes of from the dynamic topography associated with subduction (see §8.3, §5.2), and (ii) a *short-term* eustatic curve, composed of higher frequencies defining "second order cycles" or "supercycles" of duration 8–10 Myr and "third order cycles" or "cycles" of duration 1–5 Myr.

The chronostratigraphic basis for the global sea-level chart of Haq et al. (1987) is a combination of radiometric dates, magnetostratigraphy (geomagnetic polarity reversals), and biostratigraphy, but there is a limit to the time resolution of stratigraphic boundaries, which makes the question of their global synchroneity problematic (Miall 1991, 1994). The Vail–Haq global sea-level chart remains controversial. It is evident from our consideration of process stratigraphy that the timing of depositional sequence boundaries is determined by the interacting rate effects of sediment accumulation, tectonic subsidence and eustatic change. For example, we know (§7.5) that large river catchments are strongly buffered systems that have long response times to a base-level change such as eustatic rise or fall. Since different catchments have different response times (10^4–10^6 yr), a *synchronous* base-level change should result in a *diachronous* stratigraphic response. An eustatic change at a point in time should only produce a *partial* or *apparent* synchroneity in basins with different tectonic and sediment supply

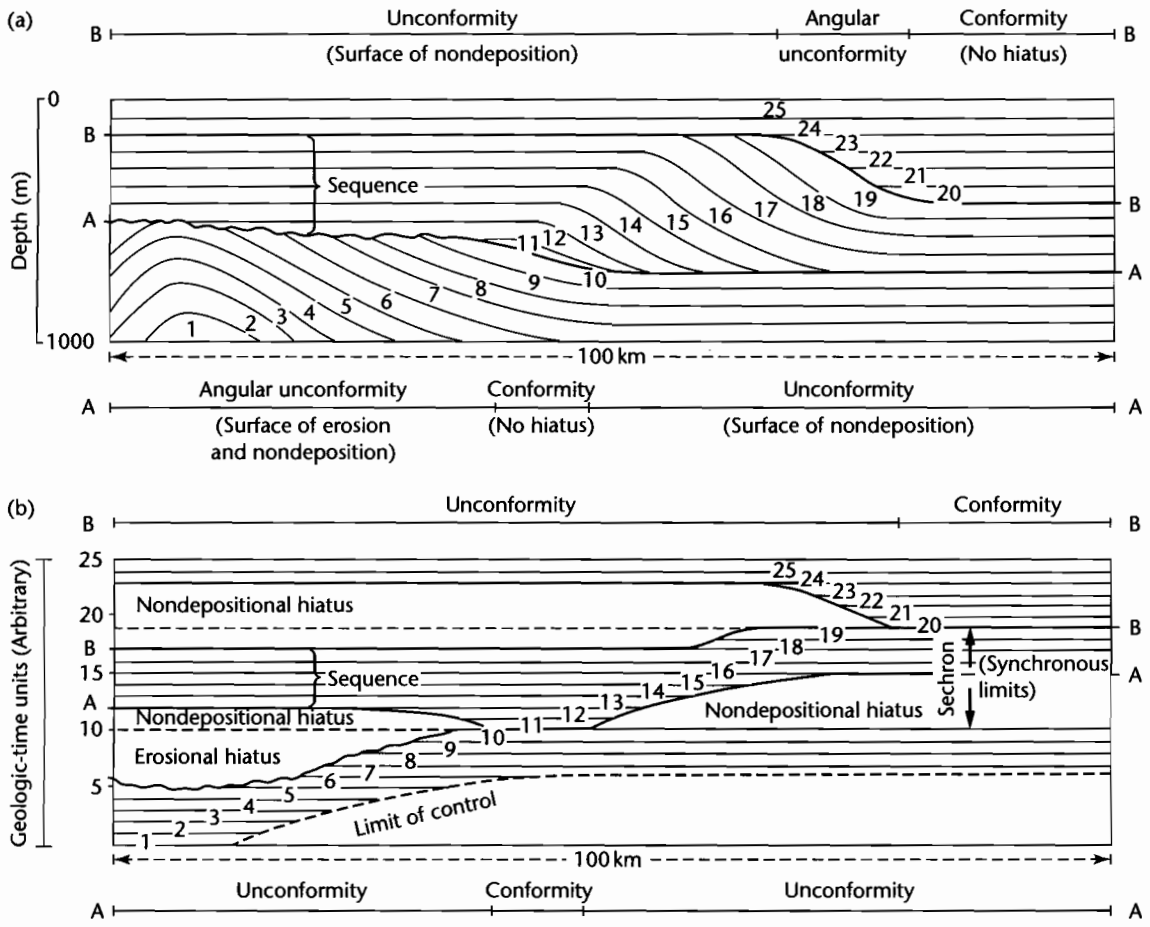

Fig. 8.8 The basic concept of the depositional sequence as outlined by Vail et al. (1977a). (a) Generalized stratigraphic section of a depositional sequence. A sequence boundary A changes from an angular unconformity in the left half of the diagram to a conformity in the centre and to a nondepositional unconformity on the right. The sequence boundary B passes from a nondepositional unconformity on the left to an angular unconformity in the centre and a lateral conformity on the right. Unconformities are dated at the points where they have become conformable. Units 1–25 represent strata deposited during successive time intervals; (b) Generalized chronostratigraphic section of the same stratigraphic sequence as in (a). The depositional sequence between surface A and B ranges in age from the beginning of 11 until the end of 19. Chronostratigraphic charts of this type are sometimes termed "Wheeler diagrams" following Wheeler (1958).

histories (see also Parkinson and Summerhayes 1985 for a thought experiment along these lines). The search for global synchroneity is therefore fundamentally futile. There is also some doubt as to whether 2nd, 3rd, 4th.... *n*th order cycles can actually be discriminated, and it is possible that stratigraphic cyclicity exists in a broad continuum of frequency (Wilkinson et al. 1998).

In summary, we believe that the Haq et al. (1987) curve is a "noisy" accumulation of a wide range of sea-level signals, and should not be used as a global benchmark.

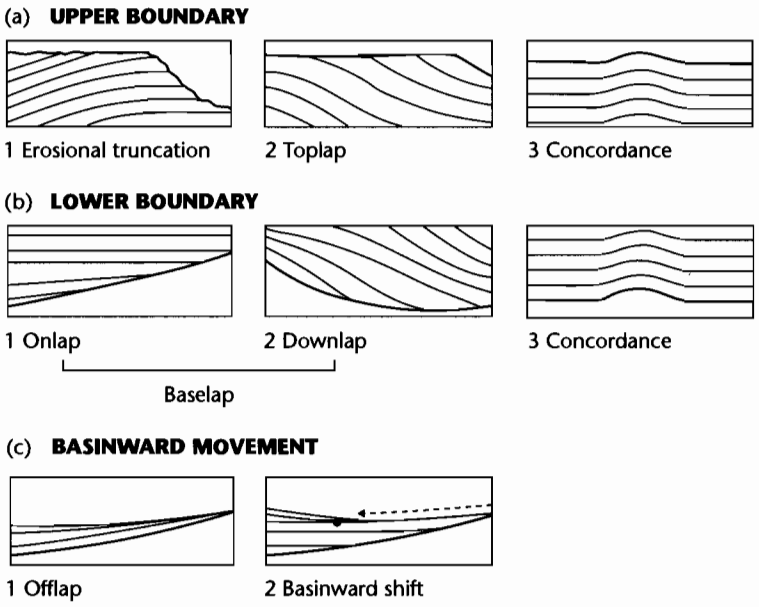

Fig. 8.9 The geometrical relationships of strata to a depositional sequence boundary or to any other surface within a depositional sequence. (a) Relations to upper surface, involving (1) erosional truncation, (2) toplap (commonly nondepositional rather than erosional), and (3) concordance; (b) Relations to lower surface involving (1) onlap where the overlying strata are near-horizontal and the surface is inclined, (2) downlap where the overlying strata are inclined, and (3) concordance; (c) Additional geometrical patterns of (1) offlap, where there is a progressive basinward migration of the stratigraphic units, and (2) basinward shifts, where the basinward movement is discrete rather than progressive.

It should never be used as a chronostratigraphic tool by assuming *a priori* that a certain stratigraphic boundary has a globally synchronous and precise age, which it is therefore safe to extrapolate into a basin with poor age control.

8.2.3 Systems tracts

Depositional sequences can be subdivided into smaller units of stratigraphy that have distinct stacking patterns of chronostratigraphic increments. These smaller units are termed *systems tracts* (Van Wagoner et al. 1988), and they are themselves composed of *parasequences*, or *paracycles*. The tracts of depositional systems (Brown and Fisher 1977) have been related to specific intervals of cycles of relative sea level (Posamentier et al. 1988; Posamentier and Vail 1988; Van Wagoner et al. 1988). Although systems tracts were defined as the stratigraphic response of a system to the competing effects of rate of relative sea-level change and rate of tectonic subsidence, they are clearly sensitive to variations in sediment supply. In the description that follows, it should be remembered that sediment supply variations may complicate and even override the effects of rate of relative sea-level change on systems tract behavior.

Systems tracts are broadly divided into the following classes according to their relationship to specific segments of the relative sea-level change curve (Fig. 8.12):

1 *Lowstand systems tract*: When relative sea-level fall is rapid, no space is available for further sedimentation, the former shelf is incised by streams (producing incised valley systems) and sedimentation is transferred to the basin floor and slope. Base-of-slope fans (*lowstand fans*) are nourished by sediment bypassed through the shelf and slope by valleys and canyons. *Slope fans* result from deposition on the middle or base of the continental slope and may be coeval with the basin-floor fan. *Lowstand wedges* are characterized by onlap onto the slope and at the same

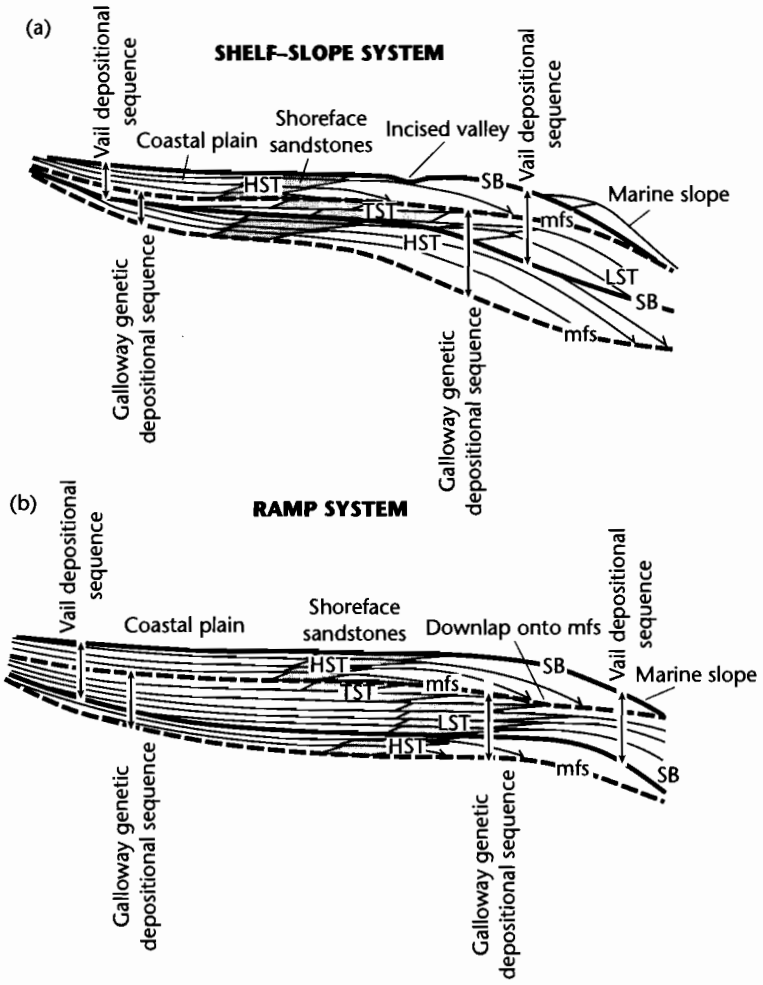

Fig. 8.10 Recognition of depositional sequences and genetic stratigraphic units using their bounding unconformities and maximum flooding surfaces respectively. A Vail-type depositional sequence is bounded by erosional unconformities or their correlative conformities, whereas a Galloway-type genetic depositional sequence is bounded by maximum flooding surfaces. HST, Highland systems tract; LST, Lowland systems tract; TST, Transgressive systems tract; SB, Sequence boundary; mfs, maximum flooding surface.

time by progradation and downlap onto the previous basin floor or slope fans. They are deposited at times of low but very slowly changing sea level, particularly during a slow relative rise. Lowstand fans, slope fans, and lowstand wedges are all associated with underlying Type I sequence boundaries. When the relative sea-level fall is gradual, sedimentation may be progressively shifted basinwards to the shelf edge where both onlap in a landward direction and downlap in a basinward direction takes place. The base of the *shelf margin* systems tract is therefore a Type 2 sequence boundary. On a ramp margin rather than a shelf-break margin, slopes are too low to allow for significant submarine canyon formation and turbidite deposition (Van Wagoner et al. 1988). Since there is little bypass of sediment to the basin floor, falling relative sea level may cause the deposition of a set of downstepping prograding wedges, known as *forced regressive wedges* (Posamentier et al. 1992) in a *forced regressive*

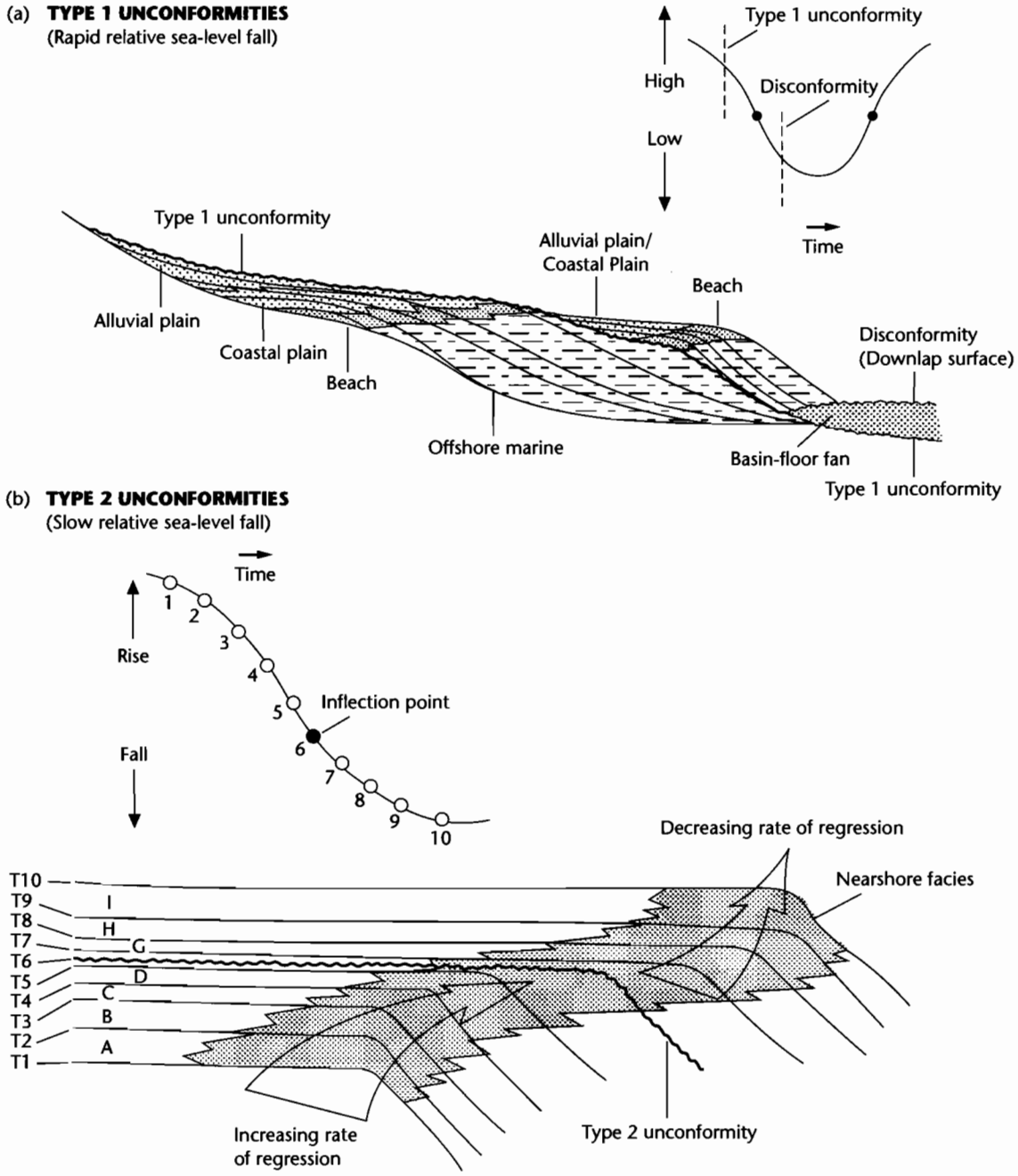

Fig. 8.11 Type 1 and Type 2 unconformities (after Posamentier et al. 1988). Type 1 unconformities (a) erode into older shelf sediments and may underlie basin-floor fans. They are believed to be formed during a rapid lowering of relative sea level. The sediments of the second depositional sequence downlap onto a disconformity or onlap the Type 1 unconformity. Type 2 unconformities (b) do not strongly erode the underlying depositional sequence, but signal a change from prominent progradation to aggradation as the rate of regression slows. Overlying sediments may onlap the Type 2 boundary landward of the shelf edge, although it is not illustrated above. Type 2 unconformities are interpreted to form at the inflection point of a slow relative sea-level fall.

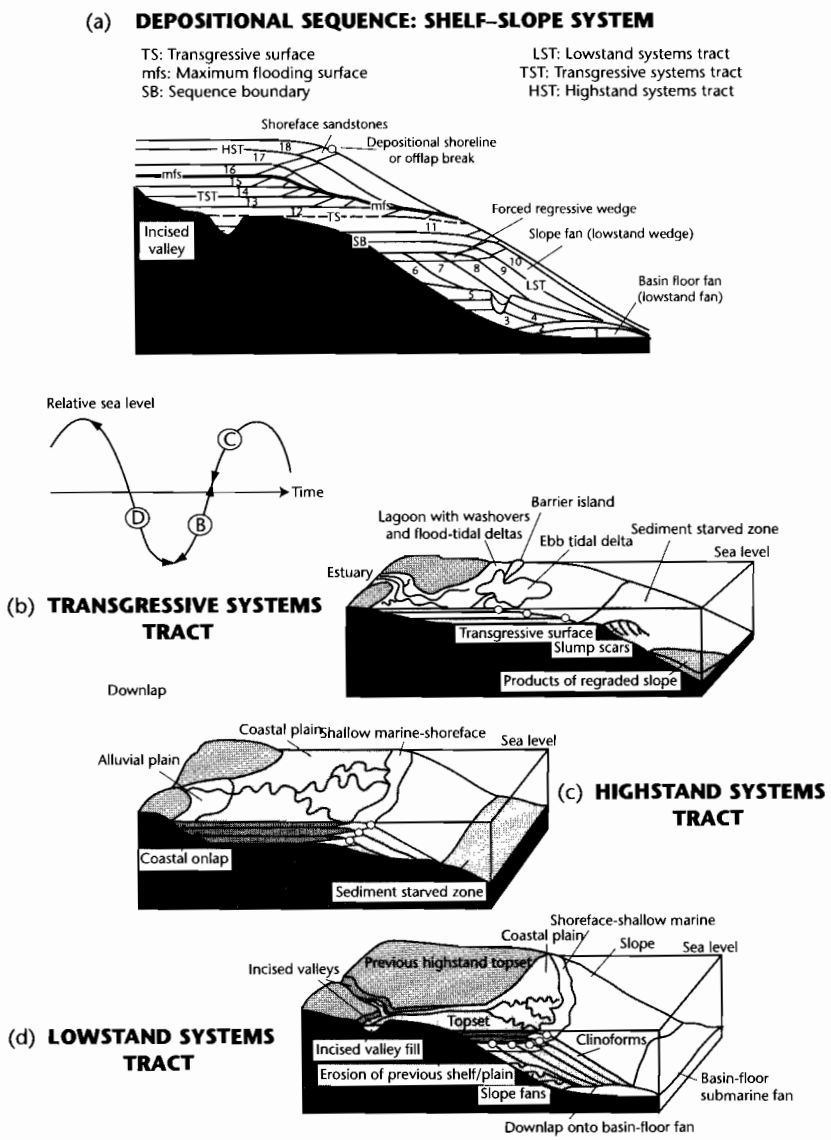

Fig. 8.12 Characteristic systems tracts and their relation to the relative sea-level curve, according to the Exxon group (Posamentier et al. 1988), modified by Emery and Myers (1996). These block diagrams are extremely idealized and have a strong vertical exaggeration. (a) Arrangement of systems tracts within a depositional sequence in a coastal plain–continental shelf-slope system. Numbers are relative ages of chrons; (b), (c) and (d) show transgressive, highstand, and lowstand systems tracts respectively. Open circles are depositional shoreline or offlap break. Reproduced courtesy of Blackwell Publishing Ltd.

systems tract (Hunt and Tucker 1992; Posamentier and James 1993).

2 *Transgressive systems tract*: During a rapid relative sea-level rise, the underlying lowstand or shelf margin system tracts are transgressed (the *transgressive surface*). Where the transgressive surface is erosional, it is called a *ravinement surface*. Sets of parasequences making up the transgressive system tract are commonly retrogradational (Fig. 8.13), that is, they back-step onto the basin margin, with strong onlap in a landward direction and downlap onto the transgressive surface in a basinward direction. As the rate of relative sea-level change slows down, the sets of parasequences change from being retrogradational to being aggradational, the surface at which this occurs being that of the *maximum flooding*. *Condensed sections* occur in the basin during times of transgression.

3 *Highstand systems tract:* After the maximum flooding, the relative sea-level rise slows and sets of aggradational parasequences are succeeded by progradational parasequences with clinoform geometries (Fig. 8.13). These highstand systems tract parasequences onlap onto the underlying sequence boundary in a landward direction and downlap onto the top of the transgressive systems tract or lowstand systems tract in a basinward direction, so that there is a prominent *downlap surface* below a highstand system tract. Marine condensed sequences occur during the early stages of a highstand systems tract before major progradation takes place (Loutit et al. 1988). Highstands offer the possibility of thick subaerial deposition of fluviatile sediments.

The methodology of systems tract recognition has been extended to carbonate-dominated systems (e.g.,

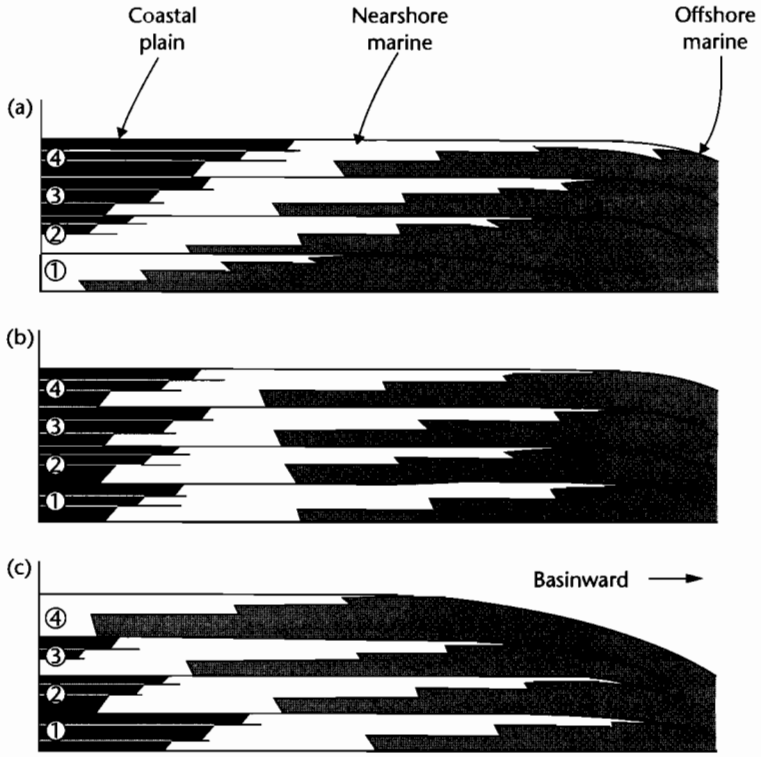

Fig. 8.13 Stacking patterns of parasequence sets (after Van Wagoner et al. 1988) are indicative of the trend in time of sediment supply and relative sea-level change or accommodation. (a) Progradational parasequence set with a basinward migration of the shoreline, characteristic of the highstand systems tract and lowstand prograding wedge; (b) Aggradational parasequence set showing no movement of the shoreline, characteristic of the shelf-margin systems tract; (c) Retrogradational parasequence set, with a landwards migration of the shoreline, characteristic of the transgressive systems tract. Reproduced courtesy of Society for Sedimentary Geology.

Sarg 1988; Schlager 1992). Although there are significant differences between siliciclastic and carbonate systems, the underlying principles are similar.

8.2.4 Smaller genetic stratigraphic units

The resolution of most seismic reflection sections generally allows only depositional sequences and megasequences to be recognized. However, log, core and outcrop data show that stratigraphy is marked by variability at higher resolution. The larger stratal geometries of depositional sequences can be linked at high resolution with their typical facies assemblages (Van Wagoner et al. 1990; Posamentier and Chamberlain 1993).

The typical small-scale cycles seen in core and at outcrop consist of an upward-shallowing trend followed by an abrupt deepening. These cycles are known as *parasequences* (Van Wagoner et al. 1990), who defined them as relatively conformable units of genetically related beds or bed-sets bounded by marine flooding surfaces or their correlative surfaces (Fig. 8.14). The boundaries of parasequences, as in depositional sequence boundaries, are thought to be synchronous surfaces. Parasquences thus defined are placed at a lower level than depositional sequences, but there is no further implication of hierarchical level (3rd, 4th, 5th order etc.). They have long been recognized in a variety of paleoenvironmental settings ranging from fluvial to deep marine, and in both siliciclastic- and carbonate-dominated systems. Parasequences are small scale but fundamental building blocks of stratigraphy, generally a few meters to <15 m in thickness. Their lateral extent varies according to the uniformity of basin tectonic subsidence and the nature of the external or internal forcing. In the Proterozoic Rocknest Platform of northwest Canada (Grotzinger 1986a) 140 to 160 progradational shallowing-up cycles can be traced for enormous distances (>100 km) both perpendicular and parallel to strike, whereas other field studies suggest that parasequences are commonly laterally impersistent.

The glacially forced sea-level changes of the Late Quaternary (§8.3.4) have a similar frequency to those required to explain some parasequences. The time scale of the fluctuation is also reminiscent of the frequency of climatic change attributed to eccentricities in the orbital motion of the Earth (Hays et al. 1976; Imbrie 1982). These variations are commonly termed *Milankovitch* cycles (see also §8.3.4). Time-series analysis of the

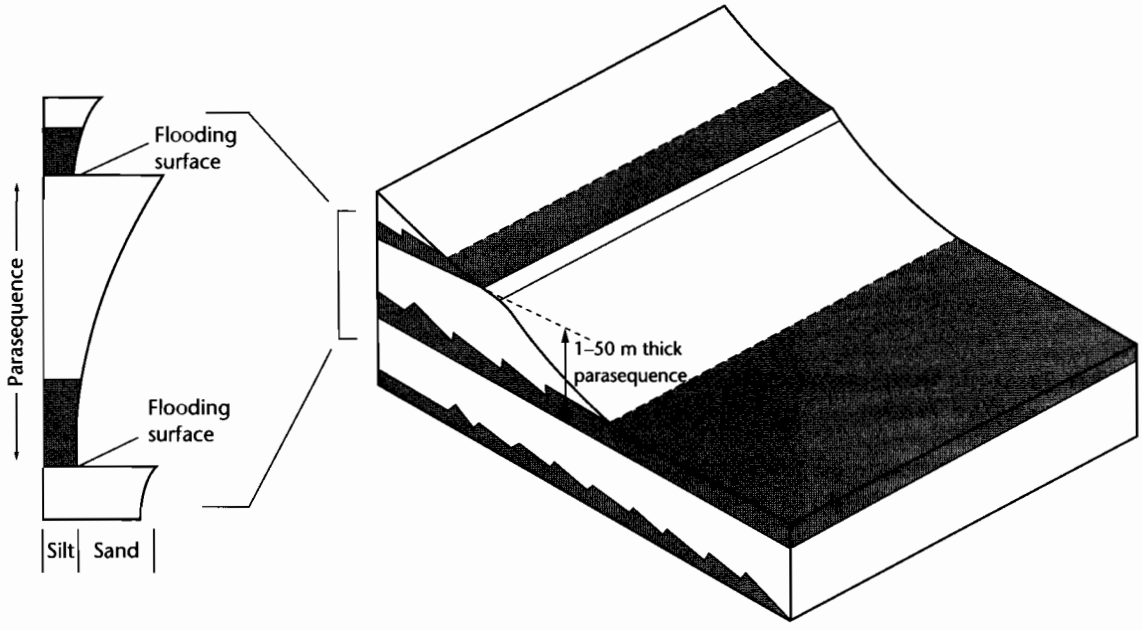

Fig. 8.14 A shallow marine parasequence involving upward coarsening, representing a shallowing of water depth over time. The parasequence is bounded by flooding surfaces. After Emery and Myers (1996). Reproduced courtesy of Blackwell Publishing Ltd.

periodicity of stratigraphic cycles, such as in the Alpine Triassic, have led to different claims about the identification of Milankovitch-type forcing (e.g., Goldhammer et al. 1990), and some cycles may be entirely unforced (Burgess et al. 2001).

Parasequences deposited at greenhouse periods, when glacio-eustatic changes are expected to have been minimal, may be unforced, or forced at a longer frequency than typical icehouse Milankovitch cycles. For example, cycles of relative sea-level change interpreted in Eocene "greenhouse" stratigraphy in the Swiss Alps appear to have a frequency of *c.* 0.4–1 Myr (Allen et al. 2001). The Oligocene stratigraphy of the New Jersey coastal plain exhibits cycles of *c.* 0.5–2 Myr duration (Kominz and Pekar 2001). Clearly, on identifying parasequences, it is not a safe assumption that they were deposited within the Milankovitch wave band.

8.3 DRIVING MECHANISMS FOR STRATIGRAPHIC PATTERNS

In Chapters 3–6 we introduced the main mechanisms for the formation and development of sedimentary basins. In this section we consider in more detail some of the mechanisms responsible for stratigraphic patterns in the basin-fill. They can be divided into tectonic mechanisms that control the spatial and temporal pattern of subsidence and the evolution of sediment routing systems, and eustatic mechanisms that essentially control accommodation and set base level. We then briefly examine the other effects of climate change, principally through sediment yield, and consider cyclicity that is unforced by external controls and which originates from the internal complexity of sediment routing systems. An overview of the depositional styles of basins in a wide variety of tectonic settings is found in §8.5.

8.3.1 Tectonic mechanisms: Flexure under applied loads

8.3.1.1 Effects of flexure on stratigraphy in basins due to stretching

The mechanisms of subsidence in stretched basins comprise: (i) a fault-controlled initial subsidence caused by mechanical stretching of the upper brittle layer of the lithosphere, and (ii) a thermal subsidence caused by the cooling and contraction of the upwelled asthenosphere (Chapter 3). These mechanisms are amplified by sediment and water loading (Chapter 9). In the period of active stretching or rifting, the lithosphere is generally viewed as being in a state of purely local (Airy) isostasy. That is, the lithosphere behaves as a very weak support for any superimposed loads in the active rift. However, the presence of gently dipping postrift sediments suggests that a broadly distributed subsidence characterizes the postrift stage. The way in which the lithosphere distributes loads in the postrift stage is by flexure. Whereas the stretching event determines the first-order depth and size of the basin, the subtleties of the flexural response of the lithosphere have a profound influence on depositional sequences in the postrift stage.

If the lithosphere behaves *elastically* over geological time periods, flexural rigidity should depend on its thermal age (§4.3.2). Basin stratigraphy should reflect this increase in flexural rigidity with time, by a progressive overstepping of younger strata at the margin of the basin. If the lithosphere behaves *viscoelastically* (and the time constant of the viscous relaxation is long), stresses are relaxed by a viscous flow, causing the flexural rigidity to decrease with time. For the same tectonic (cooling plate) driving mechanism, this different basement response produces a pattern of stratigraphic offlap, with the youngest sediments restricted to the basin center. The widths of the basins produced on elastic and viscoelastic lithosphere are therefore markedly different (Fig. 8.15). For the elastic lithosphere, the postrift sediments strongly overstep the synrift sediments giving a *steer's-head* geometry. In contrast, on a viscoelastic plate, the overstep of the postrift sediments is absent because of stress relaxation with time.

The pattern of stratigraphic onlap has been modeled in detail for the passive margin of eastern North America (Watts 1982). Sedimentation is assumed to keep pace with subsidence, maintaining a constant bathymetric profile through time. Figure 8.16 shows the initial strong onlap of sediments onto the basement at the transition from fault-controlled Airy-type subsidence to flexural-controlled subsidence. However, lateral heat flow causes thermal uplift on the coastal plain, abruptly terminating onlap. By about 16 Myr after rifting, flexural subsidence outstrips thermal uplift and the sediments again progressively onlap basement.

8.3.1.2 Role of flexure in generating foreland basin stratigraphy

The typical large-scale geometry of foreland basin stratigraphy is of wedge shaped units, thick close to the

orogenic load and thinning onto the foreland into a "feather-edge." This is a reflection of the lateral gradient in subsidence rate from the center of the load to the peripheral bulge. Superimposed on this is commonly a spatial translation (with respect to the underlying plate) of stratigraphic units ahead of a moving load, a consequence of continued convergence being accommodated in the orogenic belt. This effect causes a general onlap of successively younger stratigraphy onto the foreland (Fig. 8.17). Numerous case studies exist that demonstrate this simple geometric style, such as the Magallanes Basin of southern South America (Fig. 8.18).

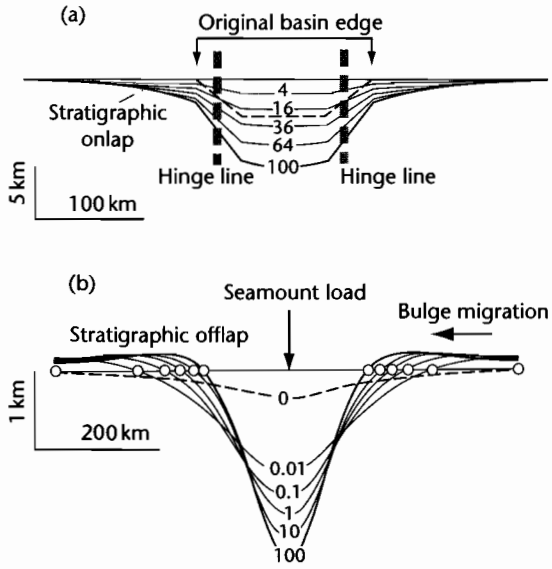

Fig. 8.15 Contrast of elastic and viscoelastic behaviors. (a) Stratigraphy of a model stretched basin with $\beta = 2.0$, overlying an elastic lithosphere where the equivalent elastic thickness is the depth to the 450 °C isotherm. T_e increases with thermal age, causing stratigraphic onlap (steer's head geometry); (b) Response of a visocoelastic lithosphere with a viscous relaxation time of 10^4 yr to seamount loading. The lithosphere weakens rapidly following loading, causing stratigraphic offlap and a gradually narrowing basin. Vertical exaggeration of × 10. Numbers are time in Myr since rifting. After Watts et al. (1982).

The deflection of a foreland plate must depend on the flexural rigidity of the flexed lithosphere, the nature of the distributed loads (topographic/thrust loads, subsurface loads, horizontal end forces, bending moments, sediment and water loads) and the presence of pre-existing heterogeneities. As a consequence, it is vital in considering foreland basin stratigraphy to consider the previous geological history of the lithosphere. The most common scenario is the *Wilson cycle* (§1.3).

The Wilson cycle implies that during continental collision, the overriding plate flexes an inherited passive margin structure in the underlying plate. Two points immediately stand out: (i) since the lithosphere has been previously heated and stretched (§3.1) it will possess a flexural rigidity or equivalent elastic thickness that reflects this history, the "memory" diminishing with time since rifting, (ii) the first loads will be emplaced on a pre-existing continental margin bathymetry rather than on an imaginary flat surface representing the regional elevation.

Stockmal et al. (1986), using a depth-dependent plate rheology, proposed four end-member models to account for the transition from passive margin to foreland basin (Table 8.1). Whereas at early stages the thermal age of the passive margin is an important, even dominant control on basin development, this effect becomes less important as the overthrust wedge is progressively emplaced on stronger unstretched lithosphere. At this stage, the thickness of the overthrust load is of greatest importance. The maximum foreland basin depths prior to postdeformational erosion vary from ~3 km for a low

Table 8.1 Four end-members of foreland basins superimposed on passive margins (Stockmal et al. 1986).

	High topographic profile* (e.g., Himalayas) Frontal slope ~3°	***Low topographic profile* (e.g., Zagros) Frontal slope ~0.5°†**
Thermally young (~10 Myr) continental margin	Young–high	Young–low
Thermally old (~120 Myr) continental margin	Old–high	Old–low

Notes:
* Seeber, Armbruster and Quittmeyer (1981);
† Chapple (1978).

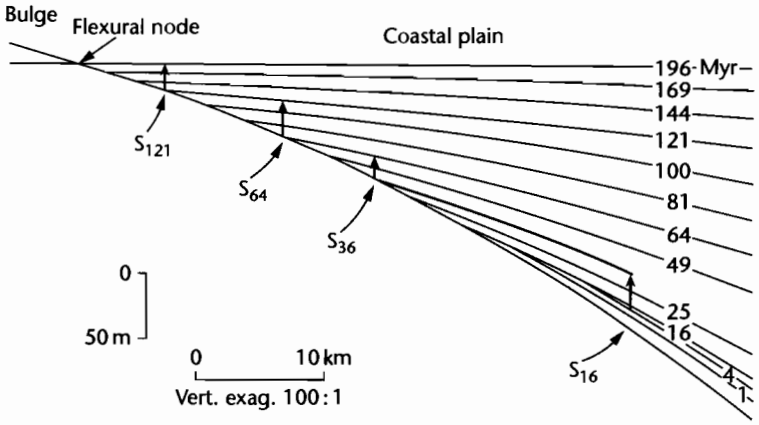

Fig. 8.16 Coastal plain and shelf stratigraphy using a model of a passive margin in which the tectonic subsidence is due to thermal contraction following stretching. Sediments rapidly infill the continental shelf, keeping a near-constant bathymetry with time. The sedimentary load flexes a cooling plate that increases in rigidity with time since heating. The initial lithospheric thickness y_L is 125 km, initial crustal thickness y_c 31.2 km, coefficient of thermal expansion α, 3.4×10^{-5} °C $^{-1}$, mantle temperature 1333 °C, initial densities of 2800 and 3300 kg m^{-3} for crust and mantle lithosphere respectively, and the uniform density of the infilling material is 2500 kg m^{-3}. The stretch factor is 3.0 and the equivalent elastic thickness is given by the depth to the 450 °C isotherm. Solid boundaries are stratigraphic units with ages in Myr since the end of rifting. Effects of compaction have been ignored. The arrowed lines show the amounts of coastal aggradation at given time periods. After Watts (1982).

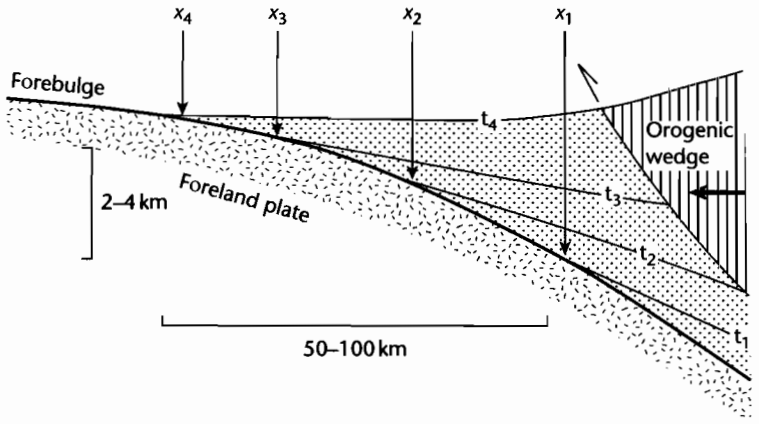

Fig. 8.17 Diagrammatic illustration of a foreland basin showing stratigraphic onlap. Locations x_1 to x_4 show the successive positions of pinch-outs corresponding to the chronostratigraphic lines t_1 to t_4.

topography (e.g., Zagros) to ~16 km for a high topography (e.g., Himalayas). Postdeformation erosion and tectonic thinning (extension) can cause massive unroofing of up to 40 km, bringing high grade metamorphic rocks to the surface. Very thick overthrust wedges can develop with little topographic expression if they are emplaced on a deep oceanic bathymetry. Further information on the development of orogenic wedges and their numerical modeling is found in §4.5 and §4.6.

8.3.1.3 The flexural forebulge unconformity

Passage of the flexural forebulge can cause a complex arrangement of unconformities (Price and Hatcher

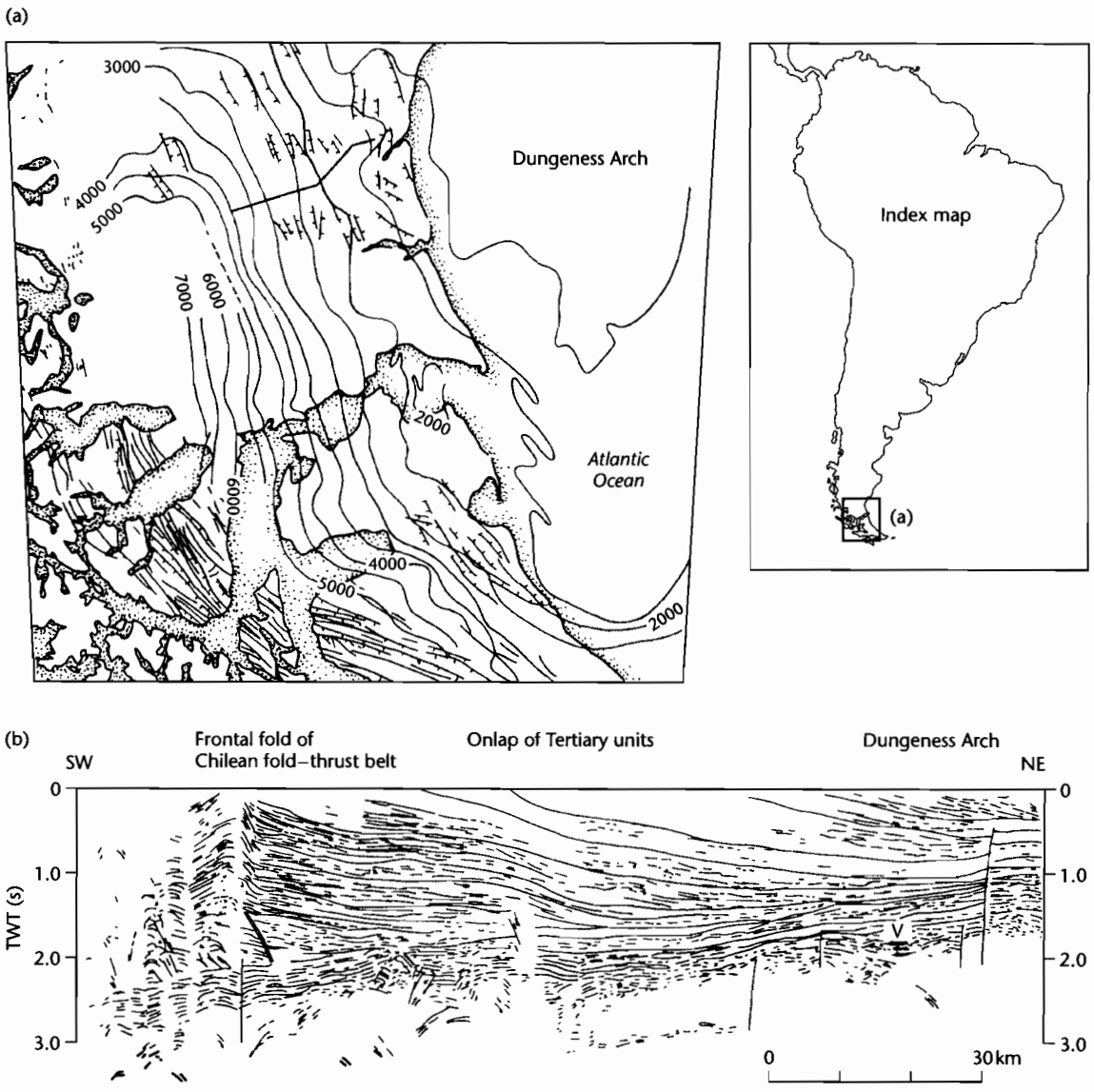

Fig. 8.18 The Magallanes Basin, southern South America (after Biddle et al. 1986). (a) Isopachs (in m) of sedimentary fill of Magallanes Basin above the level of the Tobifera volcanics, representing the last stages of rifting prior to foreland basin flexure (Bruhn et al. 1978; Gust et al. 1985). Isopachs show a clear thinning onto the Dungeness Arch; (b) Line drawing interpretation of seismic reflection record from the frontal folds of the Chilean fold–thrust belt to the flank of the Dungeness Arch. Stratigraphic units show strong onlap above the Tobifera volcanics (V). The clinoforms are thought to be fan deltas derived from the Andean mountain belt that prograded into deep marine shales.

1983). Initial uplift in the forebulge region is followed by subsidence as the bulge moves onto the craton. The unconformities should migrate in a time-transgressive manner onto the craton (Crampton and Allen 1995).

Consider a flexural forebulge unconformity generated by an orogenic load moving across a linear elastic foreland plate of flexural rigidity D. If the advance of the orogen is steady, the stratigraphic gap is dependent on:

(i) the time-average erosion rate on the forebulge, and (ii) the duration of uplift in the forebulge region, given by

$$\tau = \frac{x_2 - x_1}{V} \tag{8.13}$$

where x_1 and x_2 are the first node and second node of the deflection respectively, which is equivalent to the width of the forebulge, and V is the advance rate of the orogenic system. The width of the forebulge on a continuous elastic plate scales on the flexural parameter α (equation 4.4), with $x_2 = 7\pi\alpha/4$ and $x_1 = 3\pi\alpha/4$. Hence

$$\tau = \frac{x_2 - x_1}{V} = \frac{\pi x}{V} \tag{8.14}$$

where

$$\alpha = \left\{\frac{4D}{\Delta\rho g}\right\}^{1/4}$$

as given by equation (4.3), D is the flexural rigidity and $\Delta\rho$ is the difference in density between the mantle and the material filling the deflection. The model stratigraphic gap should increase from zero at the point of conformity corresponding to the initial position of the first node of the deflection, to a maximum at a distance corresponding to the initial position of the second node of the deflection (Fig. 8.19). In other words, this zone of increasing stratigraphic gap is equivalent to the initial width of the forebulge. In the case of inherited bathymetry from the passive margin stage, the zone of increasing stratigraphic gap is telescoped because the initial uplift of the forebulge takes place below sea level. The model prediction of Crampton and Allen (1995) compares favorably with the observed spatial distribution of stratigraphic gap at the base of the Tertiary foreland basin megasequence in the Alps of Switzerland (Fig 8.20).

In some cases, such as the Devonian (Acadian) peripheral bulge to the Appalachian orogen, the forebulge unconformity system shows an orogenward migration

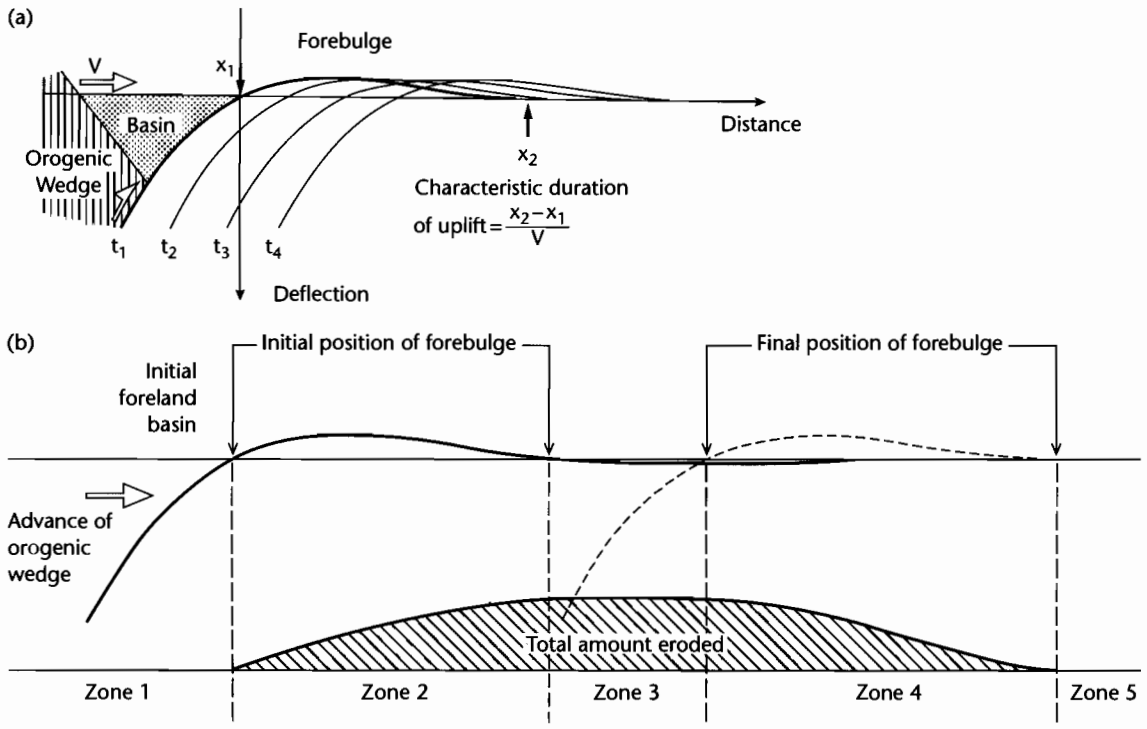

Fig. 8.19 (a) Flexural profiles at times t_1 to t_4, to show the duration of uplift in the flexural forebulge region, using a broken elastic plate; (b) Geometry of the flexural forebulge unconformity. The existence of inherited bathymetry causes zones 1 and 2 to be translated farther onto the foreland plate and zone 2 becomes narrower. After Crampton and Allen (1995). Reproduced courtesy of American Association of Petroleum Geologists.

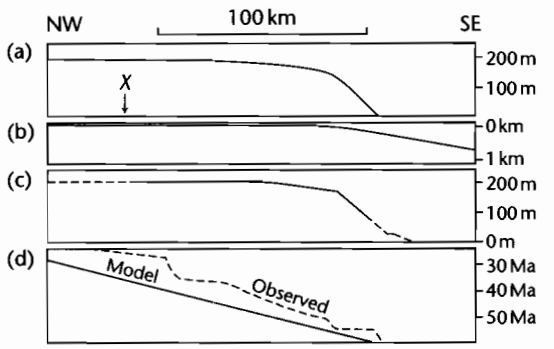

Fig. 8.20 Fit between model predictions for the forebulge unconformity and observations in eastern Switzerland, using the linear elastic model of Crampton and Allen (1995). (a) The modeled total erosion at the forebulge unconformity *versus* distance from the initial position of the orogenic wedge, with $T_e = 10$ km, orogenic advance rate 8 mm yr^{-1} and erosion proportional to elevation with coefficient 0.02. Point X is initially 200 km from the orogenic front. Note the rapid increase in erosional gap from 0 to 200 m across the zone of inherited shelf bathymetry shown in (b); (c) The observed erosion *versus* approximate restored distance from the orogen (based on Herb 1988), showing close similarity to the modeled erosion; (d) As a test, the modeled onlap of sedimentary rocks overlying the unconformity are compared with the observed onlap along a restored section (based on Herb 1988; Sinclair et al. 1991). Reproduced courtesy of American Association of Petroleum Geologists.

that has been attributed to viscoelastic relaxation of the lithosphere (Tankard 1986). A series of splaying unconformities that overstep systematically toward the orogen indicates contemporaneous uplift and orogenward movement of the forebulge at this time.

The location and geometry of a flexural forebulge may also be strongly influenced by pre-existing lithospheric heterogeneities (Waschbusch and Royden 1992). The flexural forebulge may position itself over weak zones in the lithosphere, and then episodically migrate to another weak zone, instead of migrating steadily. Reactivation of old faults may also strongly disrupt the uplift, subsidence and migration history of the forebulge region. Extensional reactivation of normal basement faults by outer arc bending stresses (Bradley and Kidd 1991) or inversion of normal basement faults by the compressional stresses generated during orogeny (Meyers et al. 1992; Ussami et al. 1999; Gupta and Allen 2000) have both been described.

8.3.1.4 Foreland basin isopachs and pinch-outs

The migration of depocenters and of feather-edge pinch-outs of stratigraphy gives an impression of the mobility of the distributed loads and/or variations in the lithospheric response. An early modeling exercise was carried out on the Cretaceous retro-foreland basin in the western United States (Jordan 1981). The progressive eastward shift of depocenters through time in the Idaho–Wyoming region (Fig. 8.21) was predicted using the palinspastically restored thrust load configuration during the Sevier orogeny. Careful matching of predicted with observed stratigraphy allowed a flexural rigidity of about 10^{23} Nm to be estimated for the Cretaceous lithosphere. There was no necessity to invoke a changing flexural rigidity with time, suggesting that the lithosphere behaved elastically over the modeled 70 Myr time span and that lateral variations in rigidity were also insignificant. Similar modeling exercises have been carried out in the Neogene Argentinian foreland of South America (Cardozo and Jordan 2001) and in the Triassic Longmen Shan foreland basin of Sichuan, China (Yong et al. 2003).

Some of the Alpine foreland basins of Europe also show a clear relationship between load mobility and depocenter migration. In the North Alpine foreland basin of western Switzerland, a classical peripheral foreland basin, pinch-outs and depocenters of stratigraphic units migrated onto the European craton during the Oligo–Miocene, corresponding to the main collisional phase of Alpine orogenesis. A palinspastic restoration of thrust units over the same time period coupled with a time-bracketing technique for dating thrust movements allowed fault tip propagation and shortening rates to be estimated (Homewood et al. 1986; Sinclair and Allen 1992). There was a close correspondence between the rates of depocenter and pinch-out migration and of thrust-related shortening in western Switzerland. This feature initially suggests, as in the Cretaceous Sevier belt, that the lithospheric response is constant through time.

If the pinch-out migration rate far exceeds the rate at which the mountain belt advances, the foreland basin should progressively widen with time (Fig. 8.22). This might result from a number of processes. For example, it would be expected if the mountain belt loaded a progressively stronger elastic lithosphere as it overrode first the passive margin, then the unstretched craton. It might also result from the forelandward shift of the center of gravity of the load by erosion and deposition of sediment

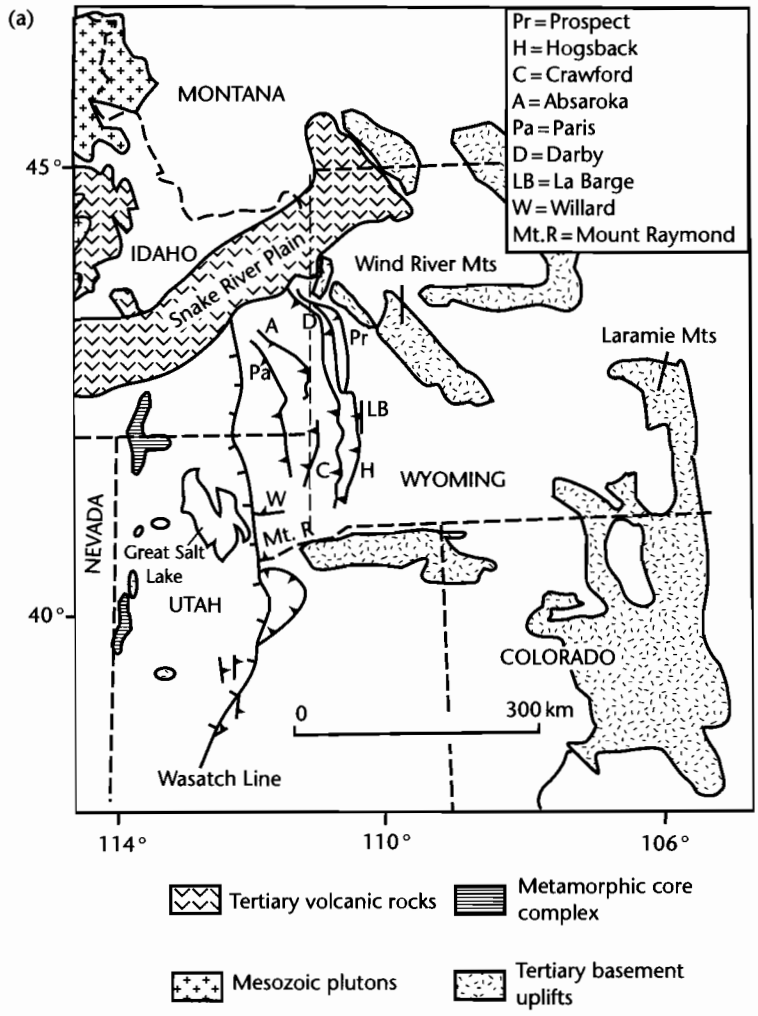

Fig. 8.21 (a) Location of Jurassic–Tertiary Sevier thrust belt in western USA. Volcanic rocks, basement uplifts, and the extensional Wasatch Line are all younger than the thrusting; (b) Plot of age versus distance (relative to the present day trace of the easternmost major thrust) showing the eastward displacement of basin depocenters through time, which is mirrored by an eastward migration of active thrusting. After Jordan (1981). Reproduced courtesy of American Association of Petroleum Geologists.

in the basin (see below). On the other hand, if the pinch-out migration rate slows relative to the rate of advance of the mountain belt or if the forebulge is dragged inwards toward a stationary mountain front, the foreland basin should narrow (Fig. 8.22). Although this kind of offlapping relationship has been interpreted to result from stress relaxation in a viscoelastic lithosphere (Quinlan and Beaumont 1984; Tankard 1986), a similar effect can be produced by thickening of the adjacent orogenic wedge loading an elastic plate (Flemings and Jordan 1989; Sinclair et al. 1991).

8.3.1.5 Underfilling and overfilling

The topography caused by thrusting in mountain belts is eroded to provide detritus to fill the foreland basin.

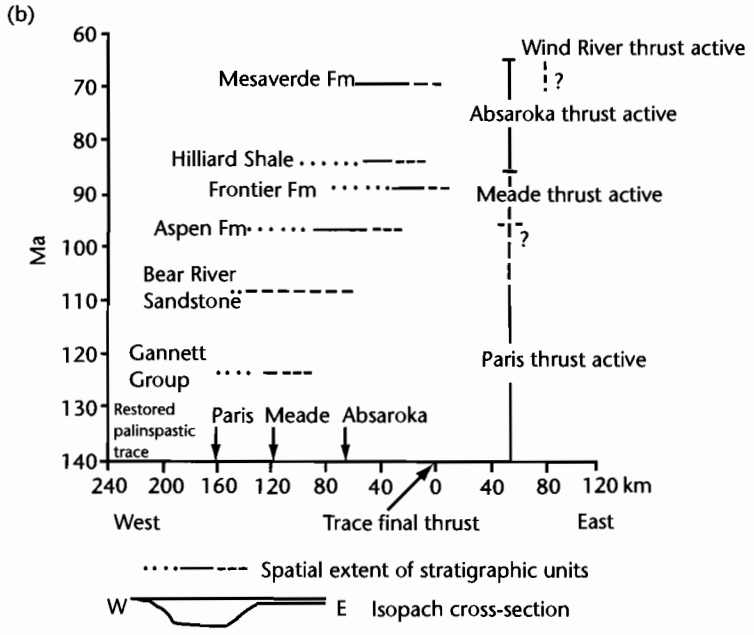

Fig. 8.21 *Continued*

Moretti and Turcotte (1985) first applied a diffusion equation to this process and Flemings and Jordan (1989) and Sinclair et al. (1991) have specifically applied 2-D diffusion modeling to the stratigraphy of foreland basins. The coupling between orogenic wedge development and basin filling has been extended to 3-D by Johnson and Beaumont (1995) and the doctoral theses of Peper (1993) and Clevis (2003) provide further valuable details.

The 2-D diffusion model provides a starting point for considering the controls on foreland basin stratigraphy. Sinclair et al. (1990) modeled the stratigraphy of the North Alpine Foreland Basin in the central Alps using a diffusion model for erosion, a thrust-wedge model based on the concept of a critical taper (§4.5 for details), and a rheology of a linear elastic plate for the flexed European lithosphere. The amount of sediment transported to the foreland basin is proportional to the slope, the transport coefficient (K) varying over several orders of magnitude according to climatic and hydrologic setting (§7.5 for details). Flemings and Jordan (1989), for example, suggest that K for fluvial transport is *c.* $10^4 m^2 yr^{-1}$ whereas it is only $10^{-2} m^2 yr^{-1}$ for the decay of isolated hillslopes. The values obtained from a study of the modern sub-Andean foreland were of the order $10^4 m^2 yr^{-1}$ (Flemings and Jordan 1989). Marr et al. (2000) estimated the transport coefficient to be $10^4 m^2 yr^{-1}$ and $10^5 m^2 yr^{-1}$ for gravel and sand respectively (§7.5.3). The magnitude of the rate of transport of sediment into the basin clearly determines whether, for a given flexural response, it is *underfilled* or *overfilled* (Covey 1986).

Sinclair et al. (1991) simulated movement of the forebulge, both vertically and horizontally, and the attendant unconformities produced in the basin-filling stratigraphy purely by varying the rate of thrust belt propagation and wedge thickening coupled with diffusive erosion (Fig. 4.34). It was not necessary to vary the flexural rigidity of the European plate through time, nor to invoke a nonelastic rheology for the flexed plate. Subtle unconformities ('sequence boundaries") associated with abrupt basinward shifts or progressive offlap could be produced by thickening the load and slowing its propagation rate. Erosion of the load then caused onlap as the center of gravity of the load migrated forelandwards through redistribution of sediment from wedge to basin. Rapid advance of the thrust tip encouraged underfilling of the basin, whereas lower values of thrust belt migration rate promoted overfilling, the sedimentation keeping pace with the creation of new space in the basin.

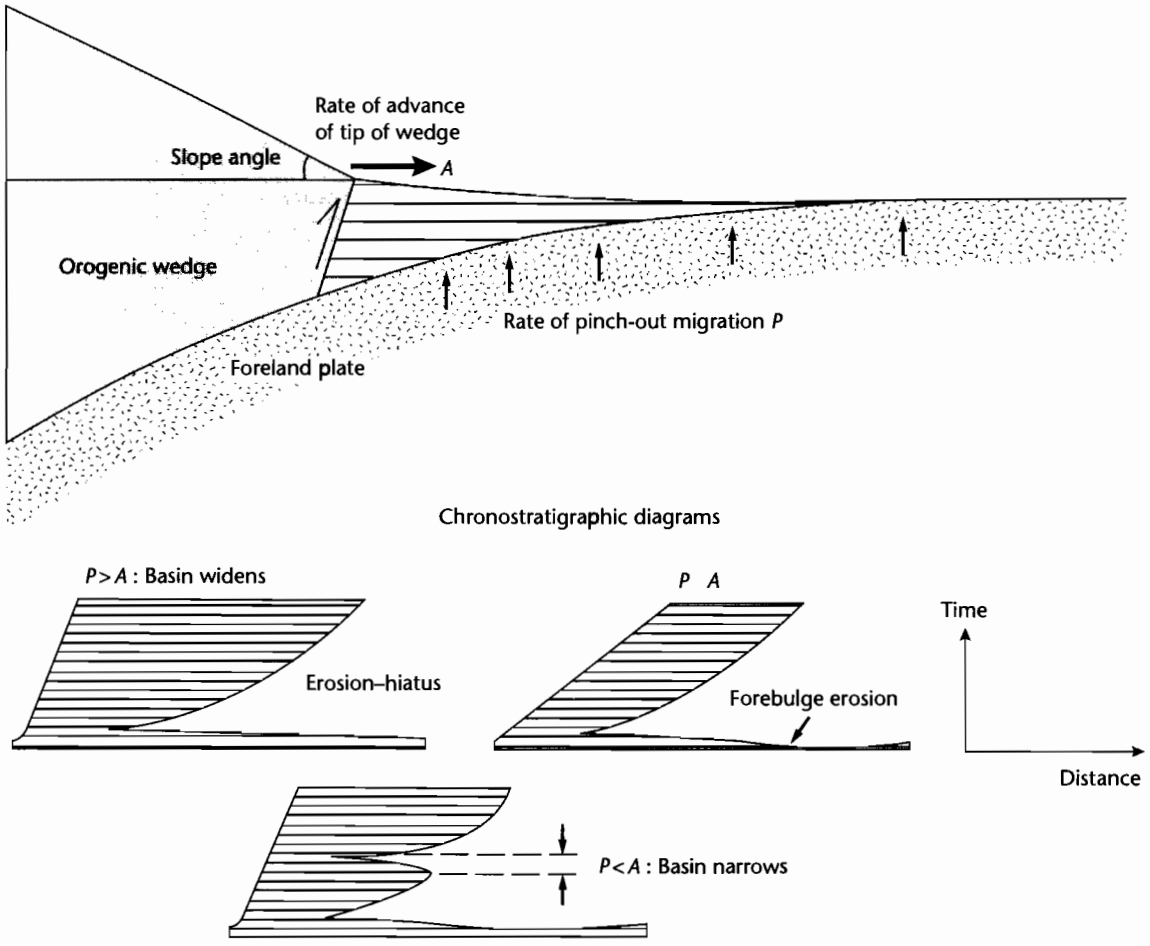

Fig. 8.22 Influence of the rates of advance of the tip of the orogenic wedge and of pinch-out migration on the foreland basin width. Note that onlap onto the foreland plate takes place even in the case of a time-constant basin width. A narrowing of the basin has been interpreted as due to viscoelastic relaxation, but can also result from reorganization of the orogenic load on an elastic plate.

8.3.2 Tectonic mechanisms: fault array evolution

Sediment deposited in rift basins does not simply fill a passive receptacle. The extending crust has an important impact on sedimentary thicknesses, stratigraphic packaging and gross depositional environments in the synrift phase of extensional basins (summarized in Gawthorpe and Leeder 2000). The extension of the crust produces an array of predominantly normal, dip–slip faults. On each fault, a slip event generates hangingwall subsidence and footwall uplift. Accommodation is therefore generated in the hangingwall, while a source of sediment is provided in the footwall. The time–space characteristics of accommodation generation are therefore closely linked to the evolution of normal fault arrays.

Crustal scale normal faults are not simple planar structures with uniform displacements along their length. Instead, they form parts of complex arrays of fault segments with cumulative displacements that vary systematically along the length of the fault segment, and which mutually interfere (Cowie et al. 2000). A single fault segment, whose length is commonly between 10 and

100 km, has a maximum cumulative displacement *d*-length *L* relationship (Schlische 1991; Dawers and Anders 1995).

$$d \approx kL \tag{8.15}$$

where k is a constant of proportionality that varies between 0.01 and 0.05 for many fault systems (Fig. 8.23). The cumulative displacement and the displacement rate are highest near the center of the fault segment, and decrease to zero at the tip. However, fault segments form part of an interacting array, so that some fault segments "grow" at the expense of other fault segments (Fig. 8.24). Faults that are able to link at an early stage with a neighboring fault may therefore continue to grow into major crustal features with large displacement, whereas other faults may quickly become dormant. Large depocenters develop adjacent to major rift faults. Eventually, the full array may become linked, with basin subsidence taking place almost exclusively along a long, linked border fault. Studies of such evolving fault arrays during the Jurassic synrift phase of the North Sea Basin suggest that linkage takes place rapidly, perhaps over 3–4 Myr (McLeod et al. 2000).

The stratigraphic patterns of rift basins reflect this underlying pattern of fault array evolution. Scenarios for fault array evolution in continental and coastal/marine settings are given in Gawthorpe and Leeder (2000) and summarized in Figure 8.25. The common evolution from small, disconnected faults to full linkage produces a stratigraphic theme of isolated continental, hydrologically closed basins with lakes evolving into open rifts connected to the ocean containing shallow marine or deep marine sediments fringed by fan-deltas. The Miocene evolution of the Gulf of Suez is a classically documented example of such a rift evolution (Garfunkel and Bartov 1977; Evans 1988; Sharp et al. 2000). It is impossible to ignore the profound effects of tectonic uplift and

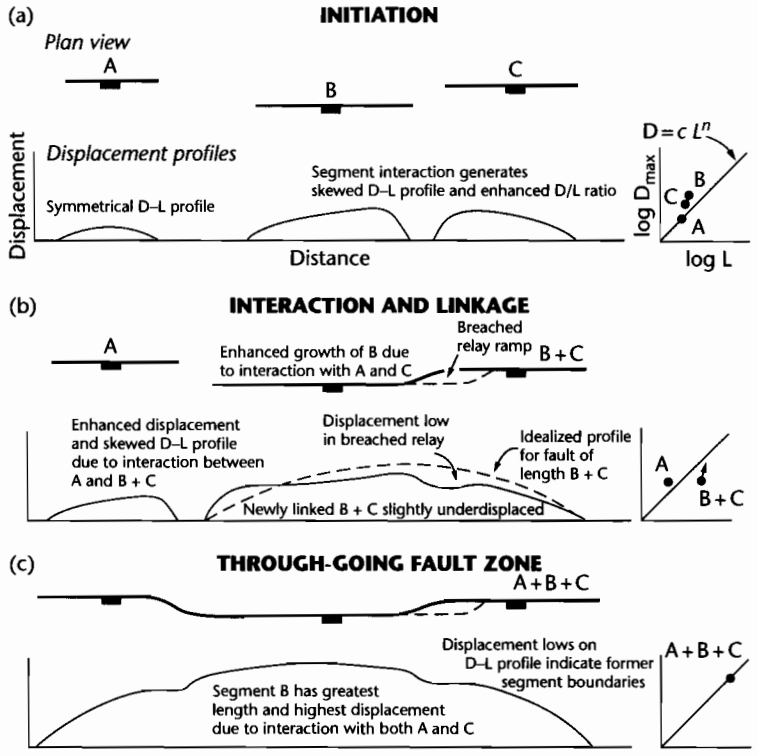

Fig. 8.23 Displacement–length relationship of normal faults. Fault segments grow from an initiation stage (a) with individualized displacement–length relationships, to interaction and linkage (b), and then to a through-going fault zone (c), where there is one displacement–length profile that may contain remnant information of the original fault segments. From Gawthorpe and Leeder (2000). Reproduced courtesy of Blackwell Publishing Ltd.

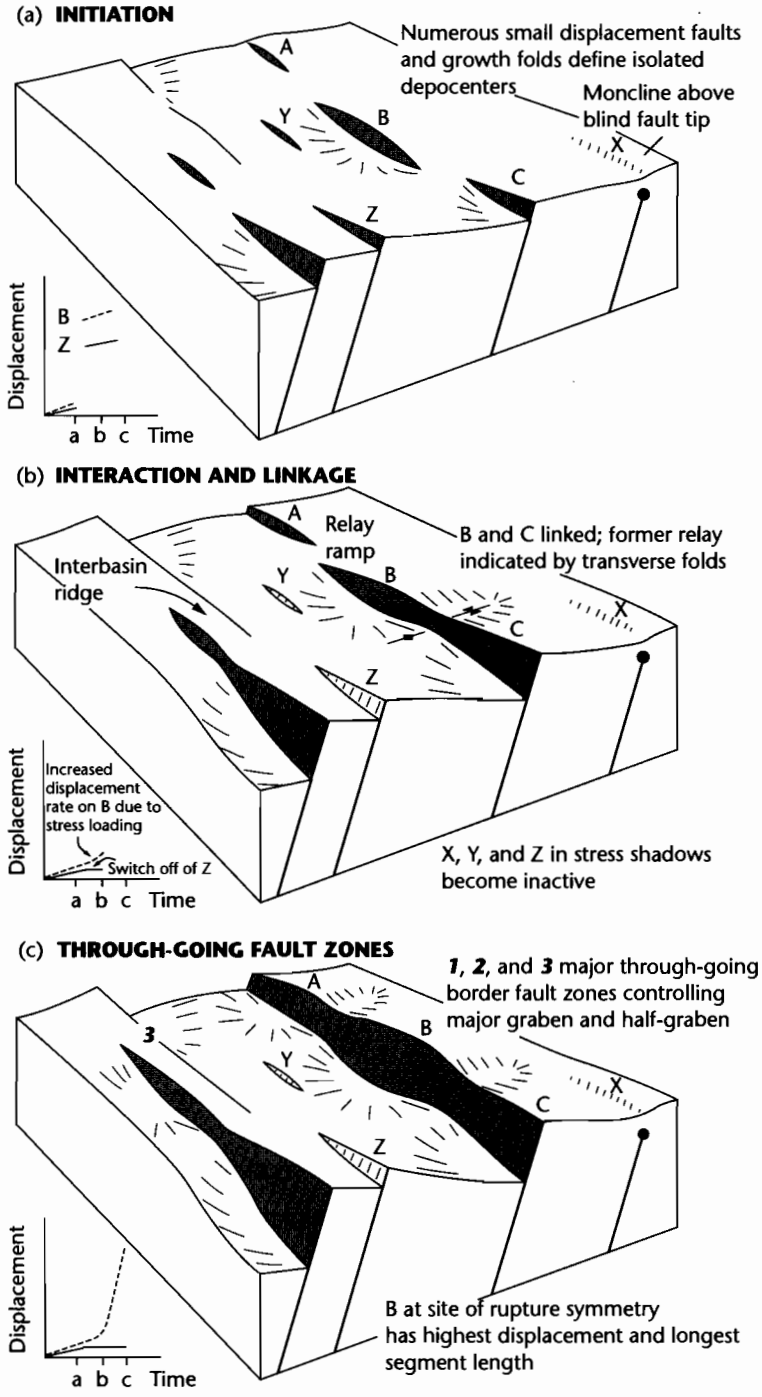

Fig. 8.24 Model of fault interaction and growth from initiation (a), interaction and linkage (b), to a through-going fault zone (c). From Gawthorpe and Leeder (2000). Reproduced courtesy of Blackwell Publishing Ltd.

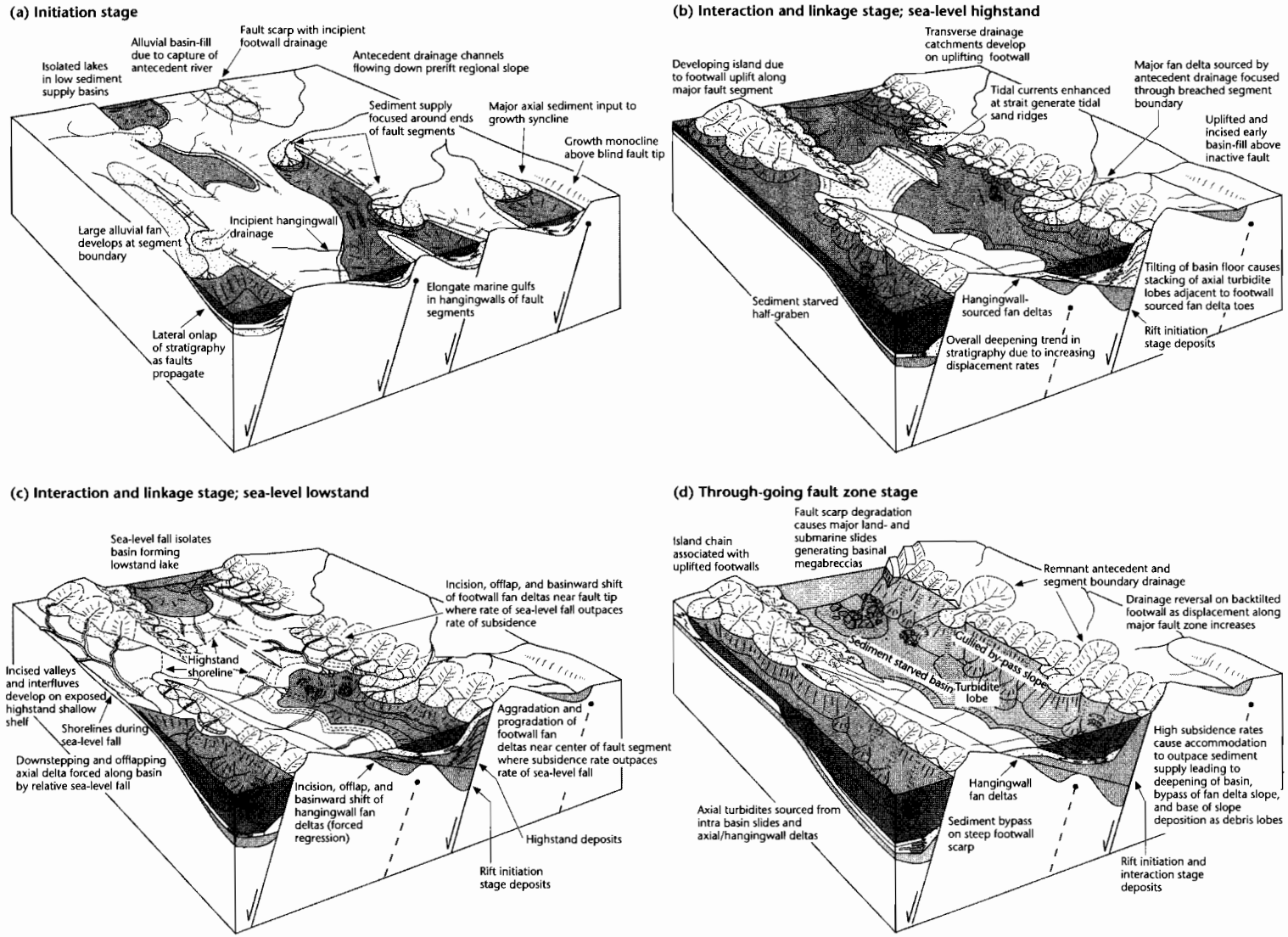

Fig. 8.25 Schematic diagrams of depositional systems related to fault growth and linkage for coastal/marine environments, after Gawthorpe and Leeder (2000). Reproduced courtesy of Blackwell Publishing Ltd.

subsidence in generating sequence boundaries and systems tracts in active rifts. For example, Underhill (1991) found from subsurface data in the Inner Moray Firth Basin, UK, that the main sequence boundaries were produced by fault activity during the synrift phase of the North Sea Basin.

Similar concepts of fault array evolution and associated folding can be applied to contractional terrains such as fold–thrust belts (Tucker and Slingerland 1996) (§7.5.4).

8.3.3 Changes of in-plane stress

Variations in regional stress fields acting within inhomogeneous lithospheric plates may cause vertical movements large enough to have a major impact on stratigraphy. The horizontal in-plane forces that might be responsible for these vertical movements include ridge push forces from spreading centers and deviatoric compression originating from sites of continental collision. Although the horizontal (in-plane) stress required to buckle an undeformed elastic plate is enormous (§4.4), in-plane stresses acting on a deflected plate may enhance or reduce the curvature of the deflection. In-plane forces may also produce long wavelength lithospheric buckles where the plate is rheologically layered, with a weak lower crust.

An early examination of the possible effects of changing horizontal stresses on a passive continental margin with an overlying sedimentary load and an age-dependent elastic thickness (Cloetingh et al. 1985) showed that the application of an in-plane force causes a modification of the deflection of the continental lithosphere. For example, changing from an in-plane tensional stress of $5 \times 10^{12}\,\mathrm{Nm}^{-1}$ (2.3 Kbar) to a compressional stress of the same magnitude on a lithosphere with an equivalent elastic thickness appropriate for an age of 30 Myr, produces a net uplift on the edge of the basin of about 100 m. The effectiveness of the in-plane force in producing large changes in the deflection increases with increasing thickness of sediment load, but decreases with the increasing age of the lithosphere. As a consequence, it was suggested that in-plane forces are particularly important on young, rapidly loaded margins. Changes in horizontal stresses also have effects towards the basin center, but because the total subsidence is large in these areas, the contribution of in-plane stresses to the deflection is masked.

Karner (1986) applied the concept of in-plane stresses to a lithospheric structure where the flexural rigidity varied not only in time (cooling effect) but also in space as a result of basin formation. He showed that the effect of a tensile in-plane stress was to reduce the curvature of the plate, and that of a compressive in-plane stress to increase the curvature. The impact of an in-plane stress change is affected by the geometry of inhomogeneities in the lithosphere, such as the basement–sedimentary basin interface and the Moho. Their effects are likely to be amplified in foreland basins; in-plane compression generates additional basinal subsidence and marginal uplift, whereas in-plane tension generates basin uplift and marginal subsidence.

According to Karner (1986) the application of a compressive ($12.5 \times 10^{12}\,\mathrm{Nm}^{-1}$ or 4 Kbar) stress on a typical extensional basin margin would cause the basin margin to uplift, producing an unconformity recognized by a sharp drop in the amount of stratigraphic onlap. In contrast, an identical tensile in-plane stress would cause a major transgression as the basin margin is depressed (Fig. 8.26). The resulting patterns of stratigraphic offlap and onlap might erroneously be attributed to eustatic sea-level change.

Later investigations of the importance of in-plane stresses have focused on the possibility of the buckling of a layered lithosphere (§4.4). Large-scale lithospheric folding is found, for example, in the oceanic lithosphere of the Indian Ocean (Stein et al. 1989) and in the continental lithosphere of central Australia (Lambeck 1983). Lithospheric buckles have been interpreted in compressional regimes such as the Himalayan syntaxes (Burg and Podladchikov 2000) and the Alpine foreland of Europe (Ziegler et al. 1995). Buckling has been interpreted as a component in the deformation of some of the major extensional basins of Europe such as the North Sea, Pannonian Basin, the south Adriatic, and the Paris Basin (Horvath and Cloetingh 1996; Lefort and Agarwal 1996; van Balen et al. 1998; Bertotti et al. 2001).

Accepting that large-wavelength lithospheric folds exist, the critical question is therefore whether in-plane stresses of significant magnitude change in sign over a sufficiently short time period to significantly influence stratigraphic packaging, and whether any such changes can be recognized in the sedimentary record of basins. Vertical motions due to changes of in-plane stress combined with the effects of dynamic topography may be highly influential in controlling the stratigraphic packaging of many of the world's cratons.

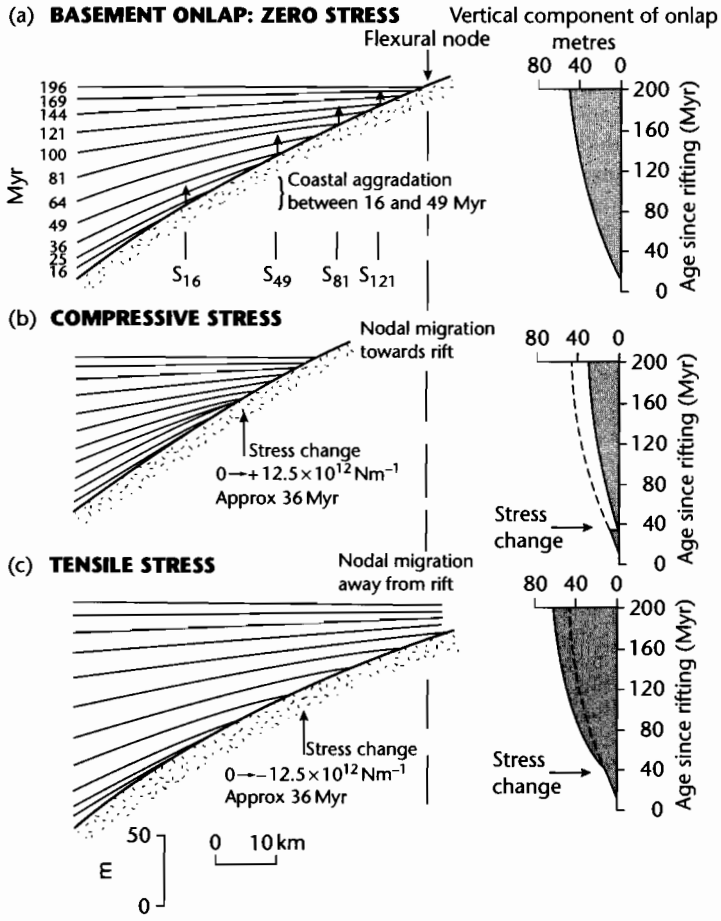

Fig. 8.26 Stratigraphic patterns in a stretched basin based on the numerical experiments of Karner (1986). Diagrams at right show the amount of coastal aggradation as a function of time, which serves as a proxy for apparent relative sea-level change. (a) Stratigraphic onlap caused by the cooling of the lithosphere following rifting; (b) Effects of applying a *compressive* in-plane force of $12.5 \times 10^{12}\,\mathrm{Nm^{-1}}$ at 36 Myr after the end of rifting, at which point the equivalent elastic thickness is 32 km. This produces basin margin uplift and a basinward shift in coastal onlap; (c) An increase in the rate of coastal onlap is produced by the application of a *tensile* in-plane force of $12.5 \times 10^{12}\,\mathrm{Nm^{-1}}$ at 36 Myr after rifting.

8.3.4 Eustatic mechanisms

In Chapters 3–5 we considered changes in basement height relative to a datum (sea level or "regional") in terms of large-scale mechanisms such as lithospheric thickness changes, flexure, and mantle dynamics. The elevation changes caused by these tectonic mechanisms may be extremely widespread, being determined by mantle convection processes, flexural response of the lithosphere or plate boundary forces, but they are not global. Global sea-level changes (absolute changes relative to the center of the Earth) result either from changes in the amount of water in the oceans or from changes in the volume of the ocean basins.

In considering absolute sea-level change, it is important to incorporate the effects of isostasy (§2.1.1). An increase in water depth in the ocean basins causes a sub-

sidence of the ocean floor due to the excess weight of the water at the new sea level. A decrease in water depth causes uplift of the ocean floor due to the removal of part of the water column. The displacement of the oceanic basement relative to the center of the Earth by changes in the water load would be found throughout the oceans, although the effect would only be observed at places such as oceanic islands. These regions would experience the same displacement as the oceanic basement, and would therefore act as a "dipstick," indicating the sea-level change.

Consider an ocean basin of depth h_1 which deepens to a depth h_2 (Fig. 8.27). The greater depth of the ocean is made up of two components: the subsidence of the ocean floor S, and the sea level rise Δ_{SL}. If rocks comprising the ocean crust have a density (ρ_m) of 3300 kg m^{-3} and the water a density (ρ_w) of 1000 kg m^{-3}, the isostatic subsidence of the ocean floor is approximately 0.4 of the sea-level change. Expressed slightly differently, the sea-level change is 0.7 of the increase in the water depth of the ocean ($h_2 - h_1$) (see also §9.3.2). These figures represent approximate upper bounds on the water loading of the oceanic lithosphere since they result from a purely local (vertical) isostasy. A flexural response of the lithosphere (§2.3.3) would reduce the water-loaded subsidence. However, the approximation is reasonable, since the wavelength of the water load (the ocean) is very large compared to lithospheric thickness.

We can examine global sea-level change in terms of five possible causes:

1 *Continuing differentiation of lithospheric material as a result of plate tectonic processes*: The volume of water in the oceans may be added to by contributions from mid-ocean ridge and island arc volcanism. Counteracting this, water may be removed by hydrothermal alteration of new crust and at subduction zones. These processes are probably roughly balanced. There is no evidence for appreciable, long-term changes in the chemical composition of the oceans during the past 1500 Myr, suggesting that the volume of sea water has not greatly increased as a result of Phanerozoic volcanism.

2 *Changes in the volumetric capacity of the ocean basins caused by sediment influx or removal*: The total sediment discharged to the oceans is *c.* 20×10^9 tons yr^{-1} (Milliman and Syvitski 1992; Walling and Webb 1996). If we ignore the volume of sediment produced autochthonously in the oceans, and the oceans have an area of 3.2×10^8 km^2, the average accumulation rate of terrestrially derived sediment is 25 mm per 1000 yr (assuming a sediment density of 2500 kg m^{-3}). This would cause a sea-level rise of 6 mm per 1000 yr (derivation in Figure 8.28). However, sediment in the ocean is removed by tectonic accretion and subduction at active margins and continued spreading creates new ocean floor. It is uncertain how much sediment is removed at subduction zones and eventually melted to contribute to arc volcanism, and how much is tectonically accreted to the edge of the overriding plate. It is likely that the balance between influx and removal of sediment, when averaged over long

$$\rho_w h_1 + \rho_m C_1 = h_2 \rho_w + \rho_m (C_1 - S)$$
$$\rho_m S = \rho_w (h_2 - h_1)$$
$$\rho_m S = \rho_w (S + \Delta_{SL})$$
$$S \left(\frac{\rho_m - \rho_w}{\rho_w}\right) = \Delta_{SL}$$

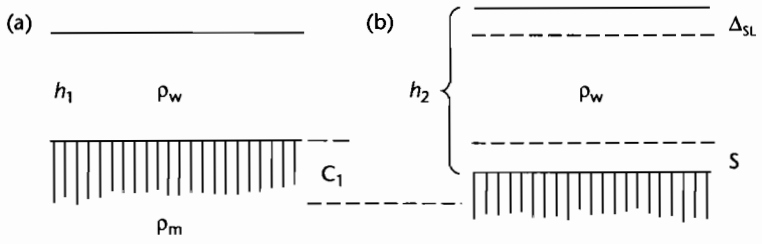

Fig. 8.27 Isostatic effect of a change in water depth in the ocean. Since the wavelength of the water load is very large, the compensation can be regarded as local (Airy). (a) Initial ocean of depth h_1; (b) An increase in water depth h_2 results in an increase in sea level of Δ_{SL}.

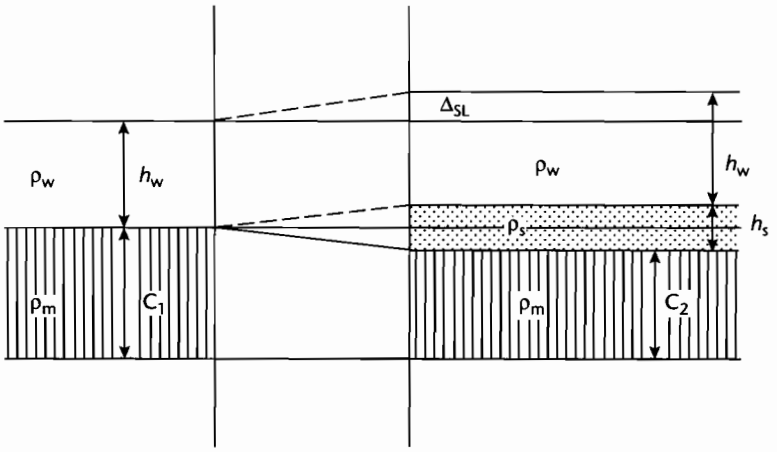

$$\rho_m C_1 + h_w \rho_w = \rho_m C_2 + \rho_s h_s + h_w \rho_w$$
$$\rho_m(C_1 - C_2) = \rho_s h_s$$
Since $C_1 - C_2 = h_s - \Delta_{SL}$,
$$\rho_m(h_s - \Delta_{SL}) = \rho_s h_s$$
$$\therefore \Delta_{SL} = h_s(1 - \rho_s/\rho_m)$$

Fig. 8.28 Derivation of the sea-level change resulting from the deposition of sediment in the ocean. If the density of mantle is 3300 kg m^{-3} and the density of ocean sediment is 2500 kg m^{-3}, the sea-level change is 0.24 of the sediment thickness h_s. Consequently, if 25 mm of sediment is deposited every 1000 yr, the sea-level change is 6 mm per 1000 yr.

periods of time, is insufficient to cause rates of sea-level change of more than *c.* 1 mm per 1000 yr (Pitman 1979).

3 *Changes in the volumetric capacity of the ocean basins caused by volume changes in the mid-ocean ridge system*: That changes in the volume of the mid-ocean ridge systems could be responsible for major sea-level changes has been argued for some time (Hallam 1963; Menard 1964; Russell 1968; Valentine and Moores 1970; Hays and Pitman 1973). This is based on the observation that the volume of the present world ridge system (*c.* 1.6×10^8 km^3) is a significant proportion, over 10%, of the volume of ocean water (*c.* 1.35×10^9 km^3). Because the bathymetry of the ocean is dependent on age, variations in spreading rates cause major changes in ridge volumes, the faster spreading ridges being hotter and therefore more voluminous. A second way of modifying the world ridge volume is through changes in the total length of spreading axes. Hallam (1977) believed that at certain geological times, the latter mechanism was the more important of the two. Bearing in mind that a change in ocean depth of magnitude Δh produces a change in sea level relative to the center of the Earth of magnitude $\Delta_{SL} = 0.7\Delta h$, the sea-level fluctuations resulting from mid-ocean ridge volume changes can be estimated if the shape of the ocean basins is known (Pitman 1979). The latter can be gauged from the *hypsometric curve*. Sea-level changes track changes in mid-ocean ridge volumes, with maximum rates of change of 4 mm per 1000 yr for the spreading history illustrated in Figure 8.29. The "first-order" or "long term" (225–300 Myr) eustatic curves of Vail et al. (1977a) and Haq et al. (1987) may be driven by variations in mid-ocean ridge volumes (Larson and Pitman 1972). The postulated sea-level changes as a result of ocean ridge volume fluctuations (Fig. 8.30) show a maximum sea level in the latest Cretaceous (Maastrichtian) when it was elevated some 350 m above present, and a fall of varying severity through the Cenozoic to the present. The Late Cretaceous maximum of 350 m above present sea level is, however, in disagreement with estimates from continental margin stratigraphy (Watts and Steckler 1979), from estimates of the flooding of continents using individual hypsometric curves (Bond 1978) and from estimates of the amount of crustal generation through time

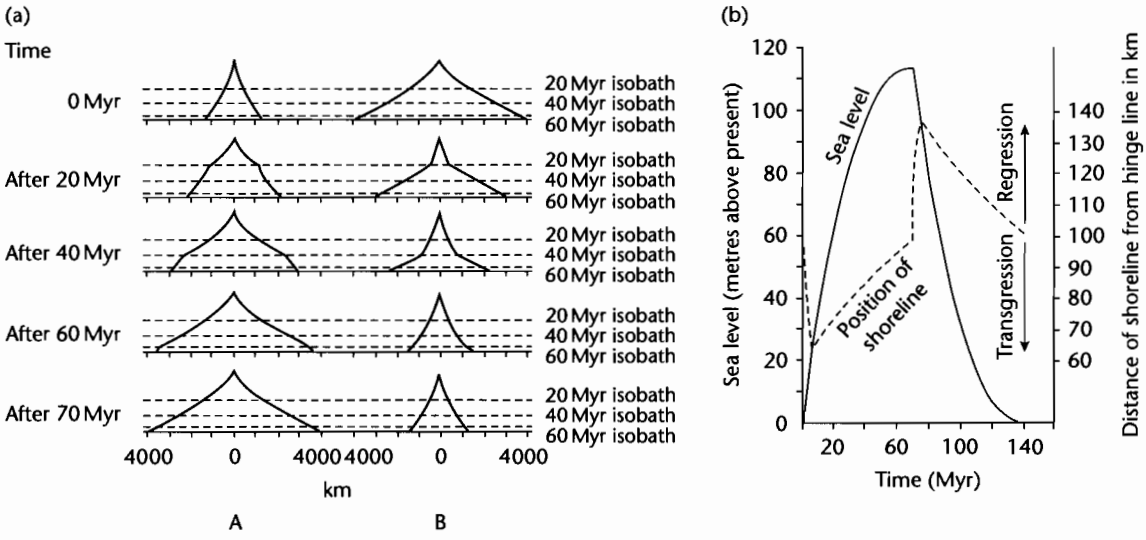

Fig. 8.29 Volume changes of spreading ridges as a function of the spreading rate (after Pitman 1979). (a) Sequence A shows a ridge that has been spreading at 20 mm yr^{-1} for 70 Myr. At 0 Myr the spreading rate changes to 60 mm yr^{-1}. Subsequent diagrams show the sequential changes in the ridge cross-section. Sequence B shows the reverse evolution: a ridge that has been spreading at 60 mm yr^{-1} for 70 Myr slows at 0 Myr to 20 mm yr^{-1}. The cross-sectional areas of equilibrium ridge profiles (after 70 Myr of spreading at the new rate) change by a factor of 3 in both cases; (b) Change in sea level resulting from the changes in spreading rates shown in sequence A of (a). The maximum rate of sea-level change occurs immediately after the change in the spreading rate.

(Parsons 1982), which all suggest a Late Cretaceous maximum of smaller magnitude (<100 to 150 m above present) (Fig. 8.30).

4 *Thermal expansion and contraction of the oceanic water reservoir*: Changes in the average temperature of the oceanic reservoir, caused by climate change, should cause changes in its volume by thermal expansion and contraction. The importance of this effect can be easily estimated by considering the volumetric coefficient of thermal expansion of water (α_v), which varies between $7.81 \times 10^{-5}\,K^{-1}$ at 2.5 °C and $34.13 \times 10^{-5}\,K^{-1}$ at 30 °C. The oceanic water reservoir is $1{,}400{,}000 \times 10^{15}$ kg, or $1{,}400{,}000 \times 10^{12}\,m^3$, its average depth is 3794 m and the area of the oceans excluding the continental shelves is $3.1 \times 10^{14}\,m^2$. The mean temperature of the ocean reservoir at the present day is about 4 °C. Taking $\alpha_v = 10 \times 10^{-5}\,K^{-1}$, a 1 K increase in temperature of the present-day oceanic reservoir therefore causes an increase in volume of water of $14 \times 10^{13}\,m^3$, which causes an increase in depth of 0.45 m. Climate change of course does not cause a uniform change in temperature of the oceanic reservoir because of the intricasies of the operation of the thermohaline system. However, the calculation above shows that the effects of thermal expansion and contraction during a climatic cycle while significant, are relatively small compared to the water depth changes caused by growth and melting of ice caps (see below).

5 *Changes of available water by abstraction in and melting of polar ice caps and glaciers*: Large sea-level changes can be caused by abstraction of water from the oceans into land-based ice-sheets, and of course, the subsequent release on melting. Ice shelves are unimportant since the floating ice displaces its own mass of water. These changes can be called *glacio-eustatic* (Fairbridge 1961; Donovan and Jones 1979). Total melting of the Antarctic land ice, some 2 to $3 \times 10^7\,km^3$, would result in an increase in water depth of between 60 and 75 m. Melting of the much smaller Greenland ice cap would probably cause an additional 5 m increase in water depth. Allowing for the water-loaded depression of the ocean floor discussed above (Fig. 8.27), the actual sea-level rise associated with the complete melting of today's land-based ice sheets is expected to be in the region of 50 m. Calculations of former ice sheet volumes are speculative. Assuming that

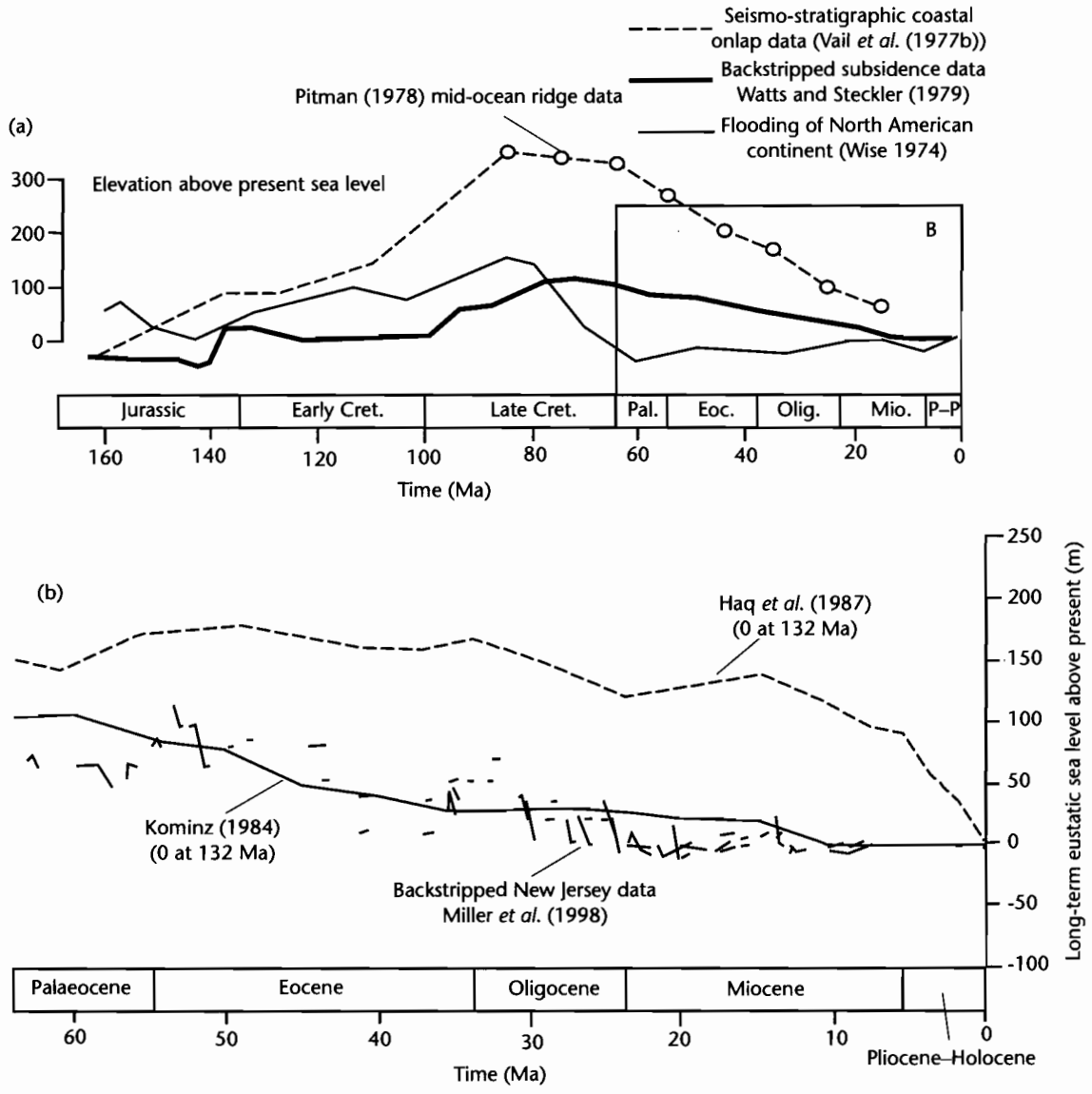

Fig. 8.30 (a) A comparison of estimates of sea-level changes in the last 160 Myr. The heavy solid line is based on the subsidence history of boreholes from the continental margins of eastern North America (Watts and Steckler 1979). The dashed line is the estimate of Vail et al. (1977b) based on patterns of coastal onlap recognized on seismic reflection lines, calibrated by the data of Pitman (1978) (circles) based on changes in the rates of spreading of mid-ocean ridges. The fine solid line is from estimates of the amount of flooding of the continental area of North America (Wise 1974); (b) The Cenozoic section of the sea-level history, showing the data obtained from backstripping of wells drilled in the New Jersey coastal plain (Miller et al. 1998), which are fitted well by the eustatic curve of Kominz (1984). The Haq et al. (1987) curve appears to significantly over-predict long-term eustatic sea level. Both curves are normalized to pass through a eustatic sea level of 0 m at 132 Ma.

former ice sheets reached an equilibrium maximum thickness, and delineating their maximum limits from Quaternary geology, the sea-level fall resulting from locking up of water in Pleistocene ice sheets is thought to have been about 100 m. The total change in sea level corresponding to the removal of Pleistocene-scale ice sheets is therefore about 150 m and liable to have major impacts on basin stratigraphy. In geological terms, the formation and melting of ice caps is a rapid process (*c.* 10 mm yr^{-1}) (Hays et al. 1976; Imbrie 1982) – about three orders of magnitude greater than those expected to result from changes in ocean ridge system volumes.

The lithosphere also responds to changes in water and ice loads; these *glacio-isostatic* adjustments (Clark et al. 1978; Peltier 1980) operate at a rate dependent on mantle viscosity. At any high latitude locality close to the former ice front, there is therefore a competition in the history of deglaciation between isostatic rebound rates and rates of eustatic sea-level rise (Belknap et al. 1987 for an example from the Late Quaternary of Maine).

Late Quaternary and Holocene sea-level fluctuations following the Pleistocene glaciation are relatively well understood compared to more ancient sea-level changes (Fig. 8.31). Sea-level curves derived from oxygen isotopes from benthonic foraminifera recovered in deep sea cores (Shackleton and Opdyke 1973; Shackleton 1977) and tropical coral terraces and related fauna (Fairbanks and Matthews 1978; Aharon 1983) show a high frequency fluctuation, with 8 sea-level maxima (and 8 minima) in the last 120,000 years. These sea-level changes vary from 20 m to 180 m in total height. They have a long primary period of about 10^5 yr, and shorter secondary periods of about 40,000 and 20,000 years.

The Serbian physicist Milankovitch first suggested that periodic variations in solar forcing might be caused primarily by orbital fluctuations of the Earth. For example, changes in the shape of the elliptical path of the Earth's orbit around the Sun (or *eccentricity*) have a periodicity of approximately 100 kyr, and may be responsible for the glacial cycles characteristic of the Pleistocene. The Earth also wobbles in its spin about its axis of rotation (*precession*), with the axis of rotation varying in its inclination with a periodicity of *c.* 21 kyr. The axis of rotation also leans with respect to the plane of the Earth's orbit around the Sun (*obliquity* of the ecliptic), the angle of lean varying on a period of *c.* 41 kyr. These three different frequencies interact to produce a complex signal that may act as a pacemaker for climate change, causing eustatic variations responsible for stratigraphic parasequences. Unfortunately, the precision of dating ancient sequences is generally too poor to allow comparison of parasequence durations with Milankovitch frequencies.

It has been shown that the Mediterranean Basin dried out during the late Miocene (Hsu et al. 1973) as it became isolated from the world's oceans. The Messinian desiccation event appears at first sight to correlate with a sea-level fall at 6.6 Ma on the global cycle chart of Haq et al. (1987). However, detailed work on ODP and DSDP cores and onshore studies in Sicily suggest that the desiccation event postdates the Tortonian–Messinian boundary (now placed at 6.5 Ma) by 0.5 Myr, so that the correlation is inexact. Perhaps more importantly, desiccating the Mediterranean by land-locking is likely to have caused a sea-level *rise* (perhaps 12 m) in the remaining oceans by reducing the volume of the ocean basins. This scale of sea-level change is considerably smaller than the variations caused by glaciations, although the rates of change of sea level would be rapid and similar to those estimated for glaciations (*c.* 10 mm yr^{-1}) (Donovan and Jones 1979).

8.3.5 Other climatic mechanisms for stratigraphic cyclicity

The influence of climate on depositional systems and depositional products is the staple diet of a number of texts in sedimentary geology and will not be repeated here. The influence of climate on weathering and erosion is also a central theme of a number of geomorphology texts (e.g., Summerfield 1991). From the point of view of basin analysis and stratigraphic cyclicity, however, the overriding importance of climate is in its influence on the sediment discharge to sedimentary basins. Climate affects vegetation and soils, precipitation and the distribution of precipitation (storminess, large floods), weathering, hillslope processes and mass wasting, the balance of solute and particulate loads, and the sediment yield from catchments. Because of its pervasive influence on such a wide set of processes, the detailed linkage between climate change, depositional processes, and stratigraphic products is poorly understood.

A very wide range of features are influenced by variations in sediment supply to the sediment routing system. Depositional water depths, cycle development, parasequence stacking patterns, formation of unconformities and ravinement surfaces, position of the maximum flood-

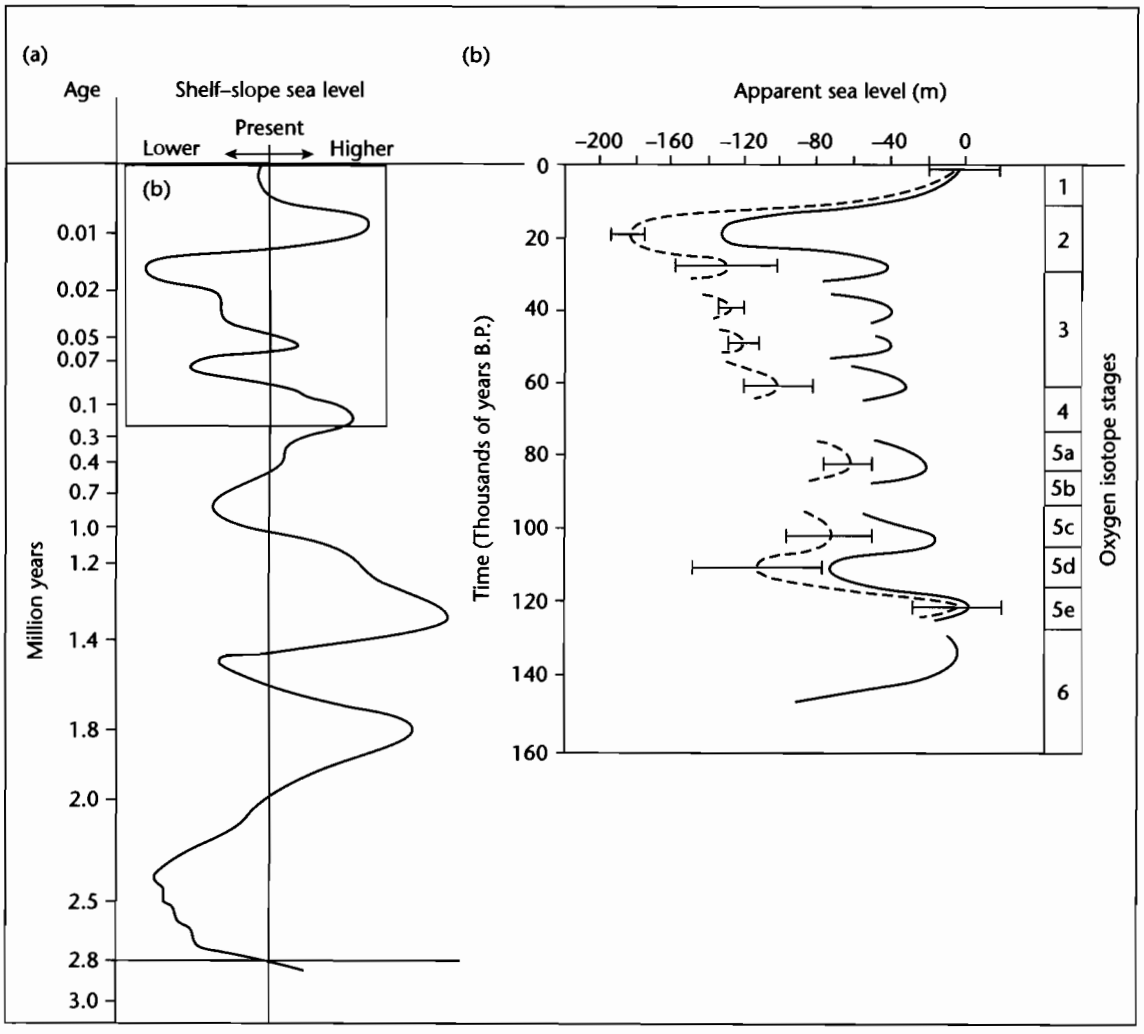

Fig. 8.31 (a) Inferred Pleistocene sea-level fluctuations in the northwestern Gulf of Mexico since 3 Ma (after Morton and Price 1987), derived by Smith (1965) from interpreted water depth and paleotemperatures, and modified by Beard et al. (1982). Note non-linear scale for age; (b) Detailed glacio-eustatic record (dashed line, Moore 1982) and oxygen isotope record based on deep sea benthic foraminifera (solid line, Williams 1984) for the last 130 000 yr (after Suter et al. 1987).

ing surface, are all strongly affected by sediment supply. The reader is referred to §7.3 for information on the effect of climate change on sediment yield, to §7.5.3 for the effects of variations in sediment flux in building stratigraphy in alluvial basins, and to §8.1.3 for a quantitative analysis of the role of sediment supply in stratigraphic packaging.

8.3.6 Unforced cyclicity

A large number of authors favor the formation of parasequences by allocyclic mechanisms such as eustatic sea-level change, commonly assumed to be driven by Milankovitch orbital forcing (e.g., Goldhammer et al.

1990; Osleger 1990). A convincing demonstration of orbital forcing should include a spectral analysis of the cyclicity. However, such statistical analyses sometimes show that apparently ordered patterns of cycles are indistinguishable from patterns produced by random depositional processes (Drummond and Wilkinson 1993; Wilkinson et al. 1996, 1997). It is possible therefore that many high frequency cycles may be produced by an unforced autocyclicity.

An early theory for the generation of shallowing up cycles in peritidal carbonates envisaged a subtidal carbonate factory, with landward transport to produce progradational supratidal and intertidal facies belts (Ginsburg 1971). Progradation was thought to reduce the area of subtidal carbonate production. Continued tectonic subsidence would therefore eventually outpace sediment production, leading to flooding. Two-dimensional (Demicco and Spencer 1989; Hardie et al. 1991; Goldhammer et al. 1993) and 3-D (Burgess et al. 2001) numerical models successfully simulate stacked autocyclic parasequences in peritidal carbonates. The internal dynamics of the numerical model developed by Burgess et al. (2001) involves an advective landward transport of sediment from subtidal areas driven by prevailing winds leading to accretion of carbonate on the seaward flanks of the islands, causing them to prograde (Fig. 8.32). A less important seaward sediment transport takes place by a gradient-dependent diffusive transport. Laterally impersistent, peritidal cycles (<2.5 m thick) are produced by the landward nucleation, detachment, and seaward migration of intertidal–supratidal islands, leaving new subtidal zones in their rear. Such cycles resemble the thin, laterally impersistent, shallowing-up peritidal cycles commonly reported from field studies (Hardie and Shinn 1986; Pratt and James 1986; Shinn 1986; Adams and Grotzinger 1996).

It is likely that external forcing and internal dynamics both take place to varying degree, and that the separation of any external signal from a system with its own internal dynamics may be difficult to achieve.

8.4 NUMERICAL SIMULATION OF STRATIGRAPHY

Numerical approaches to the simulation of stratigraphy blossomed in the last decade of the twentieth century. However, the groundwork for many numerical stratigraphic models was provided by Sloss (1962) who identified the four main variables affecting stratigraphic geometries: the quantity of sediment supply from the basin margins, the rate of subsidence in the basin relative to base level, the dispersal of sediment by various transport processes, and the composition and texture of the sediment. It is regrettable that much early sequence stratigraphic literature ignored this groundwork, and instead focused on eustatic change as the exclusive control on stratigraphic geometries. A number of approaches to quantitative modeling of the basin-fill have simultaneously developed (review in Paola 2000). This section can give a mere snapshot of the wide diversity and complexity of the modeling approaches to stratigraphy. We do so by reviewing some of the fundamental and commonly used principles upon which more sophisticated approaches are based.

8.4.1 Carbonate stratigraphy

The building of carbonate stratigraphy is fundamentally based on a notion of carbonate productivity as a function of water depth. This water-depth dependence is caused by the attenuation of light with depth, but the effects of turbidity and temperature may also be important (Lerche et al. 1987). Pomar (2001) suggested that the depth–productivity curve is also strongly affected by the type of biota. Euphotic biota produce a strong depth-dependence, with a maximum productivity in very shallow waters; oligotrophic biota produce a mid-water depth maximum, and photo-independent biota produce a weak depth-dependence (Fig. 8.33). Armed with a carbonate productivity–depth curve (e.g., Bice 1991; Bosscher and Schlager 1992; Demicco 1998), the modeler can readily simulate carbonate sedimentation in 1-D. Two-dimensional models must account for physical transport of carbonate sediment. A strong depth dependence of carbonate productivity should produce steep-edged carbonate platforms, whereas a less strong dependence on depth, or vigorous offshore transport, should flatten the carbonate platform slope into that of a ramp (Fig. 8.34). Euphotic organisms such as corals and green algae should produce steep-edged platforms, whereas oligophotic organisms such as the larger foraminifera and red algae should produce ramps. Carbonate depositional systems commonly possess clinoforms whose shape depends on the effects of lateral sediment transport, carbonate productivity, eustatic variation and accommodation generation by tectonic subsidence (Lawrence et al. 1990). Continued subsidence of clinoform geometries produced by a strongly depth-

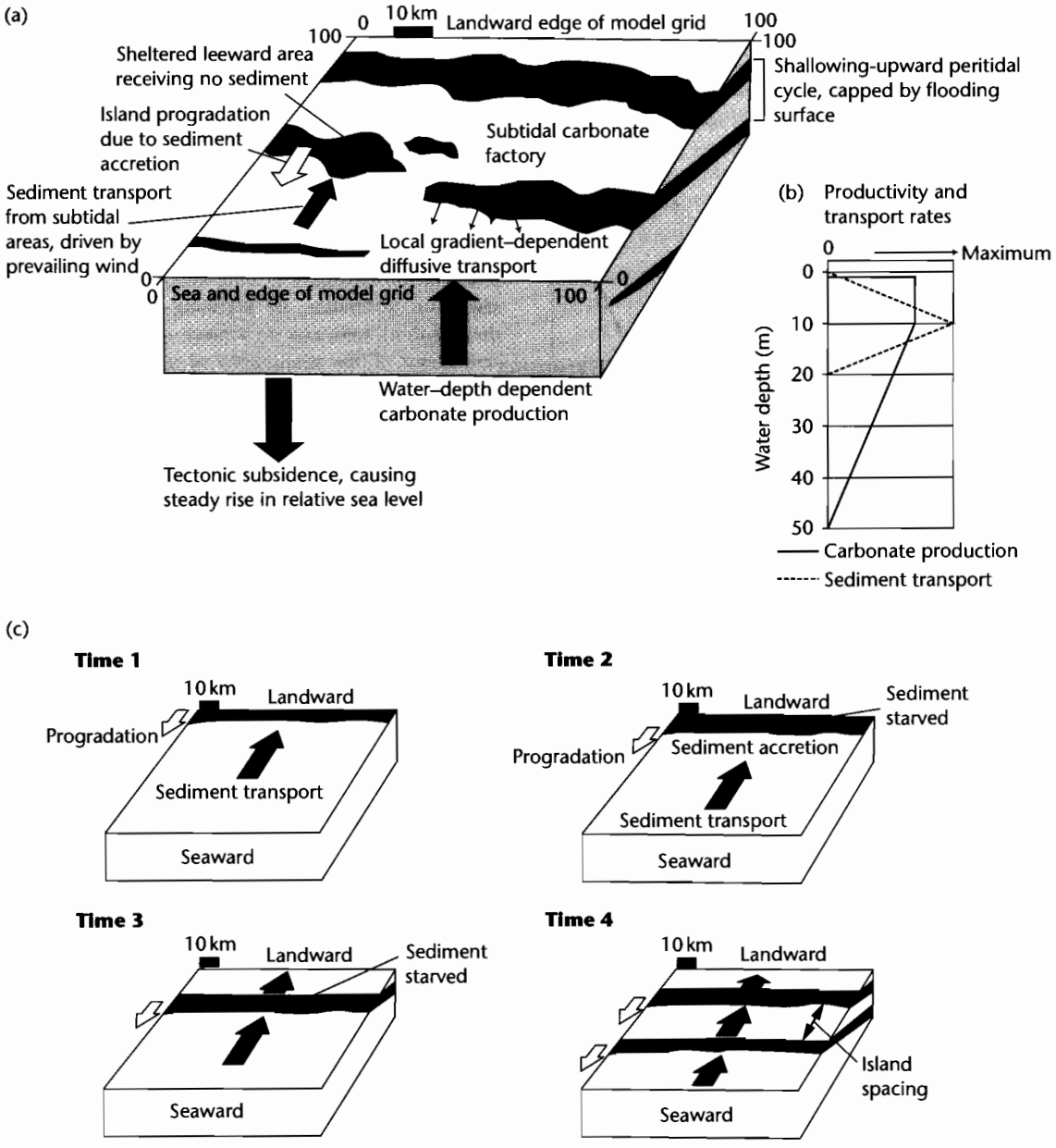

Fig. 8.32 Model for the generation of unforced high resolution cyclicity in peritidal carbonates, after Burgess et al. (2001). (a) Illustration of different processes involved in generating prograding inter- and supratidal islands and autocyclic shallowing-upward cycles; (b) Depth-dependent carbonate productivity relationship and sediment transport rate; (c) Different stages in the evolution of prograding islands. Time 1: landward transport of sediment causes accretion of inter- and supratidal flat. Time 2: Continued accretion drives inter- and supratidal flat progradation, which causes a sediment starved leeward side to develop. Time 3: Sediment starved lee subsides and prograding island forms, allowing a new subtidal carbonate factory to develop. Time 4: A second island system develops as the entire process is repeated. Reproduced courtesy of Blackwell Publishing Ltd.

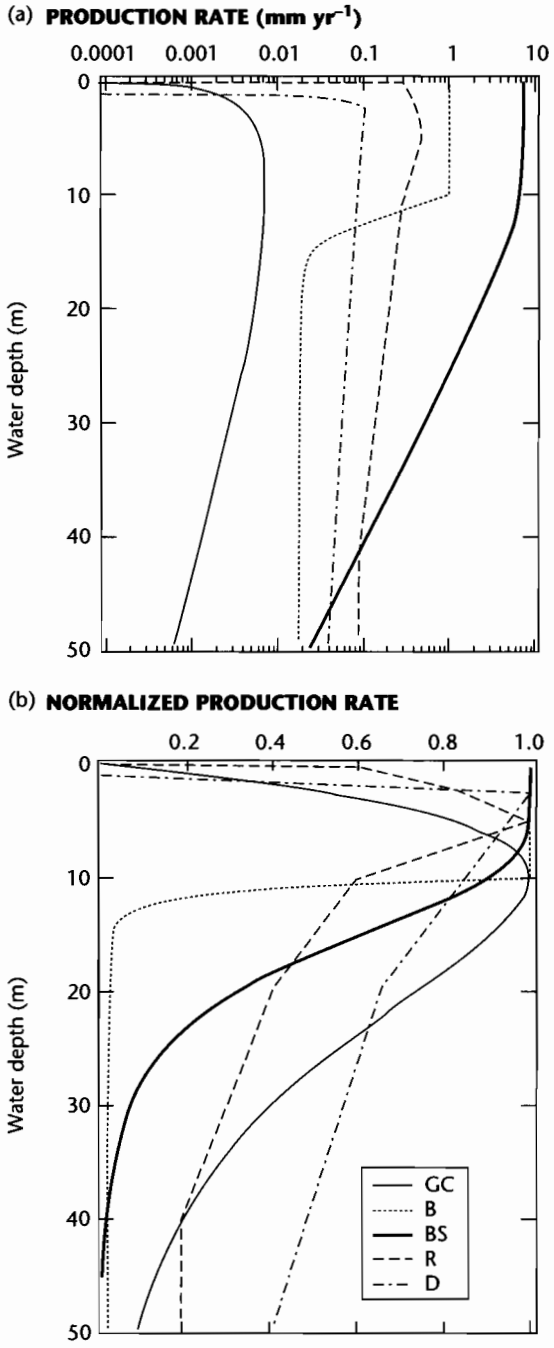

Fig. 8.33 Carbonate productivity versus depth from various authors (a), normalized by the maximum production rate in (b), after Paola (2000). GC, Gildner and Cisne (1990); B, Bice (1991); BS, Bosscher and Schlager (1992); R, Read et al. (1991); D, Demicco (1998). Reproduced courtesy of Blackwell Publishing Ltd.

dependent productivity curve may cause drowning of the platform/ramp (Schlager 1981). This may occur spontaneously, without external forcing, or during a eustatic rise superimposed on the background tectonic subsidence (Dorobek 1995; Galewsky 1998; Allen et al. 2001).

Two-dimensional geometrical models rely on sediment filling available accommodation on a template subject to tectonic subsidence. The geometrical model of Aigner et al. (1989, 1990), Lawrence et al. (1990) and Shuster and Aigner (1994) is a good example of an industry-based (Shell) model capable of dealing with both carbonate and siliciclastic sediments. By adjusting parameter values, these authors were able to achieve remarkably realistic simulations of the stratigraphy of the Paris Basin, for example. Mixed carbonate–siliciclastic sedimentation was also modeled in the model known as SEDPAK (Kendall et al. 1991a, b) and tested against the clinoform-dominated stratigraphy of the Great Bahama Bank.

More dynamic treatments of carbonate systems, such as the 3-D model of Burgess et al. (2001), combine physical processes of sediment transport (diffusion, advection) with a carbonate productivity–depth relationship to produce a dynamic mosaic of carbonate depositional environments. As we saw in §8.3.6, this model is capable of simulating the common small-scale cycles typical of peritidal sequences. Dynamic models involving the transport of carbonate sediments inevitably share much in common with models designed for siliciclastic systems.

8.4.2 Siliciclastic stratigraphy

Since the accumulation of siliciclastic sediment is not a straightforward function of depth, early simulations of siliciclastic stratigraphy were 2-D geometrical models in which the sediment filled available space up to an equilibrium profile. This was the graded stream profile on land, the shoreface profile, and the graded continental shelf (e.g., Jervey 1988; Ross et al. 1995; Burgess and Allen 1996). Commonly these models are a combination of a dynamic treatment of thermal subsidence and flexural response to sediment loads, but a geometrical treatment of the physical processes of sediment transport (Fig. 8.35) (Burgess and Allen 1996; Steckler 1999). Within this spectrum, some models (Ross et al. 1995) consider the grain size distribution of the sediment by partitioning sand and mud deposition within different depositional environments. Others (Kendall et al. 1991a, b) include the effects of sediment compaction, or incorporate a viscous relaxation time in calculations of isostatic support (Steckler 1999). However, the physical laws of erosion,

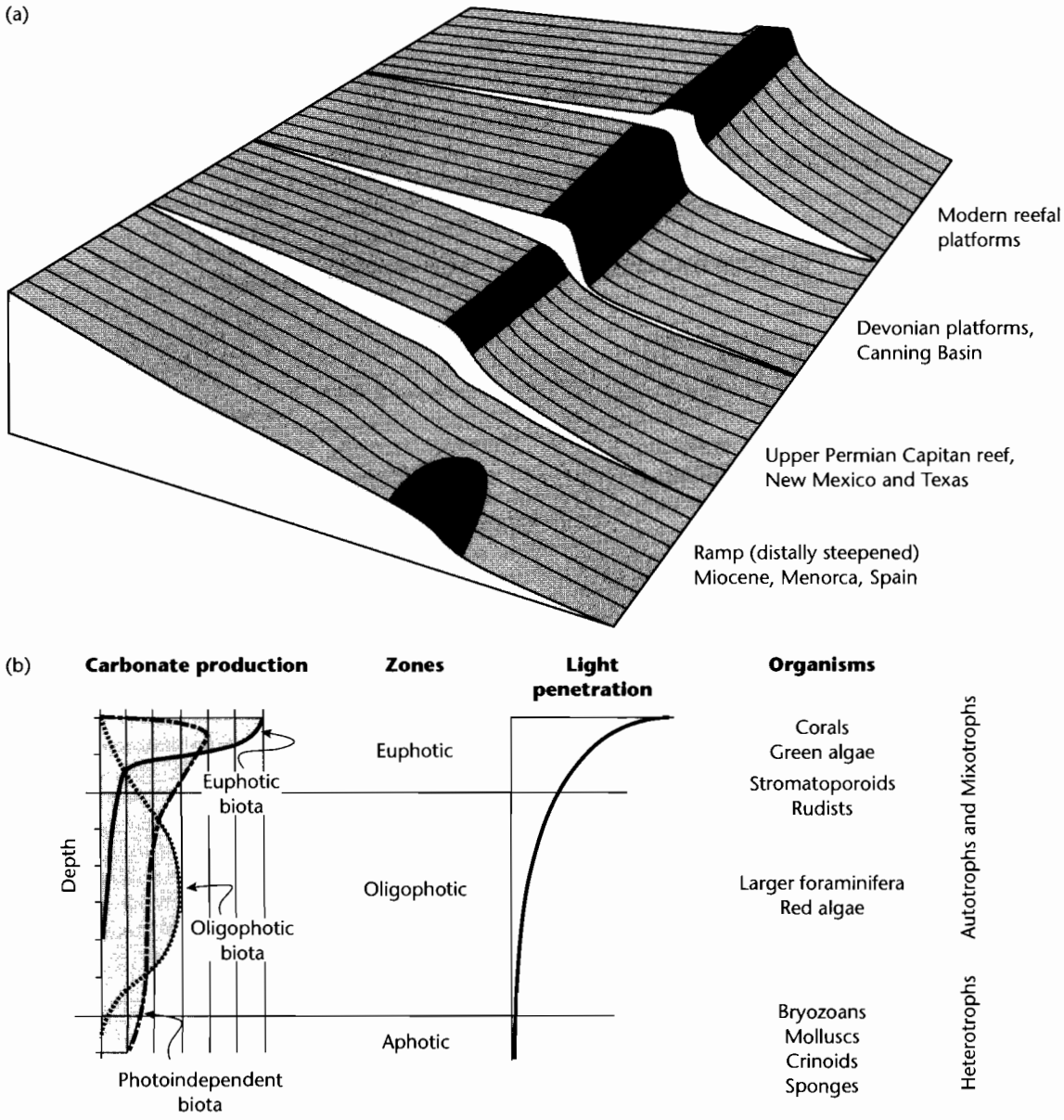

Fig. 8.34 Carbonate depositional geometries, modified after Pomar (2001). (a) Range of morphologies from ramps to rimmed platforms; (b) Carbonate productivity in relation to the type of biota. Variations in the dominant biota control the water depth range of maximum productivity. Ramps may be distally steepened where oligophotic organisms dominate. Reproduced courtesy of Blackwell Publishing Ltd.

sediment transport, and deposition are not explicitly treated in these geometric models.

We have investigated in other sections (§7.5) some of the governing laws for hillslope transport and long range fluvial transport. Other transport laws govern particle motion on the shoreface and shelf. The first dynamical models were applied to fluvial systems, which were treated as diffusive. When combined with tectonic subsi-

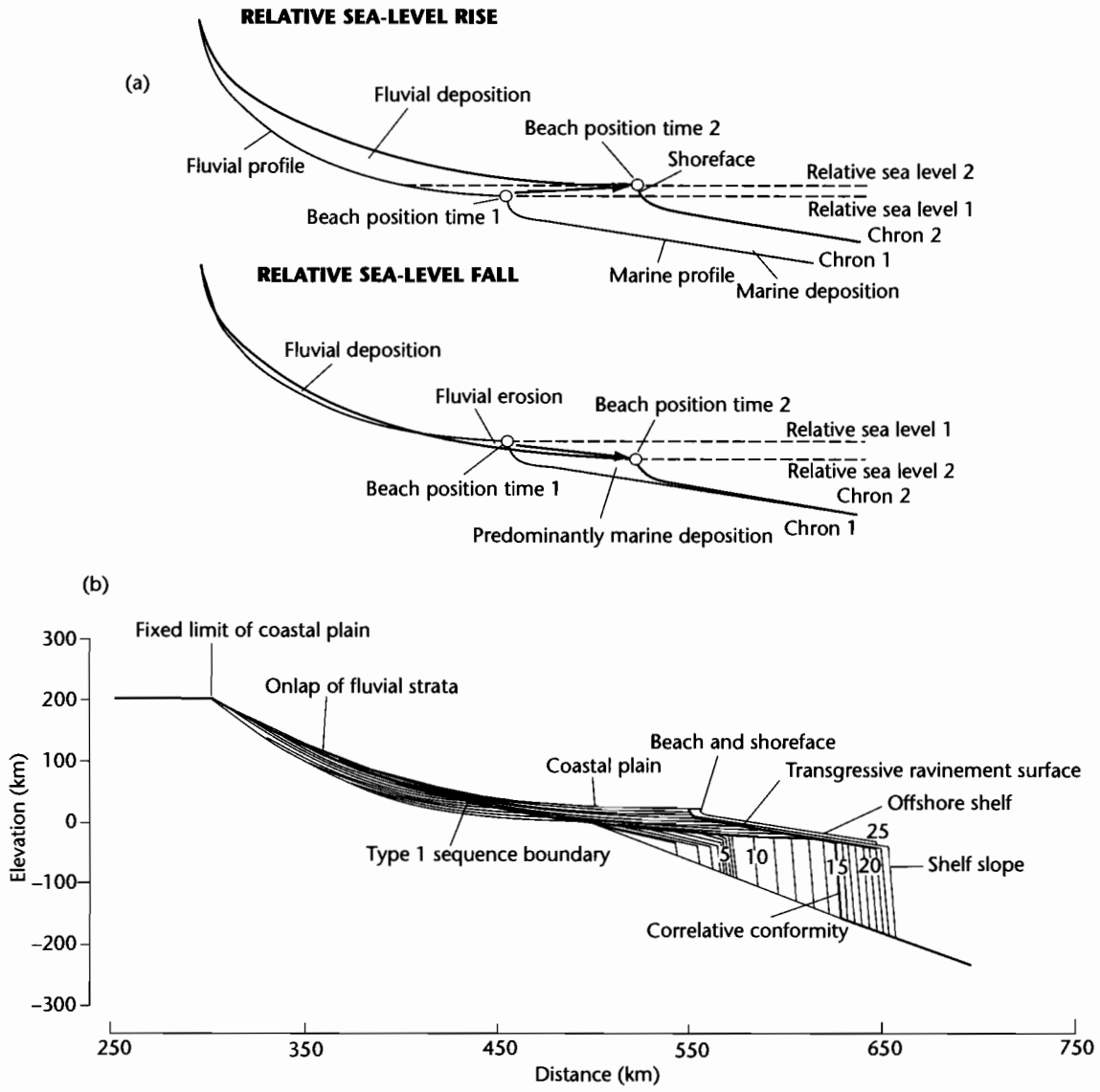

Fig. 8.35 Example of a geometrical 2-D model for stratigraphy at a passive margin (after Burgess and Allen 1996), showing how depositional sequences and bounding unconformities can be simulated. (a) Movement of the fluvial and marine profile during relative sea-level rise and fall; (b) Computer-generated stratigraphy with a Type 1 sequence boundary and its distal marine conformity and a transgressive ravinement surface generated during relative sea-level rise. Details in Burgess and Allen (1994). Small numbers are chrons. Reproduced courtesy of Geological Society of London.

dence, stratigraphy can be simulated as a function of the diffusive sediment transport coefficient as well as tectonic parameters controlling accommodation and source-area erosion (Flemings and Jordan 1989; Sinclair et al. 1991; Paola et al. 1992). Paola (2000) reviewed and justified the use of diffusive models in fluvial systems. Assuming that they can legitimately be treated diffusively, a key problem is the formulation of the diffusive transport coefficient.

Paola (2000) suggested that it depends on a number of hydrological and sediment transport parameters (§7.5.3). Interestingly, the dimensionless shear stress appears to be roughly constant (*c.* 0.05) for gravel bed rivers and a different constant (1 to 2) for sand bed rivers, implying different transport coefficients in these two regimes. Within these two regimes of gravel and sand bed rivers, the downstream variation in grain size is controlled by the size distribution of the sediment supply instead of the hydraulics.

While retaining the essential diffusive character of sediment transport, a number of approaches have been developed to deal with the problem of the transport coefficient (see also §7.5). The two-diffusion model of Marr et al. (2000) used separate transport coefficients for gravel and sand that were different by a factor of 10, whereas Rivenaes (1992, 1997) assigned transport coefficient values across a continuum according to the percentages of sand and mud, and Granjeon and Joseph (1999) invoked multiple grain size classes. These latter approaches may be more valid for the continental shelf than for fluvial systems. Kaufman et al. (1991) used a depth-dependent diffusivity for the continental shelf, which accounted for the decrease of wave energy with depth. A more dynamic approach considers the details of individual sediment transport events summed over time (Niedoroda et al. 1995). Although individual transport events may be advective, the aggregate effect may be broadly diffusive. As in fluvial systems, evaluating the net diffusive sediment transport coefficients as a function of meteorologic and oceanographic conditions is problematical. Numerical code needs to be adapted in moving from a storm-dominated continental shelf (Niedoroda et al. 1995) to a tidally dominated continental shelf (Ericksen and Slingerland 1990).

Dynamic forward models are successful in simulating many of the high resolution features seen in stratigraphy at outcrop and in borehole records, including the sand : shale ratio in the deposited layers. The evolution of the sand : shale ratio and stratigraphic geometry through a cycle of progradation and retrogradation for a fluvial-dominated delta is shown as an example in Figure 8.36 (Cross et al. 1993; Granjeon and Joseph 1999). During progradation, sand is concentrated in a high energy, narrow upper shoreface, whereas during retrogradation driven by a relative sea-level rise, sand is distributed more widely due to erosional ravinement of the underlying deltaic deposits. The same model can be used to produce a 3-D simulation at the basin-scale.

Fully coupled models do not assume that sediment supply is determined by some empirical formula related to elevation, slope or relief, nor that it is always available in sufficient quantity to fill accommodation, but instead incorporate surface process laws into a sediment routing model on a tectonically active template (e.g., Johnson and Beaumont 1995). These models provide powerful insights into the linkage between catchment development, sediment routing and depositional geometries in a fully coupled system containing geodynamic representations of tectonic uplift and basin subsidence. Models developed by different research groups may in due course be integrated into a "community" model.

8.5 DEPOSITIONAL SYSTEMS

8.5.1 Depositional systems and facies models

Depositional systems are sets of depositional environments linked by the process of sediment routing. They are responsible for large stratigraphic thicknesses, and environmental changes in one part of the system can generally be recognized in the stratigraphy of another part of the system, however distant. Depositional systems and their sedimentary products reflect the integration of autogenic (internal) and allogenic (external) controls. Sedimentary basins with different driving mechanisms (Chapters 3–6) have distinctive assemblages of depositional systems and facies. We give an overview of this linkage of tectonic environment and sedimentary character in §8.6. In this section, the main depositional systems are briefly summarized.

A hierarchy of depositional products based on scale exists from facies/beds to assemblages of facies in parasequences, to the tracts of depositional systems and finally depositional sequences. As the scale of the product increases, the cause of its deposition also changes from short-term, local and often autogenic causes at one extreme, to long-term, large scale causes involving lithospheric and climatic allogenic processes at the other extreme. In practice it may be very difficult to discriminate allogenic from autogenic causes.

The processes acting in particular depositional environments give rise to a suite of relatively small-scale characteristics of the resultant sedimentary deposits. The sum total of these small scale attributes that make a particular rock unit distinctive are embodied in the term *facies*. The term was introduced by Steno in 1669, but its

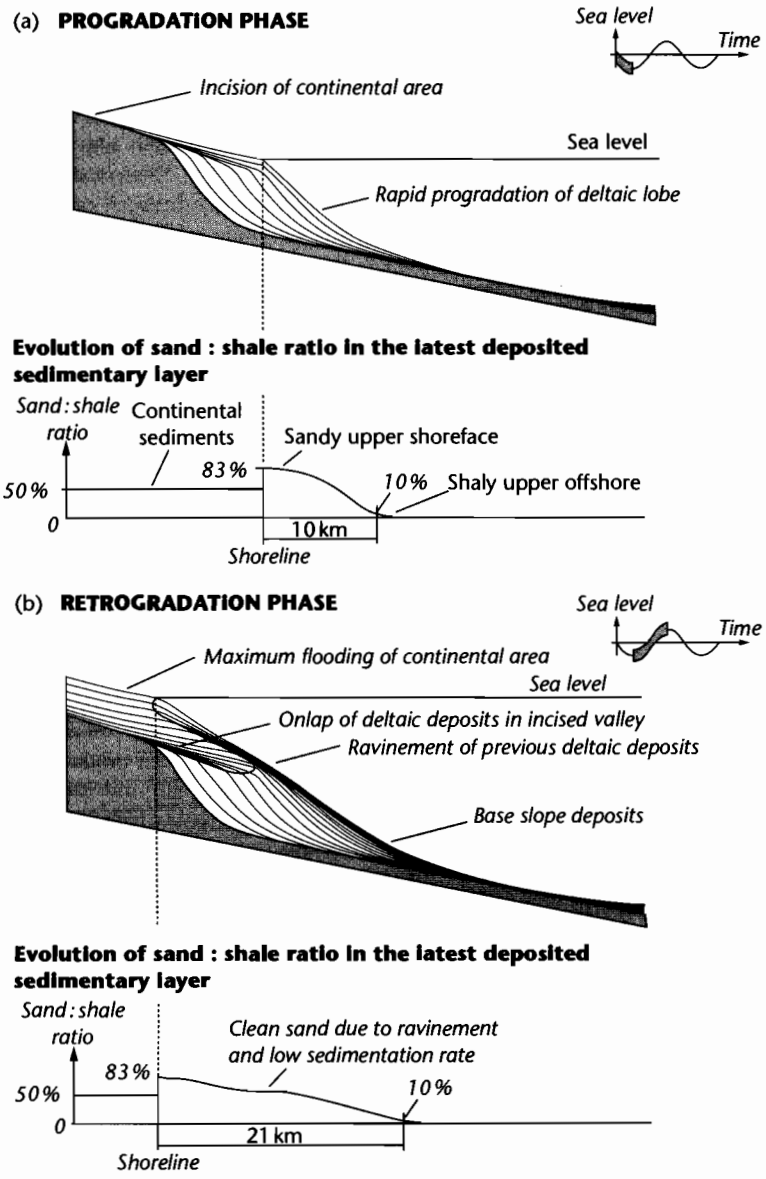

Fig. 8.36 Computer-generated 2-D transects through a fluvial-dominated delta, showing the sand:shale ratio in the preserved sediment during the progradational phase (a) and retrogradational stage (b). After Granjeon and Joseph (1999). Reproduced courtesy of Society for Sedimentary Geology.

modern usage follows Gressly (1838) who used the term to imply the full assemblage of lithological and paleontologic features of a rock unit (Cross and Homewood 1997). The term "facies" has been used subsequently in a number of ways, both purely descriptively and in terms of interpreted process of deposition (Middleton 1978; Reading 1986). A *facies model* is an interpretive device used to explain the association of facies. Facies models generally achieve this explanatory function by linking observations on modern processes and ancient deposits

into a coherent synthesis. The summary that the facies model provides should be usable in a number of different ways. It should incorporate large volumes of data into a form that generalizes sedimentary processes. It should be a stimulant for further investigations and should act as a predictor in new geological situations. Finally, it should help to give insights into the dynamic interpretation of the sediment unit (Walker 1984).

The art of facies modeling is, however, subject to its own problems. Most facies models depend on studies of *modern environments*: it is therefore necessary to assume that the present is an accurate reflection of the past. The time scale of the observations is critical, and we are often left asking the question of how typical are the last 100 years of the geological past, and what is the effect of the infrequent or catastrophic "event" on the geological record? (Dott 1983). Second, it is difficult to assess the true preservation potential of modern sedimentary sequences, and studies of present-day and sub-Recent deposits may be strongly biased compared to the ancient record.

The *vertical sequence* has played a very important role in the development of facies models. Stratigraphy is invariably cyclic at high frequency. However, the vertical profile is clearly an inadequate and sometimes misleading representation of the sedimentary evolution of a succession. Two-dimensional panels, constructed from well-exposed surface outcrops or from high quality seismic reflection lines, are now a standard tool in stratigraphic and facies analysis. Three-dimensional geometries can often be interpreted from a series of differently orientated 2-D sections. The mapping of very high resolution seismic reflection data derived from 3-D surveys also reveals remarkable detail of the geometric properties of sediment bodies and the "texture" of stratigraphic surfaces. For example, 3-D seismic mapping reveals dendritic drainage patterns etched into Type 1 sequence boundaries representing incised, subaerial continental shelves (e.g., Underhill 2001). Sedimentary geometries have been mapped digitally in the field using differential GPS and laser ranging techniques (Adams et al. 2001).

The variability of depositional units, both vertically (in time) and laterally, contribute to its *heterogeneity* (see also §10.4.2). The 2- and 3-D study of sediment geometry has given rise to the concept of "*architecture*," that is, the way in which individual sediment bodies are stacked in time and space. There are now a very large number of studies of architecture. Initially, much progress was made in alluvial and aeolian sedimentary systems. More recently, the focus has shifted to deep marine siliciclastic systems.

In the sections that follow, we outline some of the main depositional systems filling continental and marine sedimentary basins. Vast amounts of information can be found in a large number of authoritative sedimentological texts covering the entire range of depositional systems, environments, and facies. Examples are Reineck and Singh (1980), Walker (1984), Reading (1996), Leeder (1999), Einsele (2000), and Miall (2000).

8.5.2 Continental depositional systems

Terrestrial depositional systems may include the deposits of alluvial fans and fan deltas, rivers, deserts, lakes, slope wastage, and ice sheets and glaciers. Continental basins have a basic two-fold subdivision. Basins with *through drainage* are dominated by well-established river systems and perennial lakes, whereas basins with *internal drainage* are characterized by ephemeral river systems, generally shallow and short-lived lakes, continental sabkhas and deserts.

8.5.2.1 Fluvial systems

A number of specialized volumes provide a wealth of detail on *fluvial systems* and their deposits, including Collinson and Lewin (1983), Ethridge et al. (1987), Shanley and McCabe (1998), Marzo and Puigdefabregas (1993), and Miall (1997). Fluvial style is a complex response to a number of autocyclic and allocyclic controls. The primary allocyclic controls include: (i) climate, which controls run-off (discharge) and the weathering of parent rocks, and (ii) tectonics, which controls basin slopes and relief of hinterlands in the drainage basin. This interplay results in a distinctive set of characters of the river system (e.g., sediment load, discharge, slope, vegetation) which in turn determine channel patterns (braided, meandering, anastomosing), avulsion rates, and floodplain accretion rates. All of these factors control the architecture of alluvial basin-fills (Leeder 1978; Bridge and Leeder 1979; Leeder 1993; Mackey and Bridge 1995).

Alluvial basin types may be dominated by transverse (e.g., Atlantic coastal plain of North America) or longitudinal (e.g., Po system in northern Italy, Ganges of northern India) drainage systems (Fig. 8.37). Alluvial basins can also be classified according to the nature of proximal, medial, and distal elements. Tectonically active basin margins commonly have alluvial fans as proximal elements. Medial elements include braidplains and high-

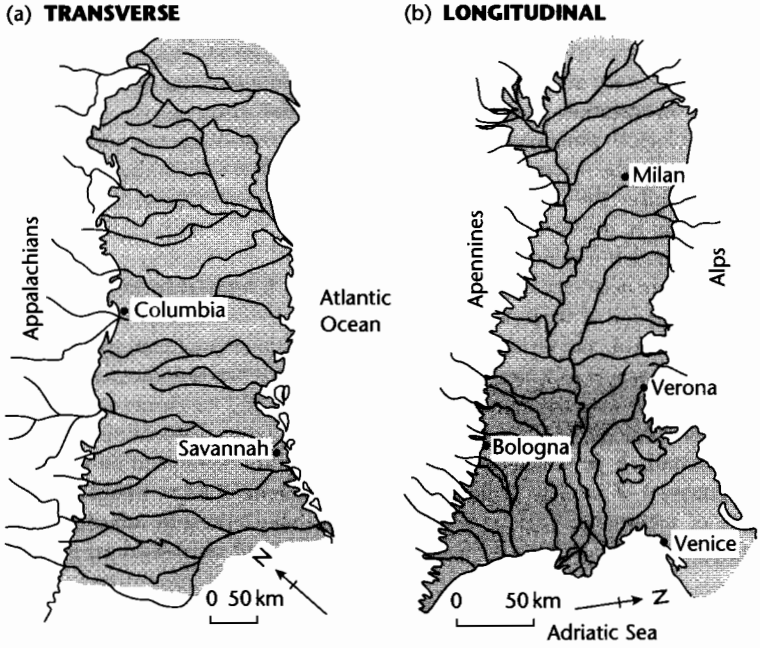

Fig. 8.37 Transverse and longitudinal river drainage patterns. (a) The Atlantic coastal plain of North and South Carolina and Georgia; (b) The Po Basin of northern Italy (after Miall 1984).

sinuosity alluvial systems of transverse or longitudinal type. Distal elements may be lake margins, terminal fans and sabkhas, deltas, and estuaries.

Alluvial fans form where rivers emerge from valleys onto an unconfined plain or major trunk valley, building semi-conical depositional landforms (Bull 1977; Blair and McPherson 1994). They are sensitive indicators of the erosional unroofing of hinterland terrains and of the accommodation generation in the neighboring basin (Whipple and Trayler 1996; Allen and Hovius 1998; Allen and Densmore 2000). Fans vary greatly in area. The classical arid-region fans of the American southwest, such as those of Death Valley, California, have radial distances of 1–7 km, slopes of 2–7° and are dominated by debris-flow processes. Other depositional systems are low-gradient, fluvial megafans with radial distances of over 100 km, such as that of the Kosi River in the Himalayan foreland (Gupta 1997). Megafans depend on an amalgamation of catchments in the mountainous hinterland to supply large quantities of sediment and water. Where fans enter a deep marine, fjord, or lake basin, its surface processes may be dominated by subaqueous mass flows and turbidity currents (Nemec and Steel 1988; Collella and Prior 1990).

Fluvial systems respond rapidly to environmental change, and the effects of tectonic activity can be assessed on-land in neotectonically active regions (Alexander and Leeder 1987) (Fig. 8.38). They therefore serve as sensitive barometers of allocyclic processes. The effects of tectonic tilting on alluvial processes can be seen in channel avulsion patterns, the preservation of asymmetrical meander loops and the interconnectedness of sandstone channel belts (Mike 1975; Alexander and Leeder 1987; Leeder and Alexander 1987; Peakall et al. 2000). River channel processes in regions of growing tectonic structures can be particularly well seen in the Canyonlands region of SW USA (Trudgill 2002). The effects of cycles of base level change at the river mouth can be recognized in systems of terraces and incisions in the river valley, as demonstrated classically by Fisk (1947) in the Mississippi Valley and later by Blum (1993) from the Colorado River of USA.

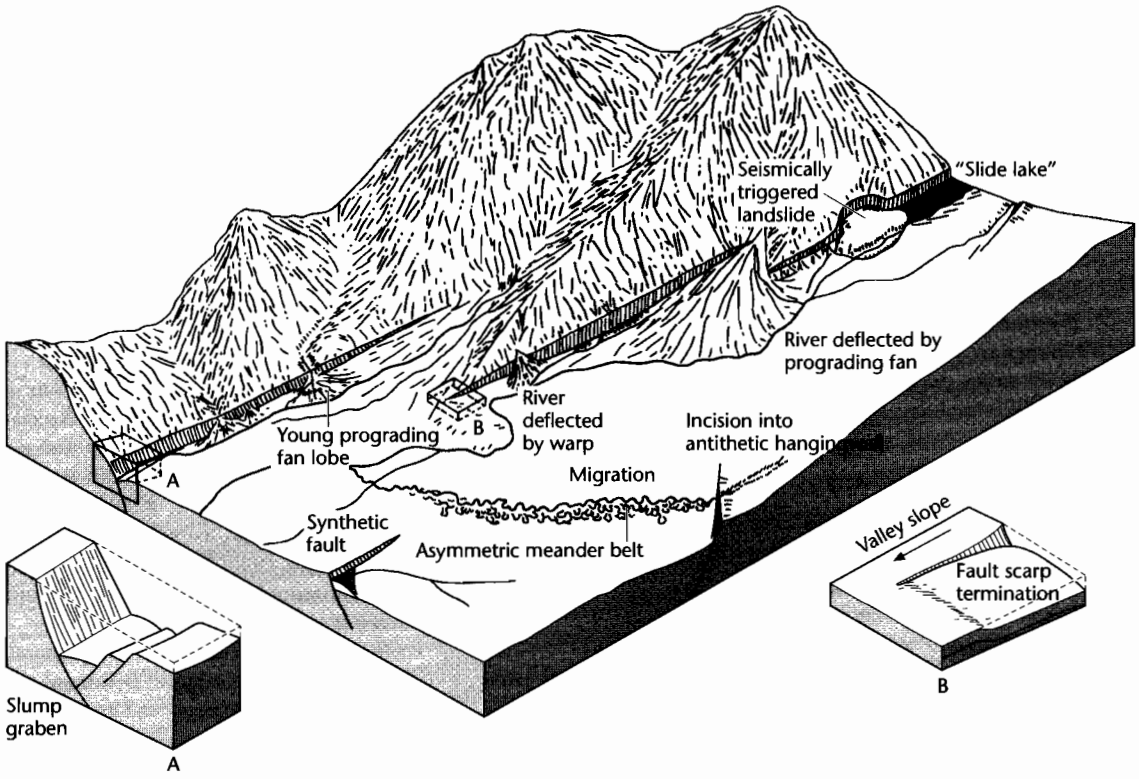

Fig. 8.38 An idealized alluvial half-graben based on studies of the Basin and Range province of western USA, showing some of the common geomorphologic features resulting from extensional neotectonics (from Alexander and Leeder 1987).

8.5.2.2 Desert systems

Deserts include a variety of environments of deposition from the giant sand seas (ergs) to stony wastelands, interdune sabkhas with temporary lakes, and dried up river courses. Deserts occur in both Arctic areas, where sediment is derived from wasting glaciers, and tropical zones where ergs are concentrated. Areas of low rainfall occur as two discontinuous belts around latitudes of 20–30° and are associated with persistently high atmospheric pressures. Deserts also occur in the centers of large continental masses. The occurrence of aeolian deposits in the stratigraphic record is therefore to a large extent a reflection of an ancient climatic zone.

Sediment transport by wind is responsible for large sand dune fields called *ergs*, accumulations of silt and clay termed *loess*, and for transport of dust into the deep sea. The largest present-day ergs occur in topographic basins in cratonic positions, such as the Saharan examples (Rub al Khali erg in Saudi Arabia is 560,000 km^2 in area), the Taklimakan and Gobi deserts of the Asian interior and those of central Australia. The average thickness of the erg may exceed 100 m with bedform (draa) heights of several tens of meters to over 200 m. Ancient examples such as the Permian Rotliegend Sandstone of northern Europe similarly occupy large continental sags. The Permian–Jurassic stratigraphy of the Utah–Arizona–Colorado region is the best-documented ancient desert succession (Peterson 1988). It contains the Lower Jurassic Navajo Sandstone, which alone is 700 m thick.

Aeolian systems can be classified as "dry" or "wet" systems. In dry systems, the water table has no effect, so there are no stabilizing factors restricting sediment transport. Erosion, transport, and deposition are controlled by aerodynamic factors. In wet systems, the water table or capillary fringe intersects the accumulation surface,

leading to stabilization. Wet interdune areas and sabkhas are preserved in the aeolian stratigraphy of wet systems, such as the Entrada Formation of western USA (Kocurek 1981a,b). Wet interdune, sabkha, and lake sediments and extremely important in contributing to the heterogeneity of aeolian reservoirs.

Distinct trends have been identified in transects from erg center to erg margin (Fig. 8.39). Such erg fringes may merge with ephemeral fluvial systems, playa lakes, or marine environments. These erg margin environments are characterized by a complex interaction of sedimentary processes (Porter 1987; Clemmensen and Blakey 1989; Langford 1989; Langford and Chan 1989), and models of *aeolian–fluviatile interaction* and *aeolian–lacustrine interaction* have been developed.

8.5.2.3 Lacustrine systems

Lacustrine depositional systems are also highly sensitive to climate. There is a great diversity of lake basins and lake waters. They can be divided into lakes that have an outlet and are hydrologically open and those that lack an outlet and are hydrologically closed (Fig. 8.40) (Allen and Collinson 1986; Talbot and Allen 1996). Their hydrological status determines lakewater chemistry and therefore the terrigeneous clastic *versus* chemical and biochemical sedimentation in the lake. Hydrologically closed lakes commonly form in the centers of endorheic (internal drainage) regions such as the Chad Basin, north-central Africa. They are characterized by a dominance of chemical and biochemical sediments and evaporites are common. Through-flowing lakes typify many continental rift systems such as in East Africa and the Baikal Rift of central Asia. They are dominated by terrigenous clastic input and, where river input is negligible, by alkaline earth carbonates. Apart from the hydrologic status of the lake, the most important controls on lacustrine depositional systems are the slope of the nearshore zone, lake bathymetry, stratification of the water column, size and shape of the lake as well as the overriding importance of climate.

Lacustrine depositional systems may change in character rapidly as a result of climatic fluctuations. A large number of present-day lakes are shrunken, saline remnants of much larger and more dilute ancestors that existed during the pluvial period coinciding with the last glacial maximum (Flint 1971). Examples are the Dead Sea and precursor Lake Lisan, Great Salt Lake, USA and precursor Lake Bonneville, and Lake Eyre, Australia and precursor Lake Dieri. The expanded lakes, such as Lake Lisan, typically accumulated alkaline earth carbonates with an abundant flora of diatoms, whereas the present-day remnant has a lake floor covered with gypsum and halite. An analysis of Holocene/Quaternary lake levels and salinities suggests that minima and maxima recur at a frequency that is most likely a result of orbital eccentricities of the Earth around the Sun. The lake level variations therefore appear to be a complex response to Milankovitch forcing.

8.5.2.4 Glacial systems

About 10% of the present Earth's surface is covered with ice and a further 20% is affected by permafrost. During some periods of Earth history, such as the Ordovician, Permo-Carboniferous and Late Cenozoic, ice and permafrost cover was much more extensive (Hambrey 1994), and during the Neoproterozoic it is thought that the Earth repeatedly froze over completely or near-completely (Hoffman et al. 1998). The assembly of plates into supercontinental assemblies appears to be a major factor in the onset of major glaciations.

Glacial environments are complex and laterally extremely variable. Moving ice is found in a number of settings, principally as polar ice sheets and as coastal ice shelves, and as valley glaciers and their marine outlets (tidewater glaciers). Glacial sedimentary facies reflect the various processes involved in ice movement and melting (Eyles et al. 1985; Ehlers 1996) (Fig. 8.41). On land, sediment is deposited by direct deposition or lodgment under active ice, some from reworking by later sediment gravity flows at the ice terminus, and some is deposited by subglacial streams or as deltas at their exit points. Sediment is also dumped from ice at its contact with lakes and in the ocean as glacilacustrine and glacimarine sediment. Rain-out diamictites are caused by the melting of sediment-loaded floating ice, which distributes a wide grain size range of sediment, including large *dropstones*, over the lake or seabed. Such dropstone-bearing rain-out diamictites are a common feature of many Neoproterozoic glacial successions.

8.5.3 Coastal and nearshore depositional systems

8.5.3.1 Siliciclastic shoreline systems

The geomorphology and oceanography of the Earth's siliciclastic coastlines reveals an exceedingly complex

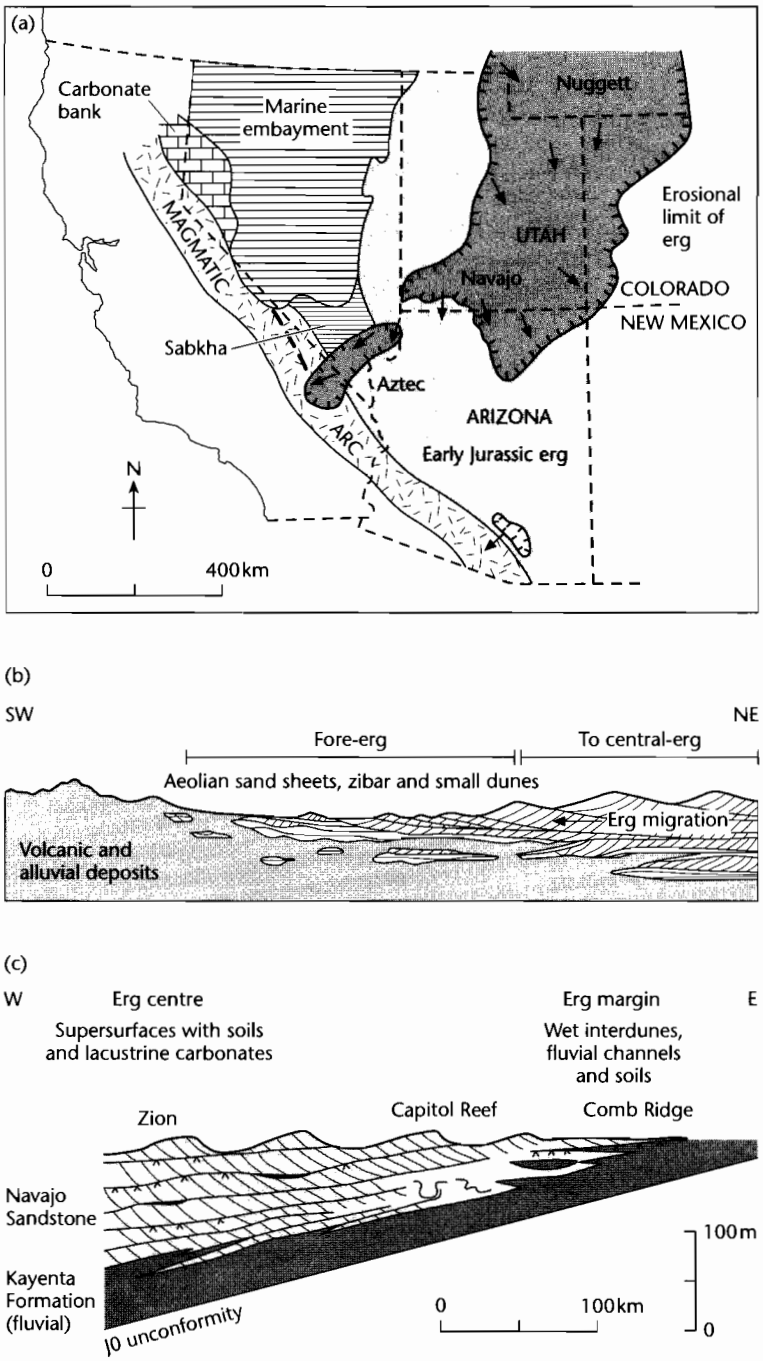

Fig. 8.39 Eolian erg centre to erg margin transect from the Lower Jurassic stratigraphy of southwestern USA (after Porter 1987; Blakey et al. 1988). (a) Generalized Early Jurassic paleogeography; (b) Schematic section across erg margin in southwest (Aztec Sandstone); (c) Cross-section of the Navajo erg showing a depositional erg margin in the east which now corresponds closely to its erosion limit. Supersurfaces show soils and locally carbonate ponds.

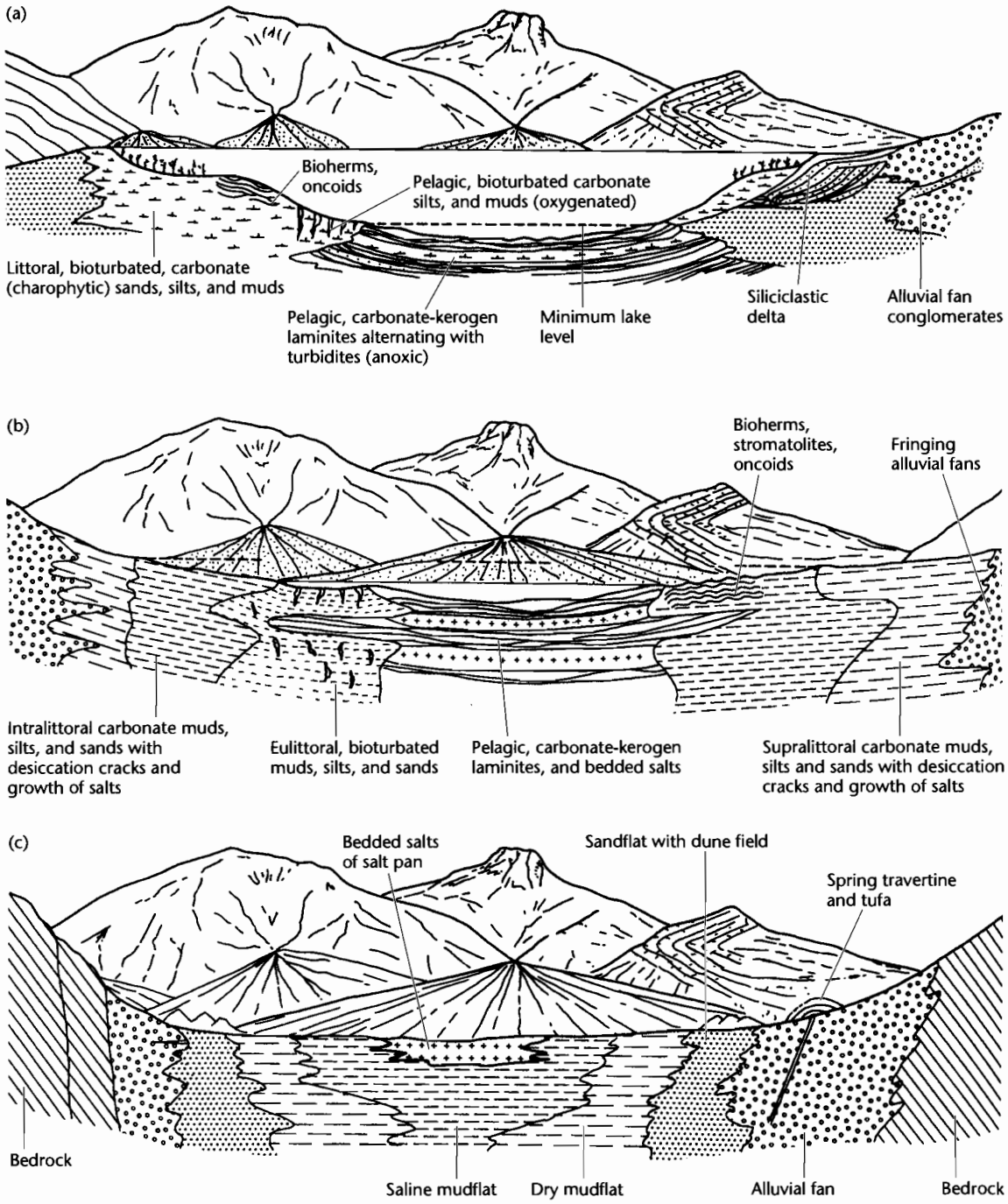

Fig. 8.40 Idealized depositional environments and facies in lacustrine systems. (a) Open freshwater lake with through drainage; (b) Hydrologically closed perennial salt lake; (c) Hydrologically closed ephemeral salt pan. After Eugster and Kelts (1983), modified from Allen and Collinson (1986).

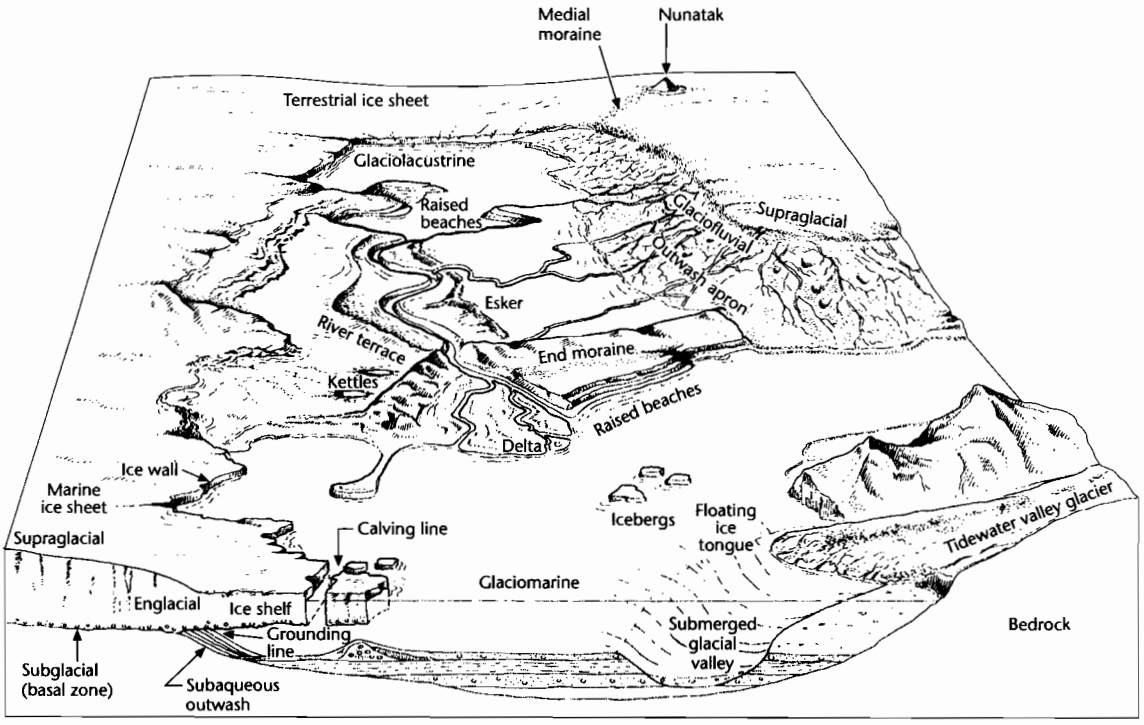

Fig. 8.41 The main depositional environments and facies at an ice margin (after Edwards 1986). Reproduced courtesy of Blackwell Publishing Ltd.

interplay between fluvial input on the one hand, and basinal parameters such as wave energy, tidal range, and storm regime on the other. The two main types of coastal depositional system are *deltaic* and *nondeltaic*. Deltaic coasts are strongly influenced by the dynamics of the outflowing river water. Nondeltaic coastal systems may be: (i) *wave-dominated*, containing beaches, microtidal barrier islands, and cheniers, (ii) *mixed wave-tide influenced*, consisting of mesotidal barrier islands with tidal inlets and ebb- and flood-tidal deltas, and (iii) *tide-dominated*, made up of tidal flats and estuaries (Hayes 1979).

Deltas develop where river systems debouch into the ocean, inland seas, and lakes. Their form is controlled by a number of factors, chief of which is the relative effectiveness of river discharge compared with the tidal and wave energies of the receiving basin (Galloway 1975; Postma 1990) (Fig. 8.42). Where tidal and wave energies are low, distributary channels are able to build out into the sea unhindered by coastal erosion producing a typical "birdsfoot" pattern, as shown by the Mississippi Delta, USA. Where wave energies are strong compared to the river inflows and tides, the sediment delivered to the sea is molded into curved ridges at the delta's front and some is redistributed along the shore as beaches and spits. Deltas of this type, such as the Senegal (West Africa) or the Grijalva (Gulf of Mexico) are roughly arc-shaped and prograde slowly because of the destructive nature of approaching waves. Deltas strongly affected by tides have tidal channels cutting deep into the coastline with associated tidal sand ridges or shoals elongated in the same direction as the tidal current pathways, such as the Ganga–Brahmaputra delta in the Bay of Bengal, and the Mahakam delta, Indonesia.

Depositional patterns at river mouths can also be studied in relation to the dynamics of outflow dispersion (Wright and Coleman 1974; Wright 1977), an extension of the original concept proposed by Forel (1892) from his studies of the delta of the Rhône River in Lake Geneva. The dispersion of the outflow into the receiving water body falls into three categories: inertia-dominated jets, friction-dominated jets, and buoyancy-dominated outflows. The dynamics of the outflow control the transport

1 Mississippi
2 Po
3 Danube
4 Ebro
5 Nile
6 Rhône
7 São Francisco
8 Senegal
9 Burdekin
10 Niger
11 Orinoco
12 Mekong
13 Copper
14 Ganges-Brahmaputra
15 Gulf of Papua
16 Mahakam

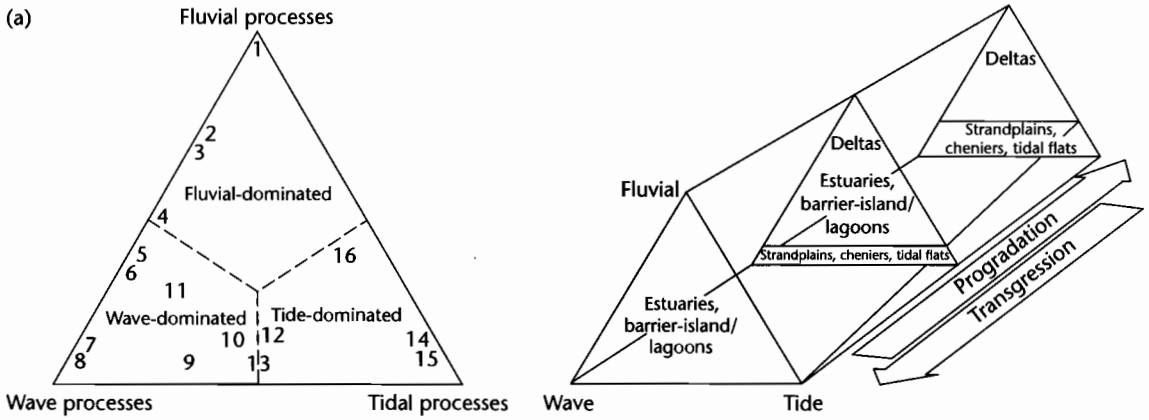

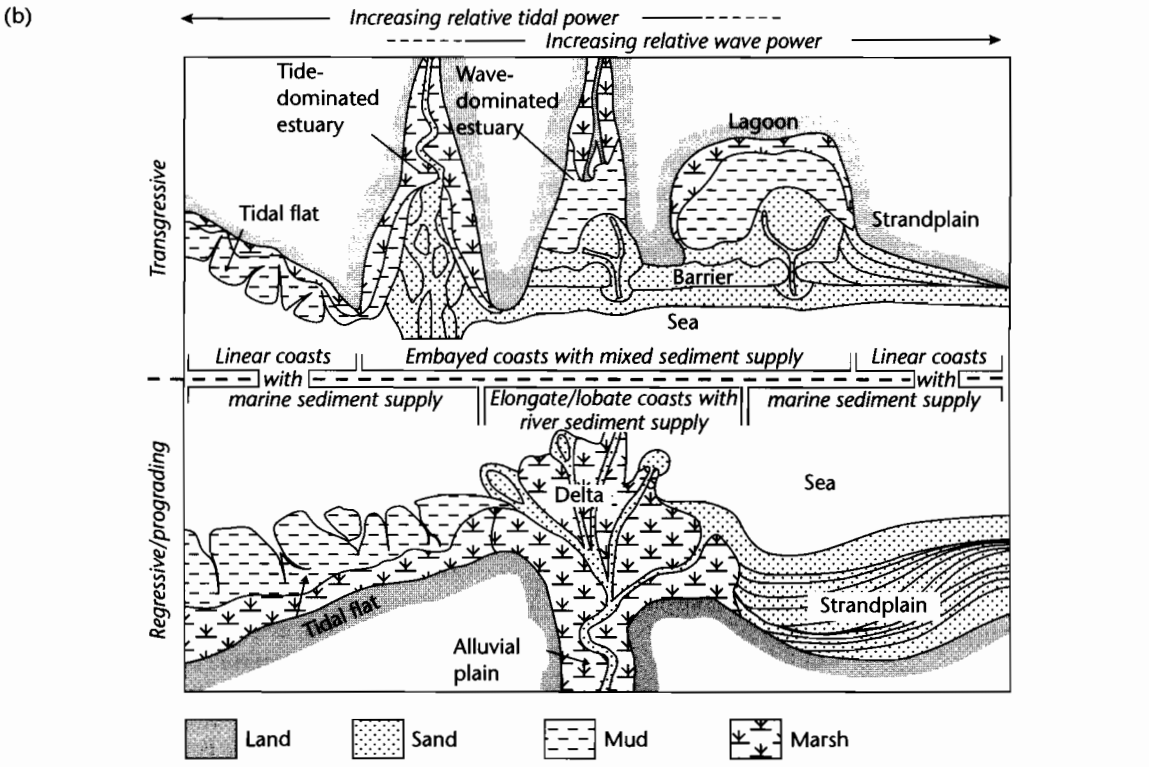

Fig. 8.42 Delta classification according to fluvial discharge, wave power and tidal range, following Galloway (1975), Postma (1990), Reading and Collinson (1996). (a) Ternary diagram and its modification into a Swiss *Toblerone*, to account for the different morphological features found during progradation and transgression of the coast. Reproduced courtesy of Society for Sedimentary Geology. (b) Plan views of trangressive/retrogradational and regressive/progradational coasts under varying conditions of wave power, tidal range, and marine and fluvial sediment supply (based on Heward 1981 and Boyd et al. 1992). Reproduced courtesy of Blackwell Publishing.

distance of particulates of different size in the estuary, lake, or ocean.

Wave-dominated shorelines may occur on delta fronts or on nondeltaic coasts. They are dominated by beaches (directly attached to the land) and barrier islands separated from the land by a shallow lagoon. Cheniers are sandy or shelly beach ridges isolated in coastal mudflats. The beachface subenvironments are controlled largely by wave approach, and vary from high energy to low energy settings. Barrier islands on wave-dominated coasts share much in common with beaches. They are found particularly in coastal environments that have a low gradient continental shelf adjacent to a low relief coastal plain, an abundant sediment supply and moderate to low tidal ranges (Glaeser 1978). An excellent example of a barrier is Galveston Island in the Gulf of Mexico (Bernard et al. 1962; McCubbin 1982). Tidal inlets are few and short-lived on wave-dominated barrier islands. Because of the limited connection to the open sea, the lagoons behind such barriers are prone to abnormal salinities (e.g., Padre Lagoon, Gulf of Mexico). Storms are capable of breaching the barrier, however, producing washover channels and fans.

Wave- and tide-influenced shorelines comprise barrier islands highly dissected by tidal inlets and associated tidal deltas. Wave-influenced tidal inlets are highly mobile, migrating in the direction of net longshore sediment transport. They therefore progressively replace the wave-built barrier with coalesced tidal inlet sequences. When tidal range is large (mesotidal to macrotidal, 2 to >4 m) estuaries dominate the coastal geomorphology (Dalrymple et al. 1992). Fine-grained sediments fringe the estuary in the form of intertidal and supratidal flats, whereas sands dominate the central zone. Tidal flats dissected by highly sinuous tidal creeks can be extremely extensive on some low wave-energy mesotidal to macrotidal coasts. Progradation of estuarine depositional systems should give rise to a fining upward sequence as subtidal and low intertidal sandflats are replaced by high intertidal and supratidal mudflats.

8.5.3.2 Carbonate and evaporite shoreline systems

Carbonate sediments are produced in great abundance in shallow, warm waters where the biological and physicochemical conditions are optimal for carbonate precipitation and fixation. Arid shorelines with low terrigenous input are characterized by deposition of carbonates and evaporites. The Trucial coast, Persian Gulf is an example of a modern carbonate-rich marginal marine *sabkha* (Fig. 8.43). A wide variety of coastal geomorphological elements are present, including beaches, barrier islands, tidal channels, and associated tidal deltas, intertidal and supratidal flats and aeolian dunes. The beaches, tidal deltas, and bars are commonly composed of oolitic-skeletal grainstones, whereas the back-barrier lagoons accumulate pelletal muds and, where predation is restricted, stromatolites. The upper intertidal zone is dominated by algal mats, constituting the lowest part of the sabkha *sensu stricto*. The supratidal zone is the main part of the sabkha and is the site of the precipitation of evaporitic minerals in the sediment column, as surface encrustations and in small ponds. Detrital carbonate grains are transported onto the sabkha by marine flooding.

Arid shorelines may also be dominated by siliciclastic sedimentation, as in Baja California, the Gulf of Elat and some parts of the Arabian Gulf. Here the sabkhas are composed of siliceous sands and muds with a possible admixture of carbonate grains. In many ways siliciclastic sabkhas are similar to their carbonate-rich counterparts. During progradation of the sabkha, normal marine sediments are first overlain by intertidal deposits, then supratidal sabkha evaporites, giving a vertical sequence indicative of increasing salinity. In some sabkhas, however, the deposits are arranged in a "bullseye" pattern, suggesting the progressive infilling of water bodies rather than shoreline progradation.

8.5.4 Continental shelf depositional systems

8.5.4.1 Siliciclastic shelf systems

Continental shelf systems are extremely complex and are highly sensitive to sea level fluctuations. *Modern siliciclastic shelves* contain sedimentary facies associations based on the physical processes operating in the nearshore-inner shelf zone, the rate of sea-level fluctuation and the nature and rate of sediment supply (Curray 1964, 1965). Some sediment on the shelf (perhaps 50% of the Earth's shelf area) is *relict*, that is, it is remnant from an earlier environment and is now out of equilibrium with the new conditions. Other sediments are termed *palimpsest*, which means that they are reworked and therefore possess aspects of both their present and former environments. Finally, some sediment is *modern* and is supplied from outside the shelf area.

Modern continental shelves can therefore be classified according to the nature of the sediment (relict, palimpsest, modern) and the hydraulic regime (wave-, tide-, storm-, or oceanic current-dominated) (Swift 1974;

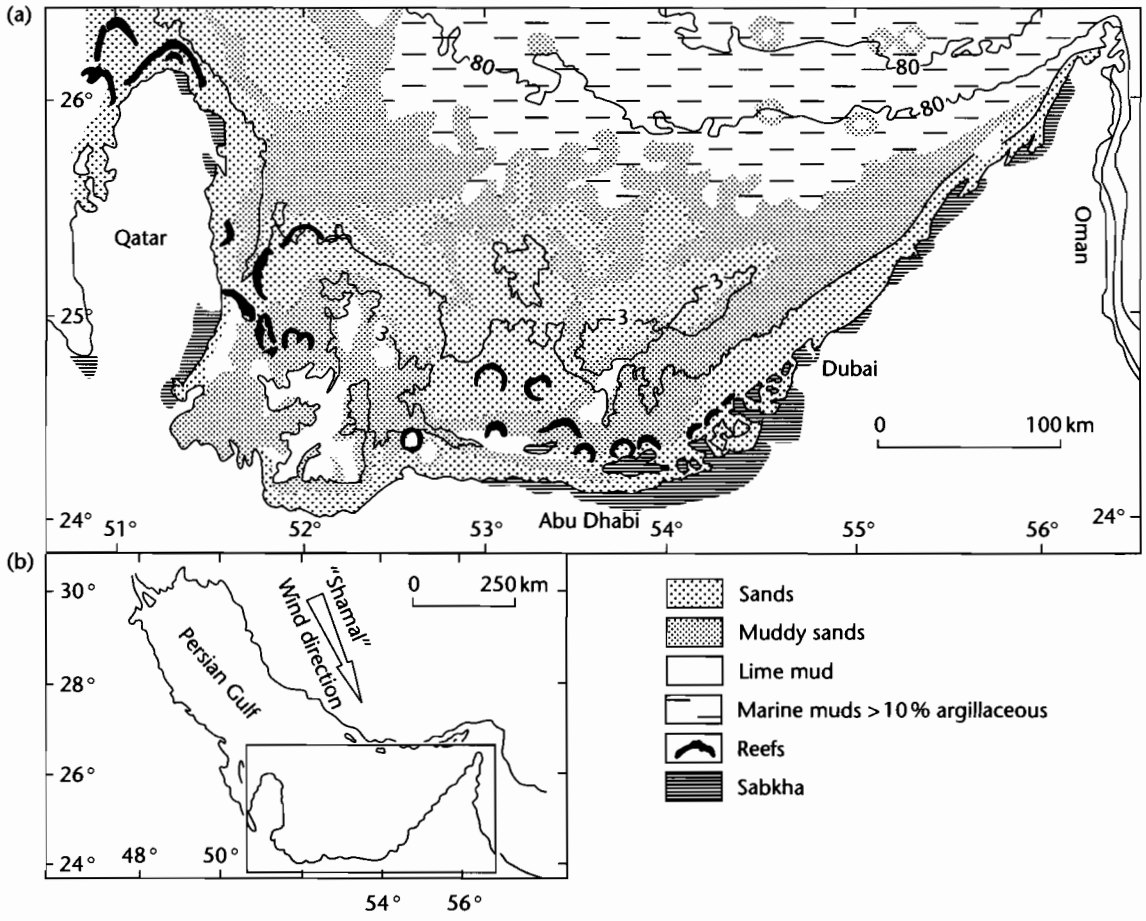

Fig. 8.43 Depositional environments of the open shelf and arid carbonate shoreline of the Trucial Coast, Persian Gulf. The Persian Gulf is an example of an open shelf, unprotected by a rim or reefs. (a) Bathymetry and facies on part of the southern shelf of the Persian Gulf (after Wagner and van der Togt 1973). Classical supratidal sabkhas are found in the Abu Dhabi area. Sediment transport on the shelf is influenced by the predominant "Shamal" wind from the NNW, shown in (b).

Johnson and Baldwin 1986) (Fig. 8.44). Classifying shelves according to the dominant shelf currents (Swift et al. 1986), tide-dominated shelves occupy 17% of the present-day shelf area, storm-dominated 80%, and shelves dominated by intruding ocean currents a very small percentage.

8.5.4.2 Carbonate shelf systems and reefs

Much of the continental shelf between the latitudes of 30°S and 30°N is an area of high organic productivity and is covered not by river-derived or relict siliciclastic sediments, but by organic carbonate material. There are two major categories of *subtropical carbonate shelf* (Ginsburg and James 1974). (i) *Rimmed shelves* sheltering protected shelf lagoons (Fig. 8.45). Their margins often fall precipitously into the abyssal depths. Some rimmed shelves are attached to continental areas as in the Great Barrier Reef of Australia. Others are now *isolated platforms* as in the Bahamas, and (ii) *open shelves* on the other hand, such as Yucatan, western Florida and northern Australia, slope gently towards the continental edge and are termed

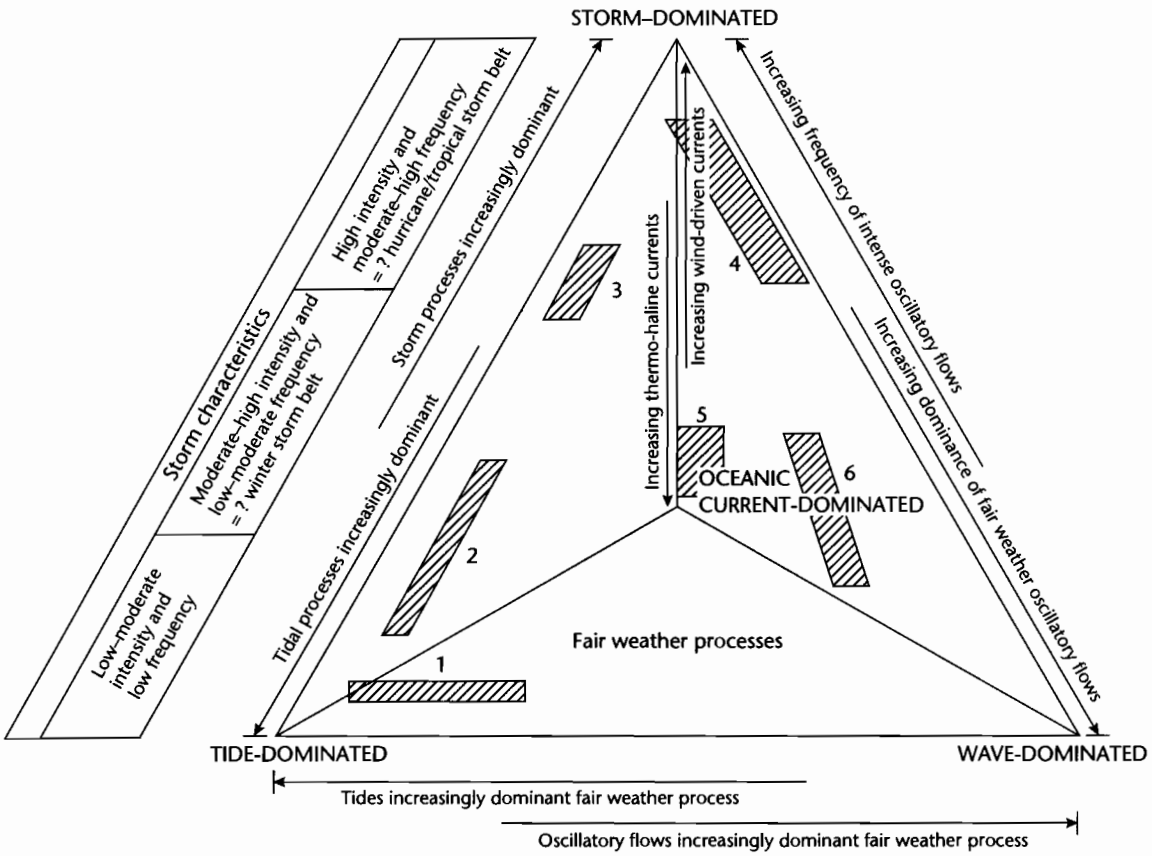

Fig. 8.44 The main types of hydraulic regime on modern shelves (modified from Johnson and Baldwin 1986). Modern shelves may be tide-dominated, ocean current-dominated or wave-dominated, where fairweather processes are of greatest importance, or storm-dominated where fairweather processes are of lesser importance. Shelf currents capable of transporting large amounts of sediment occur on shelves dominated by storms, tides, or intruding ocean currents. (1) Macrotidal and mesotidal embayments and estuaries (e.g., Bay of Fundy, Nova Scotia; Chesapeake Bay, USA; German Bight, North Sea) (2) Tidal straits and seas (e.g., English Channel, Malacca Strait, Taiwan Strait, North Sea, Yellow Sea). (3) Winter storm and tide-influenced shelf of the NW Atlantic, off eastern North America. (4) Storm-dominated shelves (e.g., Oregon–Washington and Californian shelves; SE Bering Sea; Gulf of Mexico. (5) Ocean current-swept shelves (e.g., SE Africa, Moroccan Shelf, NW Africa). (6) Low-energy embayments and shelves (e.g., Amazon–Orinoco Shelf; Niger Shelf; Baltic Sea; Hudson Bay).

ramps. Because of the lack of a protective rim, they are strongly affected by storm waves and tidal currents.

Reefs are *biogenic* constructions on the seafloor and reef facies models must successfully integrate sedimentologic and paleontologic observations. Reefs can generally be divided into: (i) a reef core comprising skeletons of reef-building organisms and a lime-mud matrix, (ii) reef flank of bedded reef debris, and (iii) inter-reef of subtidal shallow marine carbonates (or siliciclastics). Where reefs form a natural breakwater on the windward sides of shelves or islands, however, they protect a back-reef environment from wave attack. The types of reef building organisms has changed from the Precambrian through the Phanerozoic (James 1983).

8.5.5 Deep sea depositional systems

There are four fundamentally different environments of deposition of clastic sediments in the deep sea (Fig. 8.46):

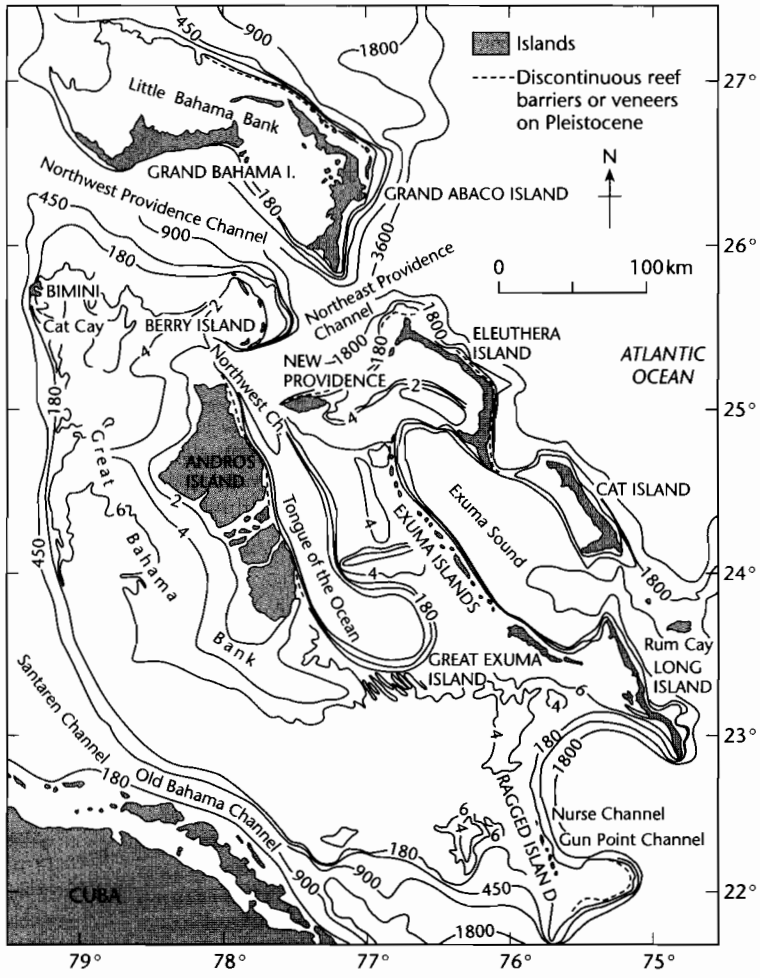

Fig. 8.45 General bathymetry of the Bahamian–Florida area, showing depths in m (after Multer 1971; Bathurst 1971, modified from Sellwood 1986). The area is a recently flooded rimmed shelf. The trace of the 6 m contour gives an impression of the former extent of the subaerial portion of the shelf prior to *c.* 7000 yr BP.

1 *Slope aprons*, which accumulate between the shelf and basin floor, vary in width from <1 km to >200 km. Normal siliciclastic slope aprons have a smooth convex–concave profile built by slope progradation. Faulted slope aprons typically have a highly stepped profile with perched basins alternating with steeply dipping slope segments. Carbonate slope aprons may form against reef edges or carbonate shoal margins. Where such margins are steep, sediment largely bypasses the slope apron so that it is dominated by calcirudite talus wedges. Where the margins are gentle, the slope apron is more actively depositional and more like its siliciclastic counterpart.

2 *Submarine fans* are constructional bodies that build oceanward at the base of the shelf slope. They receive sediment from river mouths or from alternative feeder systems such as submarine canyons. Fans vary greatly in scale and geometry, but there appear to be two end members, radial and elongate (Stow 1985). Radial fans develop concentrically around a single feeder canyon or channel (e.g., La Jolla and Navy fans off California). Elongate fans often have two or more feeder channels and extend for considerable distances from the supply margin. Examples are the enormous Bengal (off the Ganga delta), Amazon, and Laurentian (eastern North

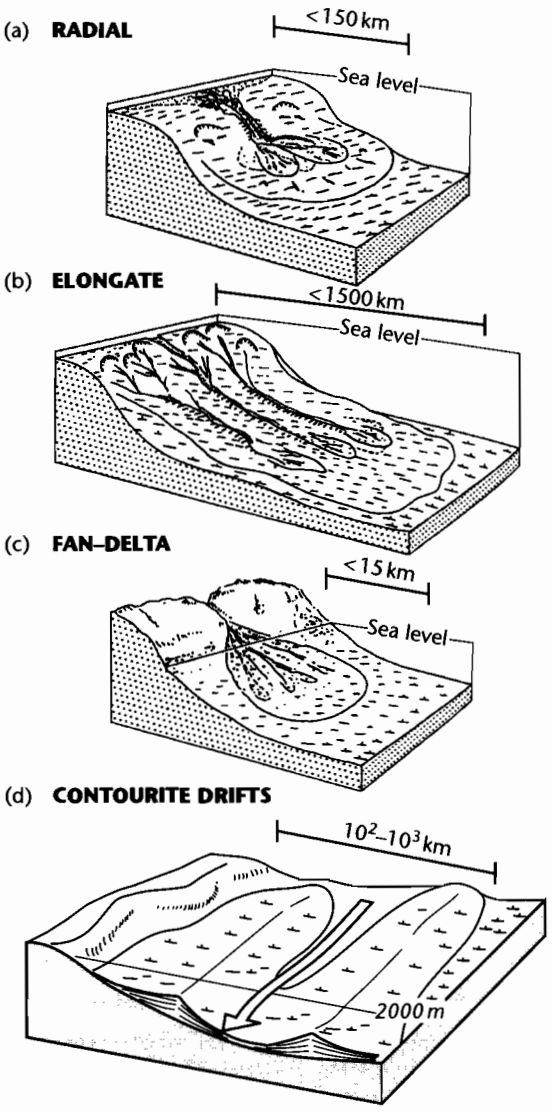

Fig. 8.46 Main types of deep sea depositional environment for siliciclastics. All diagrams are vertically exaggerated.

America) fans. Some large elongate fans, such as the Amazon, are covered with extensive debris flow deposits as well as channel-levee complexes with remarkable sinuous channels extending to beyond 4000 m depth (Cramp et al. 1995).

3 *Deep water sediment drifts* are formed by the relatively slow (generally <20 mm yr^{-1}) deep thermohaline circulation of the oceans, and to a lesser extent by wind-driven circulations where they impinge on the seabed, such as the Gulf Stream gyres of the North Atlantic. The more vigorous bottom currents may suspend diffuse clouds of sediment and organic material as *nepheloid layers*, as is found along the western margin of the North and South Atlantic (Biscaye and Eittreim 1977). Bottom currents also locally erode the seafloor, or deposit large sediment drifts composed of fine-grained *contourites*. Contourite drifts are particularly common at the edges of deep bottom water pathways (McCave and Tucholke 1986).

4 *Basin plains* are flat, relatively deep areas that act as the ultimate sediment traps for clastic sediments eroded from the continents and from submarine highs. Facies types and distributions are controlled primarily by basin geometry, tectonics, and source area (Pilkey et al. 1980). Abyssal plains are extensive and elongated parallel to the adjacent continental margin (e.g., Hatteras Abyssal Plain on the western North Atlantic). Marginal seas also have basin plains, fed from widely varied sources with a centripetal pattern (e.g., Sigsbee Basin Plain, Gulf of Mexico, Davies 1968). Deep sea trenches may consist wholly or in part of basin plains. In this case the plain parallels the highly elongate to arcuate trench orientation, and the dispersal of sediment by turbidity currents is also generally longitudinal. Strike–slip basins or borderland basins may also contain small, relatively confined basin plains.

The facies models of deep sea sedimentation of sands and gravels have been dominated by the concept of sediment gravity flows in general and turbidity currents in particular. Turbidity currents are responsible for the transport of large quantities of sand and mud into the deep sea. Turbidite beds can be recognized by their sharp, often erosive bases ornamented with sole marks, upward grading of grain size, and a vertical sequence of sedimentary structures. The greatest volume of modern turbidites accumulates in submarine fans and this depositional system has received strong emphasis in geological studies.

The seabed off northwest Africa provides an informative example of an integrated system of slope and deep marine processes and products (Weaver et al. 1992; Masson 1996) (Fig. 8.47). Catastrophic collapse of volcanic islands in the Canaries has repeatedly produced debris avalanches that load the adjacent seabed and trigger large debris flows. Some of these debris flows may have yielded turbidity currents that traveled downslope to the Madeira abyssal plain at water depths of over 5000 m.

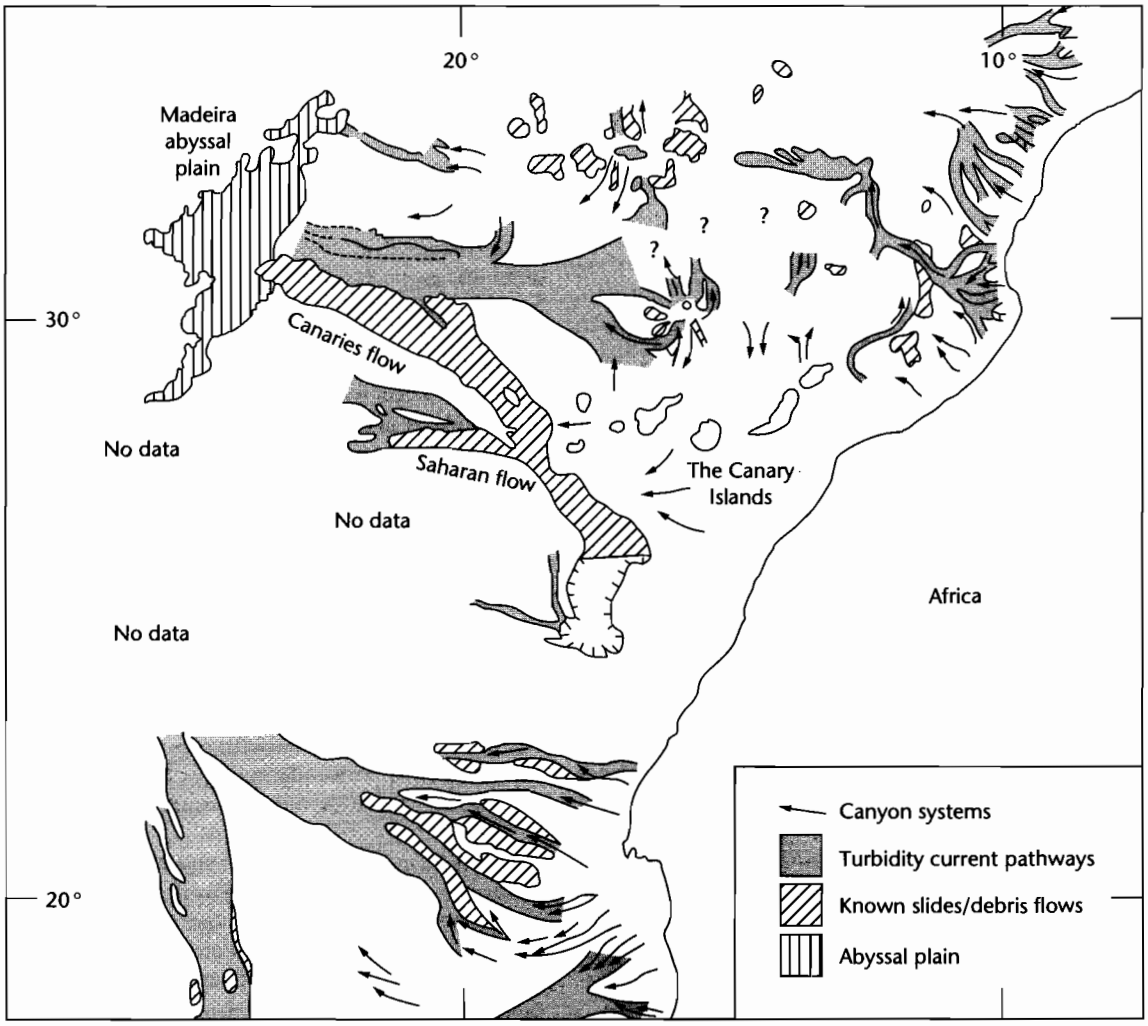

Fig. 8.47 Sediment routing systems offshore NW Africa, showing the transport paths of turbidity currents and giant debris flows. The Canaries debris flow originated by the loading of the sea bed by a rock avalanche caused by the catastrophic collapse of a nearby volcanic seamount. The Saharan debris flow, however, was due to slope failure of the continental margin. After Weaver et al. (1992).

Elongate but narrow troughs are commonly filled by turbidites deposited by longitudinal currents. The confinement of the basin, often as a result of tectonic activity, causes the turbidity currents to pond, deflect, and reflect off the basin flanks. Excellent examples are found in structurally confined basins perched at the thrust front of orogenic belts, as in the Tertiary Gres d'Annot Basins of southeastern France (Sinclair 1994) and the Tertiary Betic Sorbas Basin of southeastern Spain (Haughton 2001). In these cases traditional fan models are unlikely to closely resemble the observed facies associations.

8.5.5.1 Pelagic systems

Sedimentation in the open sea beyond the influence of the continental land masses is controlled by two major factors: the fertility of the surface water and the presence of the *calcite compensation depth* (CCD) below which carbonate

from the skeletons of marine organisms is dissolved. The biologic productivity of the oceans is highly concentrated in near-surface waters where light allows photosynthesis of phytoplankton. A small percentage (1%) of the carbon fixed by photosynthesis accumulates in dead organic tissues on the ocean bed. In low oxygen conditions, this organic matter is converted into black, laminated, organic-rich shales known as *sapropels*. Highest productivity is where there is an ample supply of nutrients, as in upwelling zones. Nutrient supply may also be strongly influenced by climate change, with increased productivity during glacial periods when nutrients such as iron are blown into the ocean from expanded desert regions.

Above the CCD, calcareous oozes derived from microorganisms such as formanifera predominate. Below this, the silica skeletons of radiolaria and diatoms produce siliceous oozes. There are also regions of seafloor dominated by red and brown clays derived from volcanoes, meteorites and dust blown from continents. The CCD has varied in its depth in the ocean during geological time, commonly as a result of variations in temperature and productivity, as at the Eocene–Oligocene boundary (Kennett and Shackleton 1976).

8.6 RELATION OF DEPOSITIONAL STYLE TO BASIN SETTING

Sedimentary basins form by deformation of the lithosphere (stretching, cooling, bending) and their gross stratigraphic patterns primarily reflect the various allogenic processes, principally climate and tectonics, causing base-level or relative sea-level change. It follows therefore that basins of a similar genetic type may show a consistent pattern in their sedimentary evolution, whereas basins of different type show correspondingly different sedimentary styles. Knowing the formative mechanism of a basin consequently has predictive power in assessing the basin-fill. In the following sections some characteristic sedimentary histories of various basin types will be sketched out. However, this should not be done in isolation from the particular "basin-specific" tectonic and burial history. The examples and generalizations that follow are a snap-shot of a subject area with an almost limitless bibliography. Further details can be found in Allen and Allen (1990), Ingersoll and Busby (1995), Leeder (1999), Einsele (2000), and Miall (2000), and in the various contributions of Bill Dickinson, who pioneered the linkage between tectonics and sedimentary geology (e.g., Dickinson 1974, 1976, 1993).

8.6.1 Basins related to divergent plate motion

Some basins on continental lithosphere appear to be purely sags with no obvious rifted basement. Others are clearly fault-bounded rift valley basins and yet others are rift basins that have since undergone a widespread subsidence unrelated to active tectonics (failed rifts or aulacogens). Large amounts of stretching lead to the formation of proto-oceanic troughs and passive margins. The underlying process that unites these various basin styles is lithospheric thinning and associated thermal disturbances. In this section we overview the typical kinds of sedimentary infillings of these basins formed on continental lithosphere.

8.6.1.1 Intracratonic sags

Intracratonic sags are characterized by prolonged but slow subsidence and a lack of strong syn-sedimentary structural activity. The sedimentary systems filling intracratonic sags are most commonly terrestrial, often in the form of rivers draining into centrally located, shallow lakes. Such endorheic systems are found in the Chad Basin of north central Africa and the Eyre Basin of southern Australia. In other intracontinental sags, shallow seas are able to enter the basin, as in the Paleozoic Hudson Bay Basin and Michigan Basin of North America.

There are a number of plausible mechanisms for the development of intracratonic sags, some of which may act in combination: subsidence as a response to recovery of the lithosphere following a thermal disturbance; subsidence driven by phase changes in the underlying mantle; subsidence related to the dynamic topography associated with subduction of oceanic slabs around the plate margin; subsidence over a mantle downwelling; long wavelength buckling of a layered lithosphere. Whatever the primary mechanism, the subsidence of intracratonic sags is strongly amplified by the effects of water and sediment loading. Fringing uplifts may act as an annulus that simultaneously serves as a source region for sediment and a topographic load on the lithosphere.

The *Chad Basin* is situated deep in the African interior >500 km from the nearest sea. The watershed bounds a roughly square area with sides of about 1200 km. The shallow (<10 m) centrally located lake occupies at present a relatively small area (30,000 km^2) compared to the extent of its late Pleistocene precursor Lake Mega-Chad (almost 1.5×10^6 km^2, Grove and Warren 1968). Most of the subsidence of the Chad Basin has taken place in the

Neogene and it has been concentrated in the zone within the confines of the beach ridges represented by the maximum limit of Lake Mega-Chad (Fig. 8.48). Sediment supply is thought to have been from fringing uplifts that acted as a dynamically supported annulus around the basin (Burke 1976). The intracratonic sag overlies an Early Cretaceous rift system, but cannot simply be due to thermal relaxation following stretching, because sedimentation in the modern basin is Neogene to present. Hartley and Allen (1994) suggested that the Chad Basin might be situated over an asthenospheric downwelling, which causes slow basin subsidence.

The *Michigan Basin* of northern USA (Wilson and Burke 1972; Burke and Dewey 1973) (Fig. 8.49) has undergone subsidence at varying rates for 500 Myr, yet the greatest thickness of basin-fill, found in the basin center, is still only 4 km. The Cambrian to Jurassic sediments are largely unaffected by structural activity, but the strong positive Bouguer gravity anomaly trending NW–SE across the basin and the sedimentary rocks penetrated by a deep borehole (Sleep and Sloss 1978) suggest the existence of a turbidite-filled Precambrian rift (~1100 Ma) underlying the basin (Hinze et al. 1975; Fowler and Kuenzi 1978).

Subsidence probably started in the Cambrian (Catacosinos 1973; Haxby et al. 1976) and continued through the Paleozoic with episodes of erosion producing continent-wide unconformities (Sloss 1963; Sloss and Speed 1974) (Fig. 8.49). Although the Cambrian contains extensive shallow marine sheet sandstones, the bulk of the Middle Ordovician to Devonian succession is made of carbonates, shales, and evaporites. The limestones, which are also found in the Illinois Basin to the south, are well known for their build-up complexes. In the Silurian, barrier complexes grew around the perimeter of the Michigan Basin, whilst so-called "pinnacle reefs" developed closer to the basin center where biogenic construction kept pace with the greater rate of subsidence (Wilson 1975 for synthesis) (Fig. 8.50). Evaporites are interfingered with and overlie the carbonate build-ups. Whereas the origin of the carbonate build-ups is undisputed, the evaporites are controversial. Deep water, shallow water, and supratidal environments have all been suggested. Since both the shelf carbonate reefs and the more basinal pinnacle reefs show signs of subaerial exposure (calcretes, dolomitization, travertine cements, karstic erosion, and solution features), and the associated evaporites possess a range of shallow water or supratidal features, it is believed that the entire shelf region became periodically desiccated, attesting to the very low depositional slopes typical of intracratonic basins.

More details on intracratonic basins, such as the Williston and Illinois Basins in North America and the Baltic and Siberian Basins of northern Eurasia, can be found in the volume edited by Leighton et al. (1990).

8.6.1.2 Continental rift basins

The location of continental rifts is sometimes determined by the existence of old fundamental weaknesses in the lithosphere. A number of examples of this phenomenon are the opening of the modern Atlantic Ocean along the Paleozoic Iapetus suture (Wilson 1966), the Cretaceous separation of southeastern Africa from Antarctica along a Paleozoic failed rift (Natal Embayment) (Tankard et al. 1982) and Cenozoic rifting in the East African Rift system, which follows Precambrian structural trends (McConnell 1977, 1980).

Continental rifting is the initial stage of a sequence leading to complete splitting and ocean floor generation (Veevers 1981). The duration of the rift phase is highly variable (§3.2.1, §3.6) and a series of rift events may be interspersed with relatively quiescent periods, as in the East Greenland Rift Basins (Surlyk et al. 1981) and North Sea (Glennie 1986). Nevertheless, within individual rift phases, the evolution of fault arrays may be rapid, with initial rifting developing into full linkage within a small number of millions of years (§8.3.2).

The nature of the sedimentary fill of a rift basin depends on its climatic zone, uplift pattern of the rift shoulders or arches acting as sediment sources or barriers, subsidence rate of central rift valleys determining alluvial base levels and lake water depths, and tectonic evolution of linked extensional fault systems. We can view the sedimentary fill on two scales – firstly the large scale features traceable along an entire rift, perhaps over some hundreds of kilometers, and secondly, the more detailed response of sedimentary facies to subsidence and uplift in rift compartments or in individual graben or half-graben. The broad features of the initial deposits of rifts are that they are predominantly nonmarine, comprising arkosic, commonly volcaniclastic fluviatile deposits, lacustrine (freshwater or evaporitic), and aeolian deposits. Fault-controlled subsidence commonly outpaces sedimentation at later stages of rift development, encouraging marine incursions in the rift climax phase (Prosser 1993) (Fig. 8.51), as seen in the Miocene of the Gulf of Suez (Gupta et al. 1999; Young et al. 2000). Shallow marine sediments may be overlain by deeper marine sediments as the rift evolves towards a site of seafloor spreading, as in the Mesozoic rifts of East Greenland (Surlyk 1990).

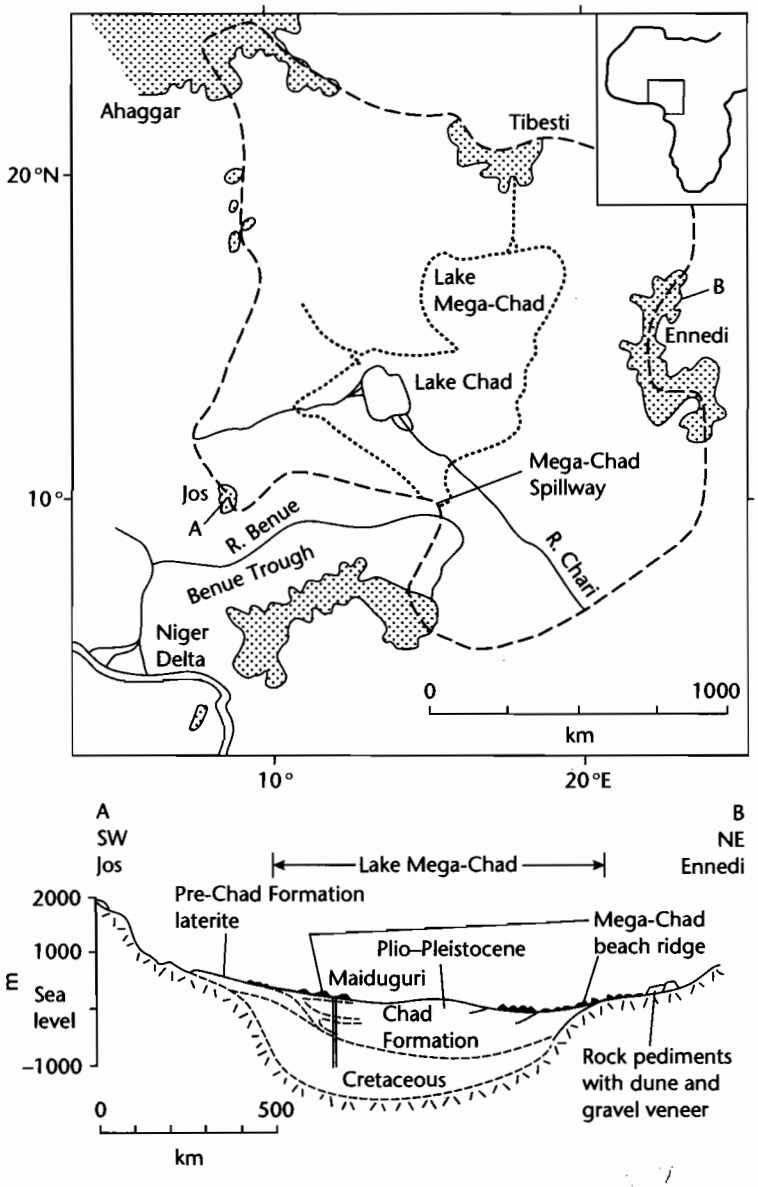

Fig. 8.48 The Chad Basin of the southern Sahara, showing the basin watershed (dashed line) enclosing an area of about 20×10^6 km, and the extent of Lake Mega-Chad (dotted line). This expanded lake spilled over to the Atlantic *via* the River Benue. Areas higher than 1 km above sea level represent peripheral uplifts (stippled). Cross-section along A–B shows that Quaternary sediments are restricted to the limits of ancient Lake Mega-Chad. This depositional area is fringed by a wide annular area of pediment and high ground. A borehole at Maidiguri penetrated 600 m of Quaternary Chad Formation (after Burke 1976).

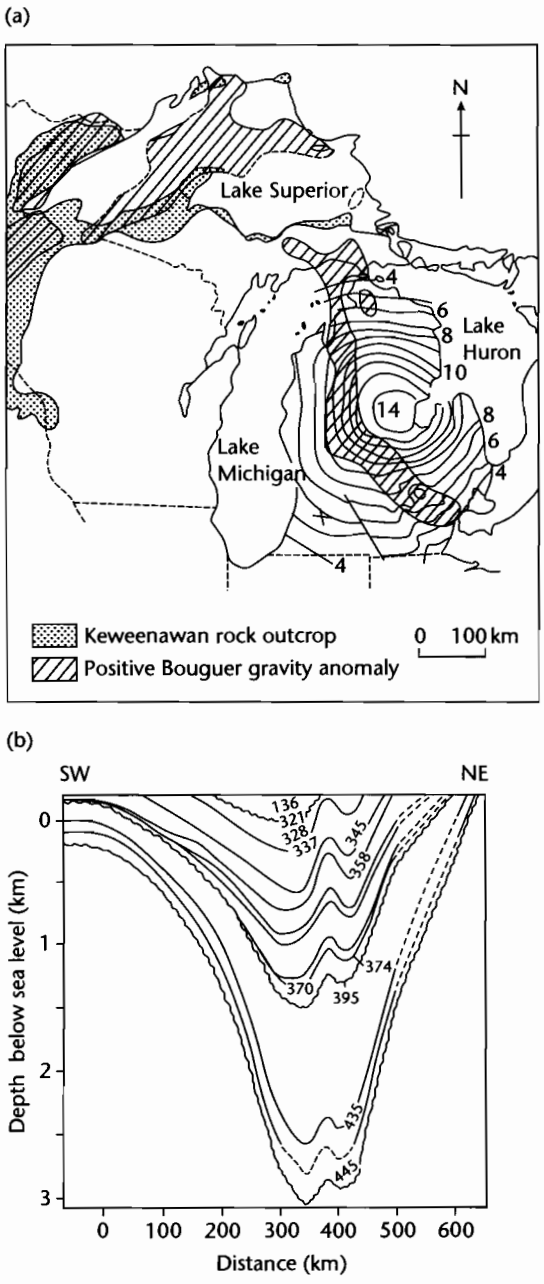

The Neogene East African Rift System demonstrates some typical stratigraphic and sedimentologic responses to continental rifting. The Neogene rift valleys of East Africa are located within broad plateaux rising as high as 4.5 km above a background mean elevation of about 0.5 km. Rift valleys split the plateaux centrally, as in Ethiopia, or occur on the flanks of individual arches as in the Central Plateau of Tanzania, Kenya and Uganda (Fig. 3.1). There are also rift divergence zones where well-developed single rift valleys pass into zones of diffuse extension composed of tilted fault blocks (as in northeast Tanzania). Seismic investigations of some rift valleys such as that of Lake Tanganyika (Rosendahl et al. 1986; Morley 2001) suggest that they are composed of a linked, alternating arrangement of arcuate half-graben (Fig. 8.52). Individual half-graben are separated by interbasinal ridges, trending oblique to the rift axis, which serve as barriers to sediment spillover between the various rift compartments (Contreras and Scholz 2001). The structural template implies that the amounts of subsidence and extension and sediment infill are all dependent on location within the rift valley zone. Sedimentary facies within the Lake Tanganyika Basin result from an interplay of river input of clastics and input of fanglomerates along border fault scarps and background "rain" of biogenic sediment from lake waters. The entry points of clastics into the Lake Tanganyika basin are: (i) the axial flowing River Ruzizi entering the lake in the north, (ii) rivers flowing over platforms, e.g., Malagarasi River entering the lake from the east, (iii) as conglomerates and breccias derived from slope wastage along border faults, and (iv) rivers entering over the shoaling sides of half-graben (Fig. 8.52).

Climatic variations cause major oscillations of lake level and therefore strongly control stratigraphic architectures (Scholz et al. 1998). Major climate-driven

Fig. 8.49 (a) Location of the Michigan Basin, USA and structural contours on the Precambrian basement surface in thousands of feet (after Hinze and Merritt 1969; Fowler and Kuenzi 1978). The basement depth increases gradually into the centre of the basin, which is almost perfectly circular in plan view. A buried Precambrian Keeweenawan rift, recognized by a positive Bouguer gravity anomaly, is thought to underlie the basin; (b) Cross-section of the Michigan Basin from Middle Ordovician to Jurassic (after Sleep and Snell 1976). Major unconformities are from Sloss (1963). Youngest units are found in the center of the basin, and some unconformities (e.g., at 395 Ma) are associated with a basinward shift in onlap. The anticline in centre right is due to Paleozoic tectonics.

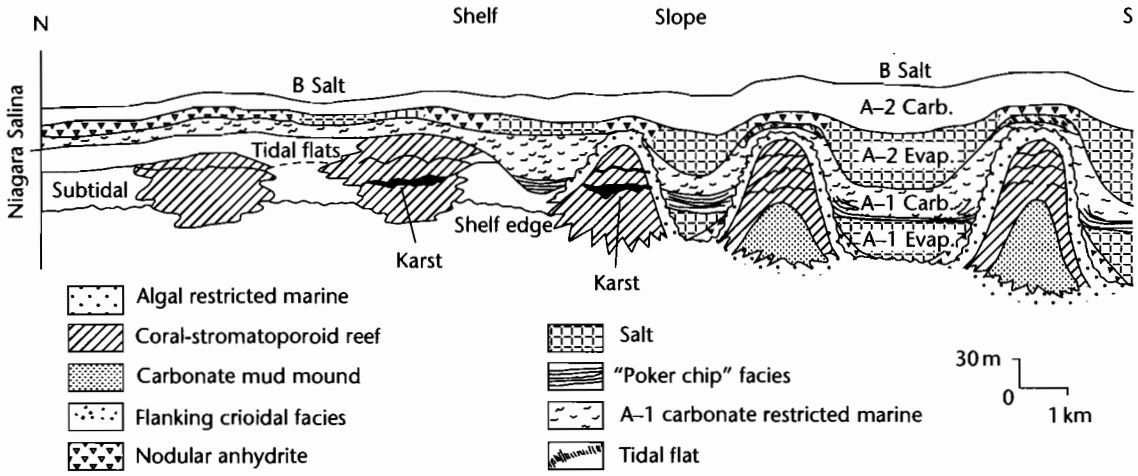

Fig. 8.50 Reconstruction of the facies and stratigraphy of the evaporite-dominated Upper Silurian of the northern part of the Michigan Basin (after Sears and Lucia 1979, 1980).

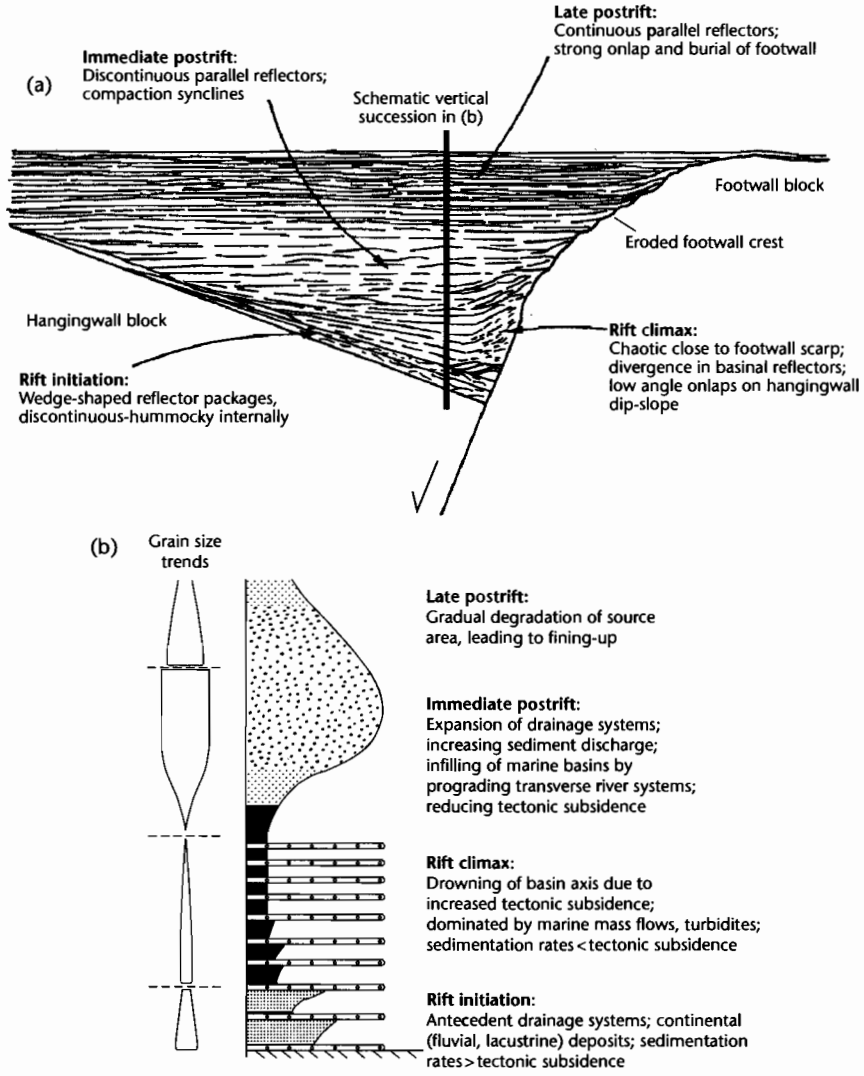

Fig. 8.51 Cross-section (a) and stratigraphic column (b) for an extensional basin evolving from rift initiation through rift climax to the postrift stage, based primarily on seismic stratigraphic data (modified from Prosser 1993). Reproduced courtesy of Geological Society of London.

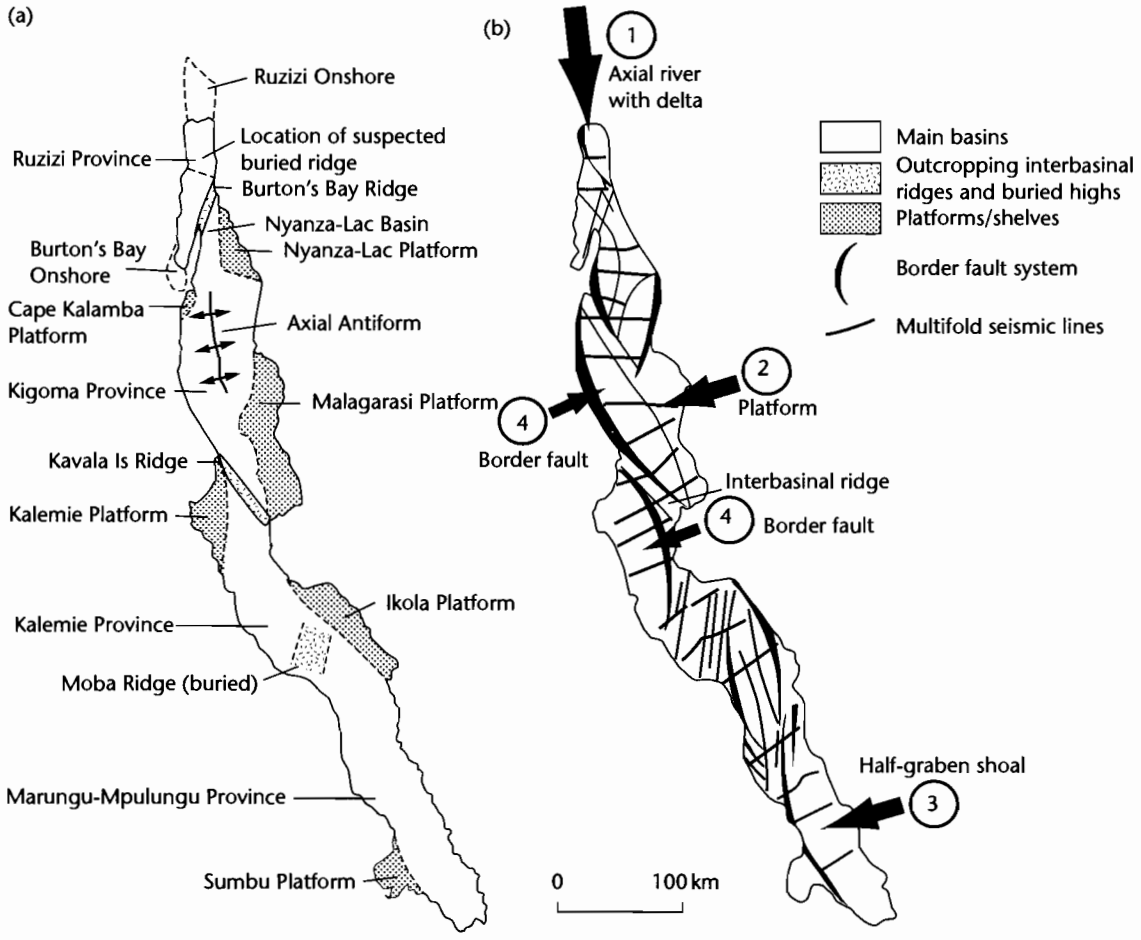

Fig. 8.52 Structural geometry, basin compartments, and sediment entry points into the Lake Tanganyika rift system (after Rosendahl et al. 1986; Contreras and Scholz 2001).

oscillations in lake level are particularly important in low-latitude lakes, such as those of the East African Rift system. Lake level variations may be rapid and high in amplitude (>100 m over 10^2 yr, >350 m over 10^{3-5} yr, Owen et al. 1990) because of the dominance of evaporation in the hydrological cycle. (In contrast, high-latitude lakes, such as Lake Baikal, do not experience severe lake level fluctuations.) Sequence architectures are dominated by these climate-driven lake level changes. Lake drawdown, enhanced by tectonic tilting, produces sequence bounding unconformities and basinward shifts of progradational deltas. Subsequent lake level rise encases the delta bodies in deep marine shales. During the rift initiation stage, individual half-graben sub-basins are fed with sediment from flexural margins and axial rivers. During the rift climax, however, the deeply subsiding sub-basins are walled off by major border faults, and sediment input is concentrated at accommodation (transfer or relay) zones and at axial deltas. Today, much of the East African Rift system is in a semi-arid climatic zone. Consequently, river deltas are markedly ephemeral in their discharges, perhaps flowing for only a few hours each year (Frostick and Reid 1986). Only a few deltas are fed by large perennial streams (e.g., River Omo, Lake Turkana). Some lakes, especially in the north of the rift system have internal drainage and, under a negative water budget, precipitate evaporites.

Volcanic activity has a major influence on rift sedimentation, as exemplified by the eastern rift of Kenya and the Rio Grande Rift of southwestern USA (Mack

and Seager 1990). Volcanism exerts this influence by the intercalation of subaerial and subaqueous lava flows within the terrestrial and lacustrine stratigraphy, by diversion or damming of surface drainage by volcanic eruptions, and by overloading of streams with volcanic, especially pyroclastic, detritus. Leaching of volcanic material leads to alkaline to hyperalkaline groundwaters and hot springs that then influence lake chemistry, as in Lake Magadi, Kenya. Inorganic cherts and Na-Al-Si gels, the precursors of zeolites, have been described from the lake (Eugster 1967). The chief mineral precipitating today is the evaporite mineral trona, which is interbedded with thin beds of wind-blown volcaniclastic sand and silt and black anoxic muds. The centrally located salt pan and fringing mudflats, ephemeral streams and springs provide an arid-region closed rift-lake model that can be identified in the stratigraphic record, such as in the Eocene Green River Formation of eastern USA (Eugster and Hardie 1975).

8.6.1.3 Failed rifts

Failed rifts are those basins in which rifting has been aborted before the onset of seafloor spreading and passive margin development. Their rift phase is identical to that outlined in the previous paragraphs. During cooling, failed rifts widen and postrift sedimentary rocks onlap the previous rift shoulders, producing a steer's-head geometry. A sedimentary evolution from nonmarine to shallow marine in the synrift phase and deeper marine in the postrift phase seems to be typical.

The Benue Trough of central-western Africa and the North Sea are two excellent examples of aborted rifting. The Benue Trough is 1000 km long, 100 km wide, and is filled with <5 km of fluvial, deltaic, and marine Cretaceous sedimentary rocks. At the southwestern end of the failed rift, the Tertiary Niger delta has built a wedge of fluvial, deltaic, and submarine fan deposits 12 km thick.

In the northern North Sea a major period of rifting took place in the Middle Jurassic. At this time sediment was dispersed longitudinally along the graben. In the N–S oriented Viking Graben, fluviatile deposits pass northwards into deltaic and shallow marine deposits of the Brent Group (Morton et al. 1992). The mid-Cretaceous saw the end of the rift phase and sediment onlapped the graben shoulders onto the East Shetland Platform in the west and the Norwegian Platform in the east. Thick deposits of Cretaceous chalks, Paleogene submarine fan sandstones and basinal shales, and Neogene mudstones typify this postrift phase. In the southern part of the North Sea, the basin was filled by major sediment supplies from rivers draining the European mainland, producing megaclinoforms due to westward delta progradation (Huuse and Clausen 2001; Overeem et al. 2001) (Fig. 8.53). The southern-central North Sea therefore shows the tendency for basin filling during the later stages of the thermal subsidence phase of failed rifts.

8.6.1.4 Proto-oceanic rifts

At high amounts of stretching, continental rifts, or backarc basins may evolve into new oceanic basins through a stage known as a proto-oceanic trough. The transition can be seen in northeastern Africa and Arabia. The southern Red Sea contains young (<5 Ma) oceanic crust along its 50 km-wide axial zone, with flanking shelves underlain by stretched continental lithosphere. To the south the Red Sea undergoes a transition to the continental Afar Rift, and to the north into the continental Gulf of Suez Rift. The sedimentary evolution of the Red Sea area involves Oligo-Miocene synrift sedimentation of basin margin fans and fan-deltas and shallow marine carbonates and silicilastics. As stretching continued through the Miocene, thick evaporites formed in the periodically isolated proto-oceanic trough. During the Pliocene to Holocene, the Red Sea has accumulated pelagic foraminferal-pteropod oozes in deep water.

At the transition from rift basin to youthful ocean basin subsidence commonly outpaces sediment supply, leading to the deposition of a number of distinctive facies associations indicative of sediment starvation:

- *Evaporites*: The intermittent connection of developing rifts with the sea during the incipient stage provides ideal conditions for the formation of thick evaporites. Such evaporites occur along the margins of the Atlantic Ocean (Emery 1977; Rona 1982) and under the Red Sea (Lowell and Genik 1972);
- *black organic-rich shale:* High organic productivity and restricted marine circulation may allow the preservation of organic-rich shales. Such conditions are likely to prevail where youthful ocean basins contain submarine sills restricting the throughput of water;
- *pelagic carbonates*: In new ocean basins with little clastic supply, deep water pelagic carbonate facies may directly overlie the foundered prerift "basement" or newly created seafloor. The faulted basement topography controls the type of deposit, with uplifted fault block edges and seamounts accumulating shallow water carbonates, and intervening troughs being the sites of fine-grained pelagic sedimentation. This pattern of sedimentation related to fault block shoulders

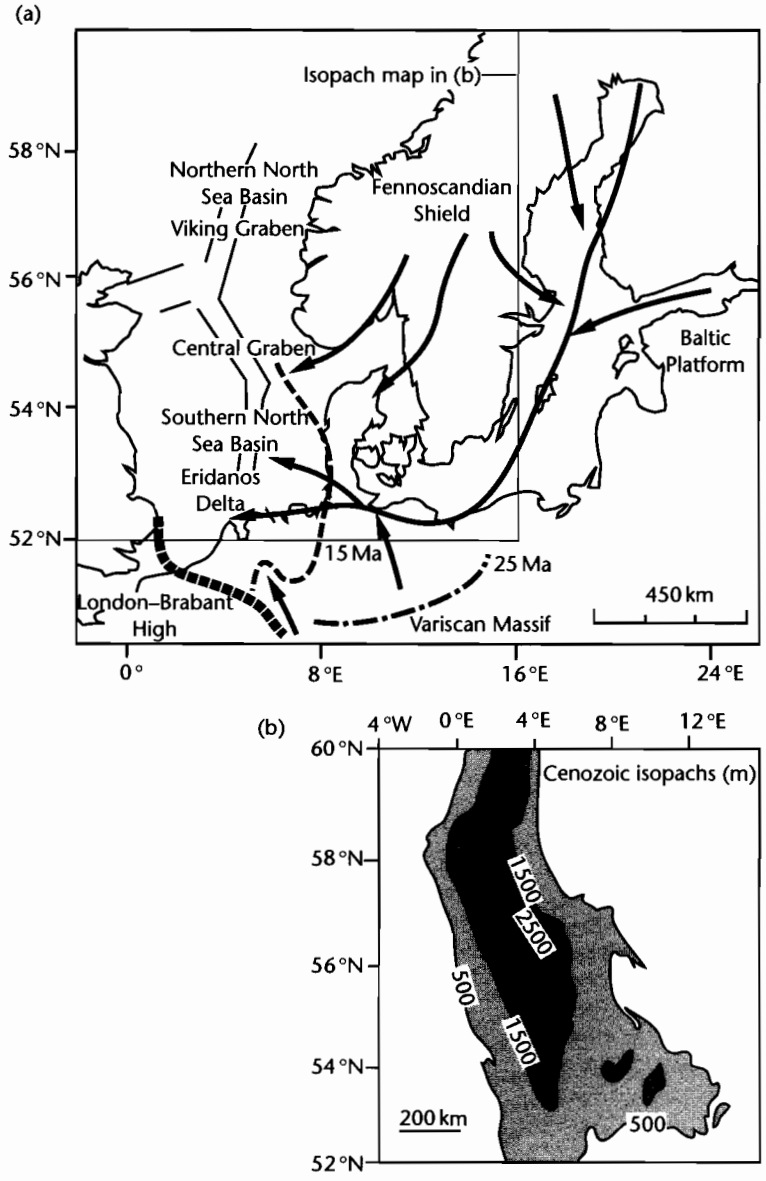

Fig. 8.53 Postrift stratigraphy in the southern North Sea is dominated by megaclinoforms produced by delta progradation related to major river systems draining Europe, such as the Eridanos delta (after Overeem et al. 2001). (a) Drainage system for the Eridanos delta, with the shoreline shown at 25 Ma and 15 Ma; (b) Cenozoic isopachs (excluding Danian) in the North Sea (after Huuse and Clausen 2001). Reproduced courtesy of Blackwell Publishing Ltd.

and troughs has been interpreted from the Triassic–Jurassic of the Tethyan realm of southern Europe. By the Late Jurassic, most of the fault blocks had been buried beneath radiolarites, red marls, and fine-grained pelagic white limestones (Bernoulli and Jenkyns 1974).

8.6.1.5 Passive margins

The formation of juvenile oceanic spreading centers, as in the 20 Myr-old Red Sea–Gulf of Aden, and then mature (<40 Myr) ocean basins is accompanied by the development of passive margins on the adjacent stretched continental lithosphere (Fig. 8.54) (review in Bond et al. 1995). Fully developed passive margins, such as those bordering the Atlantic Ocean, are characterized by extensional faulting, large-scale gravitational tectonics (slumps, slides, glide-sheets) and salt tectonics (§3.2.2). Extensional faulting dies out in the postrift phase with only minor reactivation of older normal faults. Growth faults are common in areas of high sedimentation rate (e.g., off the Niger delta, African coast). Gravitational mass movements, from small slumps to gigantic slides, are very important during the postrift drifting phase. The continental slope and rise off southwestern and southern Africa was subject to major slope instability during the Cretaceous and again in the Tertiary (Dingle 1980). The slide units are over 250 m thick and can be traced for 700 km along strike and for nearly 50 km down paleoslope. The recent 3500 km^3 Storegga slide (8150 yr BP) off the Norwegian margin (Bondevik et al. 1997) is a reminder of the on-going gravitational instability of continental margins.

Deep seismic reflection images of continental margins show a strongly elevated Moho, tilted extensional fault blocks with wedges of syn–rift sedimentary rocks, and an overlying, onlapping postrift stratigraphy. The Atlantic margin of Iberia shows all of these features (e.g., Pickup et al. 1996). The sediment supply to the passive margin prism comes principally by erosion of the continent by rivers, but significant quantities of sediment may be accreted to the lower continental slope by thermohaline current-driven drifts. Major river systems build out large embankments and submarine fans that may extend directly onto oceanic crust, as in the case of the Amazon fan.

Evaporites typify the closed lake basins of the rift stage and the first marine incursions during the incipient ocean phase of the proto-oceanic trough. When buried under an overburden of passive margin sediments these evaporites become mobile, producing diapirs. The Brazilian continental margin and the western Grand Banks, Newfoundland show examples of major diapiric activity (Fig. 8.54).

The Atlantic margin shows great variety in the nature of the passive margin prograding wedge (Fig. 8.54). The Senegal margin of western Africa contains a thick carbonate bank extending over the stretched continental crust. Further to the SE the Niger has built a thick deltaic clastic wedge, provoking growth faulting and mud diapirism. Further south off Gabon and remote from the Niger delta, oceanic muds overlie thick diapirs of evaporite. Off the coast of southwestern Africa a "normal" siliciclastic margin exists with seaward prograding clinoforms reaching far out into the basin and overlying the oceanic crust. This latter type is also common to the highly sediment-nourished North American Atlantic margin, where a well-developed coastal plain and continental shelf extend to 200 m water depth, with a continental slope descending to the abyssal plain of the Atlantic Ocean at water depths in excess of 4 km.

8.6.2 Basins related to convergent plate motion

8.6.2.1 Morphological and tectonic elements at arc-related margins

The main components of convergent arc-related systems are, from overriden oceanic plate to overriding plate (Dickinson and Seely 1979) (Fig. 8.55),

- An *outer rise* on the oceanic plate recognized as an arch in the abyssal plain. This is the flexural forebulge of the descending oceanic plate (§3.1);
- a *trench* or deep trough, commonly >10 km deep situated oceanward of the arc (review in Underwood and Moore 1995). The sediments of trenches are dominated by fine-grained turbidites and pelagic deposits. The bathymetric expression of the trench much depends on the sediment supply into it and, associated with this, the rate of encroachment from the arc of the accretionary wedge. The trench is the bathymetric expression of the deflected (flexed) oceanic plate (§3.1);
- a *subduction complex* composed of tectonic stacks of fragments of oceanic crust, its pelagic cover and arc-derived turbiditic sediments, together with *perched* or *accretionary basins* ponded on top of the accretionary wedge. The subduction complex makes up the inner slope of the trench. Where accretion rates are high, the

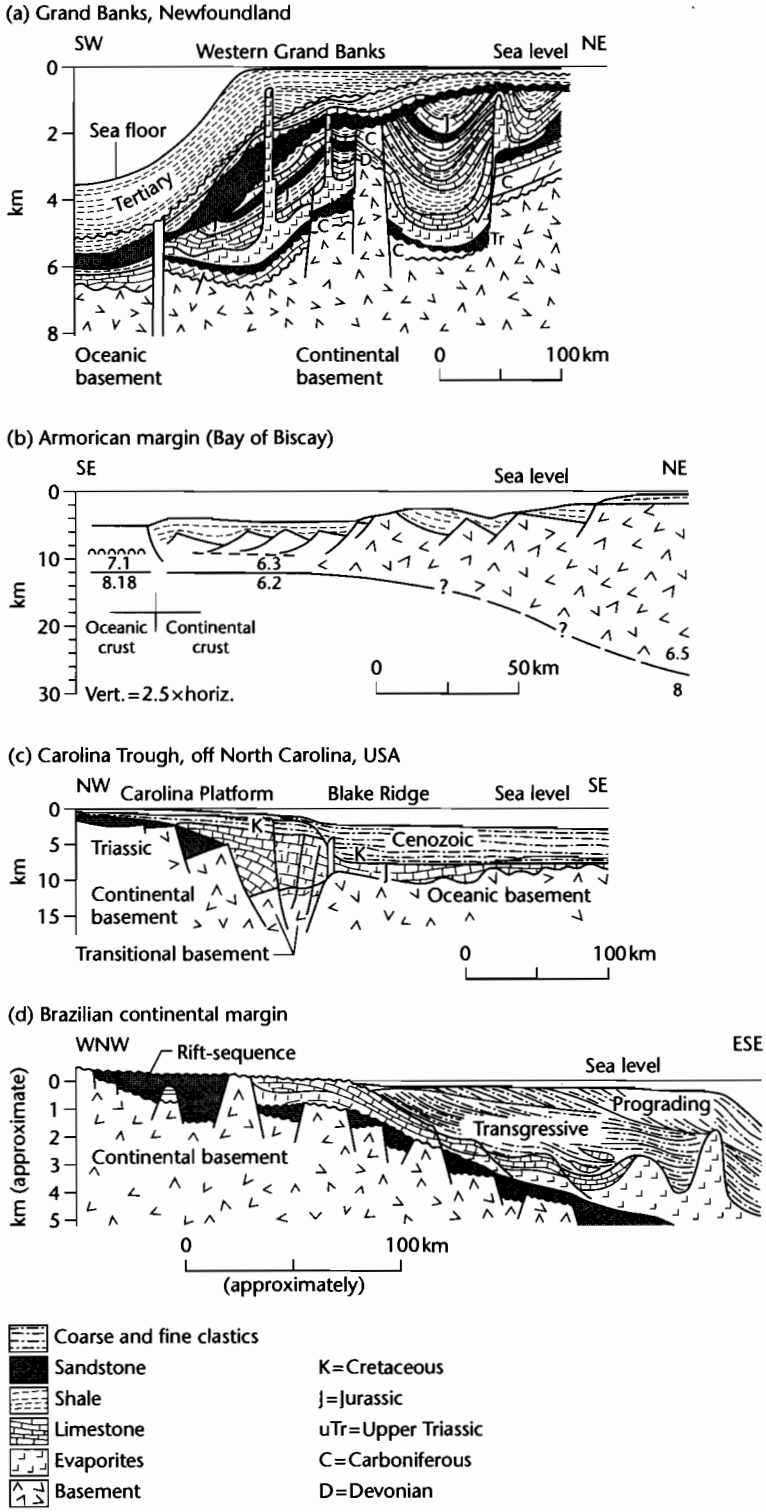

Fig. 8.54 Types of passive margin stratigraphy around the Atlantic Ocean. (a) The sediment-nourished margin of Grand Banks, Newfoundland shows complex unconformities and salt diapirism originating from the Jurassic; (b) The sediment-starved Armorican margin (Bay of Biscay) retains deep water depths; (c) Carolina Trough, eastern US seaboard has a thick Jurassic carbonate bank extending onto oceanic basement; (d) Brazilian continental margin shows salt diapirism originating in the Lower Cretaceous and prograding clastic wedges. Modified after Miall (1984).

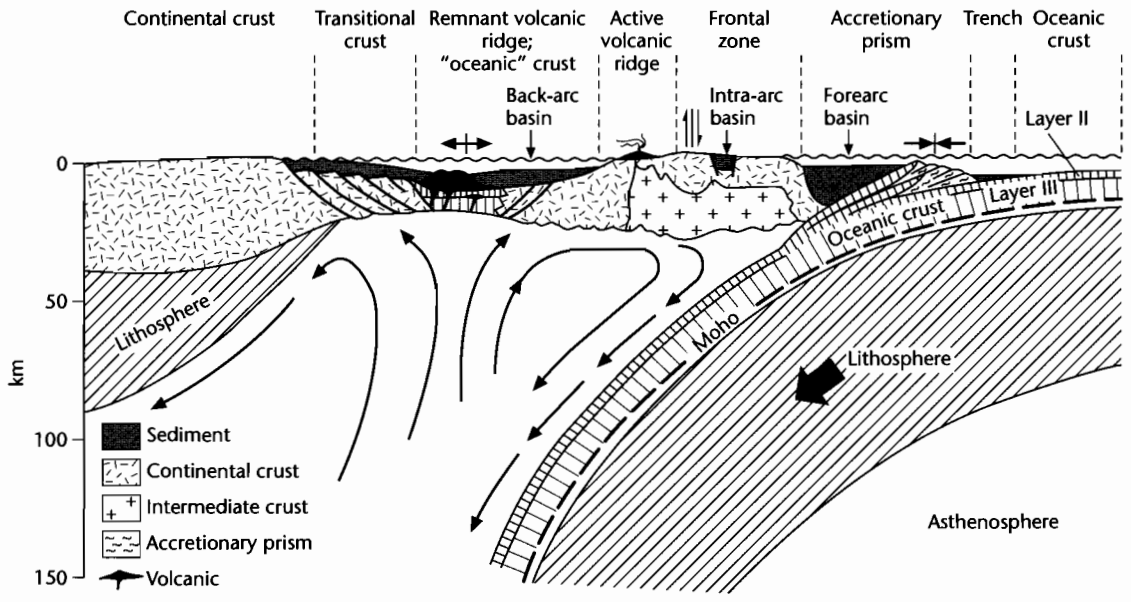

Fig. 8.55 A convergent ocean–arc boundary showing the location of the trench, accretionary wedge, forearc basin, intra-arc and backarc basins. Modified from Dickinson and Seeley (1979). The intra-arc or intra-massif basin and the forearc basin both contain deep marine to nonmarine sediments. The accretionary basin on the subduction complex contains tectonic slices of abyssal plain, slope and trench deposits together with ophiolites and metamorphics.

subduction complex may rise to shelf depths or even become emergent;

- a *forearc basin* between the ridge or terrace formed by the subduction complex and the volcanic arc (review in Dickinson 1995);
- the *magmatic* arc caused by partial melting of the overriding plate and possibly subducted plate when the latter reaches between 100 and 150 km depth. The volcanism is predominantly andesitic. Small intra-arc basins may form by extensional or strike–slip tectonics or in collapsed calderas (Smith and Landis 1995);
- the *backarc* region floored by oceanic or continental lithosphere (review in Marsaglia 1995). Where the lithosphere is oceanic, the backarc region typically undergoes extension. Backarc basins are some of the most rapidly extending regions of the Earth's crust today, a prime example being the Aegean Sea of the eastern Mediterranean. Where the lithosphere is continental, as in Andean-type margins, the backarc (or retroarc) region is typically a zone of flexural subsidence related to major fold–thrust tectonics along the arc boundary. These retroarc basins are therefore discussed in the section below on foreland basins.

8.6.2.2 Brief outline of ideas on kinematics of arcs

Molnar and Atwater (1978) first attempted to answer the question of why some convergent margins consist of oceanic arcs and extensional backarcs and some consist of magmatic arcs on continental crust with active backarc compression (Cordilleran-type). These two possibilities are exemplified by the western and eastern margins of the Pacific Ocean respectively (Tamaki and Honza 1991) (Fig. 8.56).

In the western Pacific the convergent margins are generally subducting oceanic lithosphere of Mesozoic age (i.e., ~100 Ma) and backarc extension is widespread. In the eastern Pacific the subducting lithosphere is much younger (<50 Ma). Here the arcs are located on the overriding continental plates, with fold–thrust belts and retroarc foreland basins in the backarc region. Since oceanic lithosphere cools and thickens with age, the older Mesozoic lithosphere of the western Pacific should be more gravitationally unstable than the <50 Ma lithosphere of the eastern Pacific. The older lithosphere should therefore subduct more rapidly and may exceed

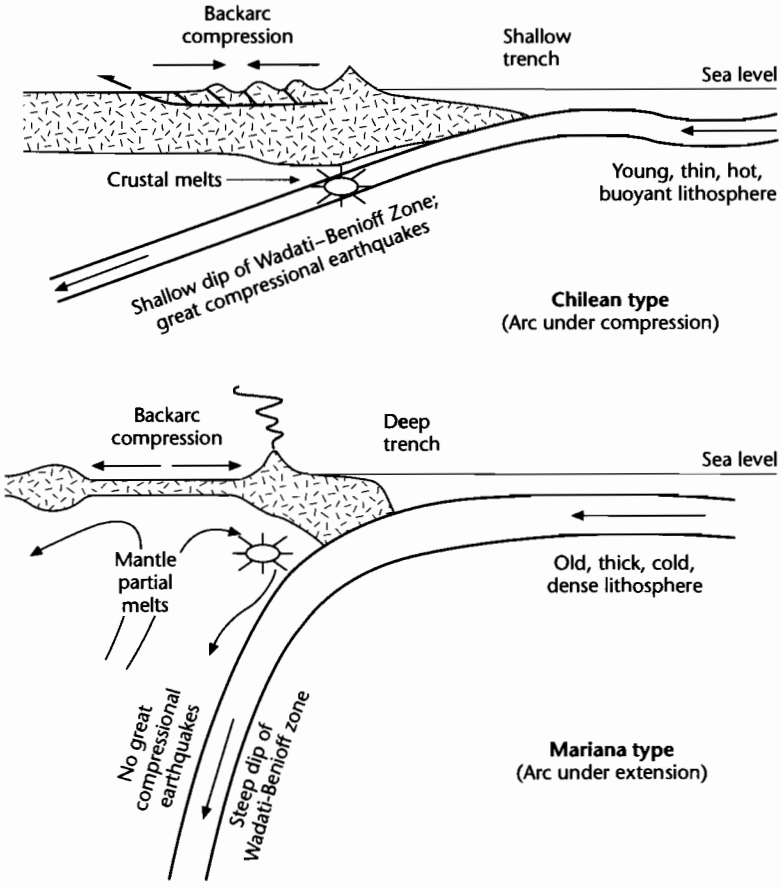

Fig. 8.56 End-member types of subduction zones, based on the age of the lithosphere being subducted, after Uyeda and Kanamori (1979) and Stern (2002). Reproduced courtesy of American Geophysical Union.

the convergence rates of the plates. This should cause an oceanward migration of the subducting hinge together with the forearc elements. This process has been called *roll-back* (e.g., Dewey 1980). It leads to extension in the region behind the rolled-back forearc, that is, backarc spreading. Others believe that backarc extension is related to secondary mantle convection above the subducted oceanic plate (Fig. 8.55) (Toksöz and Bird 1977; McKenzie 1978b).

Dewey (1980) suggested that there are three families of arc-systems. (i) *Extensional arcs* where the velocity of roll-back exceeds the oceanward velocity of the overriding plate, producing backarc extensional basins. As the arc migrates oceanward the forearc region becomes isolated from continental sediment sources and consequently is starved of major sediment supply. Examples are the Mariana and Tonga arcs, eastern Indonesia, (ii) *neutral arcs* where there is a balance between the rates of roll-back and oceanward movement of the overriding plate, producing well-developed subduction complexes but no backarc extension. Examples are the Alaska–Aleutian and Sumatran (western Indonesia) arcs, and (iii) *compressional arcs* where the subducting crust is young and the velocity of roll-back is low. This places the forearc region in compression, causing thrusting in both overriden oceanic and overriding continental crust. Examples are the Canadian–western USA Cordillera and the Peruvian Andes.

Arc behavior may change through time as the age of the subducted oceanic lithosphere changes. If the age of the subducted oceanic lithosphere gets progressively older for example, backarc basins may form, then be

closed and margins change from western Pacific type to Cordilleran type.

8.6.2.3 Continental collision – basic scenarios

Suturing of two continental plates produces a complex amalgam of intense structural deformation, regional metamorphism, plutonism, and basin formation (see summaries in Dewey 1977; Hsu 1983; chapters in Ingersoll and Busby 1995). The ocean closing process may involve a number of variations in the manner of continent–continent docking: (i) the continental plate may initially collide with an arc–backarc system before continent–continent suturing, causing inversion of extensional backarc basins, and choking of subduction complexes with continental fragments, (ii) the continental plates may compress a number of microplates in the collision zone, and (iii) the collision may be highly irregular or oblique, triggering diachronous orogenic activity and major strike–slip displacements. The lithospheric shortening, thickening, metamorphism, and plutonism involved in continental collision is accompanied by the formation of sedimentary basins in a number of settings. Foreland basins form both in front of (pro- or peripheral foreland basins) and behind (retro-foreland basins) the overriding plate. Intermontane basins are found within the megasuture. Extensional and strike–slip basins are located in shear zones produced by "escape tectonics" from the collision.

8.6.2.4 Foreland basins (peripheral and retroarc types)

In the simplest terms foreland basins develop at the front of active thrust belts where the bulk transport direction is towards the evolving basin. Because the thrust load is inherently mobile the foreland basin itself becomes involved in the deformation. To what extent the basin becomes dissected or becomes completely detached depends on a number of variables including the propagation rate of the thrust tips, availability of subsurface easy-slip horizons underlying the basin, and the angle of convergence. The foreland basin system (DeCelles and Giles 1996) contains four depositional zones (Fig. 8.57):

- Basins that rest on moving thrust sheets as a *thrust-sheet top* (Ori and Friend 1984) or *piggy-back basin*, which receives sediment from the eroding orogenic wedge (Fig. 8.58);
- a basin ahead of the active thrust system in a *foredeep*, which is supplied with sediment from both the continental foreland and the orogenic wedge (Fig. 8.58);
- sediment may also accumulate on the flexural forebulge if accommodation is available, for example because the foreland lithosphere is submerged below sea level as a result of negative dynamic topography (§5.2)
- a shallow, broad backbulge basin filled with shallow marine and continental sediments; ongoing convergence should cause the backbulge depozone to be uplifted and eroded in the flexural forebulge.

Individual foreland basins may contain examples of these four depozones, but foredeep and thrust-sheet-top basin-fills are by far the most common. In the North Alpine Foreland Basin of Switzerland (Allen et al. 1991; Sinclair 1997) the first clastic wedges (Early Oligocene), composed essentially of turbidites, were shed partly into ponded basins located on top of thrust sheets and partly overspilled into foredeeps. As the foreland basin evolved through the Oligocene, thrust-sheet-top basins became far less conspicuous features of the inner margin of the basin. Postdepositional tectonics (Late Miocene–Pliocene) detached the entire basin in western Switzerland, using Triassic salt as an easy slip horizon, as deformation progressed into the Jura province (Homewood et al. 1986).

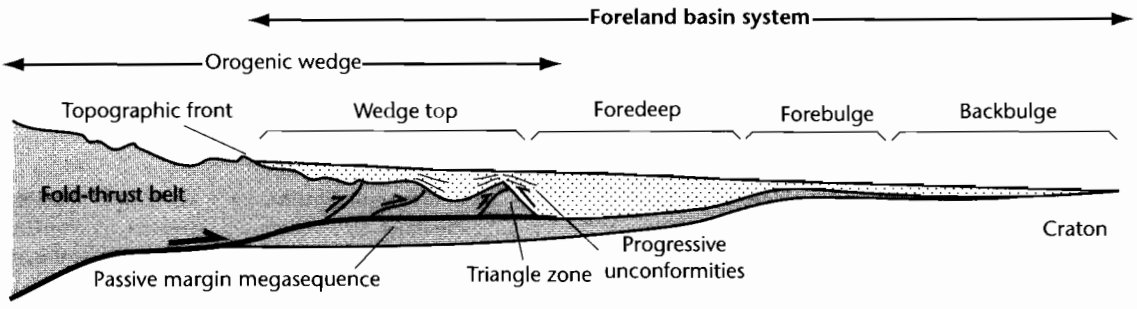

Fig. 8.57 The four depositional zones of a foreland basin system as envisaged by DeCelles and Giles (1996).

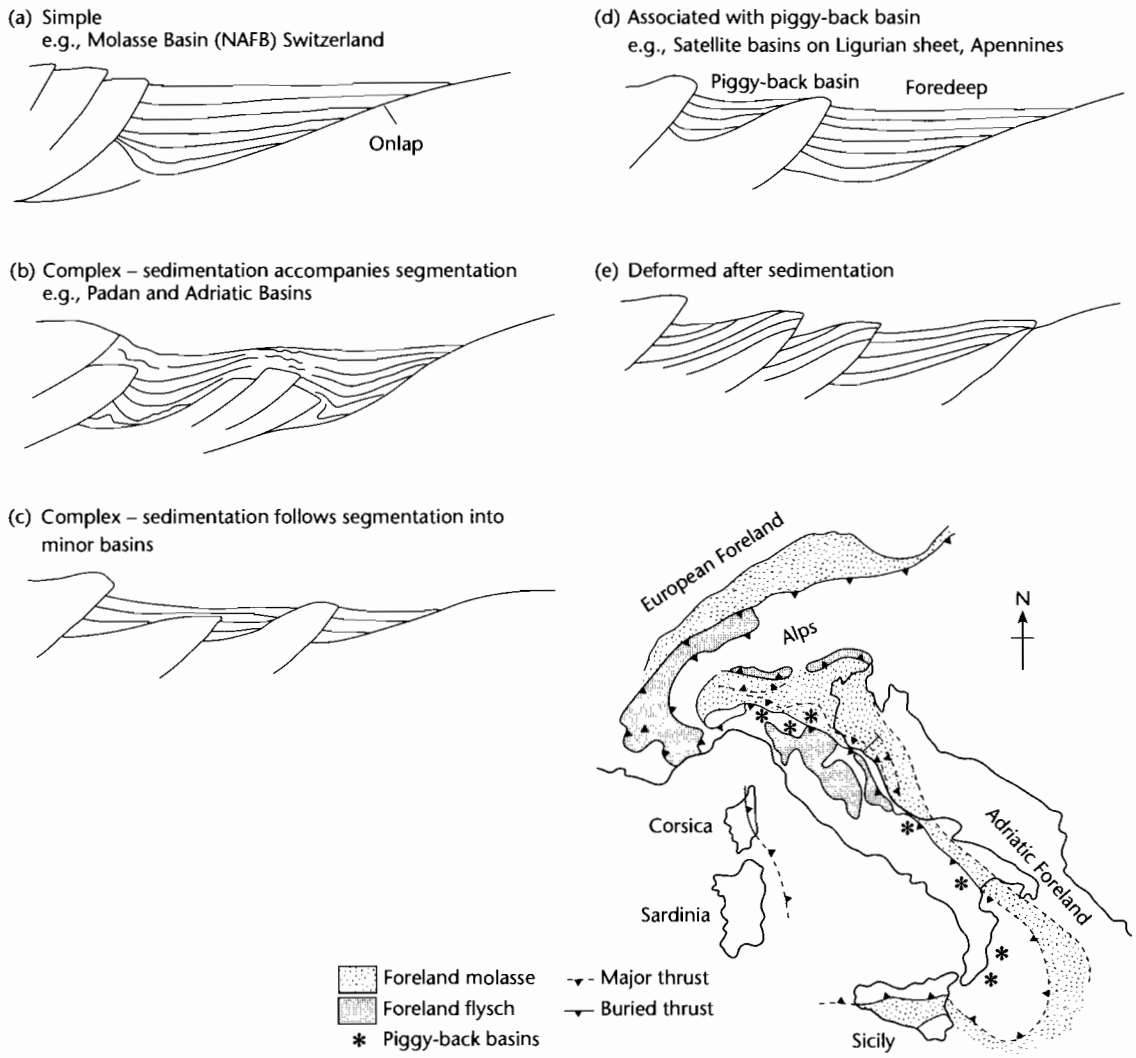

Fig. 8.58 Foreland basin–thrust belt interactions, based mainly on seismic records from the Apennines and forcland of Italy (after Ricci-Lucchi 1986). Basins may bc *simple*, asymmetrical wedges with stratigraphic onlap onto the foreland plate (a). Basins may be *complex* as a result of segmentation during thrusting. Some complex basins were segmented contemporancously with sedimentation (b), whereas others were dcformed and then passively draped with sediment over the thrusted basement topography (c). The minor basins may be subequal or of markedly different size and shape. Foredeeps may be associated with distinct thrust-sheet-top or piggy-back basins (d). Forcland basins may also bc deformed after sedimentation, leading to erosion of part of the foreland basin successions (e). Inset shows location of main foreland basin depocenters and satellite basins in Italy and thc Adriatic.

A lucid picture of a linked system of inner thrust-sheet-top basins and outer foredeeps is provided by the Apenninic chain of Italy (Ricci Lucchi 1986 for synthesis). The entire system of basins migrated eastwards onto the foreland. Scdimentation was initially dominated by turbidites and some hemipelagics. As deformation continued, the inner thrust-sheet-top basins became uplifted at the end of the Miocene and cannibalized to provide erosional detritus for the foredeep. Sediments range from continental coarse clastics to shelfal mixed carbonate-

siliciclastics and turbiditic deep-water sandstones. The Apenninic foreland basin depocenter has now extended into the Adriatic Sea where penecontemporaneous thrust deformations have produced submarine structural culminations. These seafloor highs have been subsequently denuded by slope failure and submarine erosion (Ori et al. 1986). Three depositional seismic units have been recognized in the Plio-Pleistocene of the Adriatic section of the foreland basin comprising initially turbiditic and hemipelagic deposits and subsequently deltaic deposits shed from the Apennines and Southern Alps.

Tectonics have a primary influence on sediment dispersal patterns. Uplifting thrust fronts may not act as major sediment suppliers but may instead form barriers to basinward sediment transport. This is well illustrated in the Miocene of the Southern Pyrenees. Alluvial dispersal patterns in the foreland basin south of the Pyrenees are controlled by the position of the frontal and lateral ramps of the thrust front (Fig. 8.59). The apices of major fluviatile systems are located at structural lows or re-entrants in the thrust front, whereas small, locally developed fans with highly restricted drainage basins typify the structural salients in the thrust front (Hirst and Nichols 1986). This same bimodal picture of small, locally sourced fans coexisting with large megafans sourced from deep within the orogen is also found in the Andes (Horton and DeCelles 1997) and Himalayas (Gupta 1997).

Structural re-entrants are commonly provided by lateral or oblique ramps or through-going strike–slip faults unrelated to the boundaries of thrust sheets. They act as conduits for the removal of erosional detritus from the orogenic belt to the foreland basin, and if they traverse the basin itself can be responsible for large thickness variations in the sedimentary fill. Transverse faults, such as the Sillaro Line and Forli Line had a strong influence on sedimentation in the Apennines. The Sis paleovalley is an example from the Southern Pyrenees (Vincent 2001).

Foreland basins contain a gross stratigraphic evolution related to the geodynamical controls on subsidence and sediment supply. The oldest deposits of foreland basins are commonly predominantly fine-grained, often turbiditic sediments that accumulated in sub-shelf water depths, which pass distally into shallow water carbonates deposited close to the flexural forebulge (Dorobek 1995; Sinclair 1997; Allen et al. 2001). The later deposits of foreland basins are, in contrast, predominantly shallow-water or continental and typify the term "Molasse." This kind of vertical megasequence is found in the North Alpine Foreland Basin (NAFB) of Switzerland (Matter et al. 1980; Sinclair et al. 1991; Allen et al. 1991; Schlunegger et al. 1997a, b) (Fig. 8.60) in the form of a basal deepening-up trend, followed by two shallowing-upwards megasequences. The shoreline unit at the top of the Lower Marine Molasse (Fig. 8.60) can be thought of as the pivot point between an early *underfilled* stage (Covey 1986) and a later steady-state stage (see §8.3.1). During the underfilled stage the topography of the orogenic wedge was most likely relatively subdued, sediment delivery rates were low and the orogenic advance rate relatively high, which collectively caused deep-water conditions in the foreland basin (Sinclair and Allen 1992). After the mountain belt had grown to a steady state, rapid erosion counterbalanced tectonic uplift, the advance rate was slow, and the basin was filled to the spill point with detritus. During this phase any excess sediment was exported from the foreland basin by fluvial and/or shallow marine processes.

Retroarc foreland basins such as the Cretaceous Rocky Mountains foreland basin in western USA and the series of basins east of the Andes do not fundamentally differ from peripheral foreland basins. Their main distinguishing characteristic is that they commonly evolve from regions of backarc extension, and the composition of the sedimentary fill reflects the large amounts of plutonic and volcanic rocks in the orogenic belt. Excellent examples are the Magallanes Basin of Argentina (Biddle et al. 1986), the basins of the northern Argentinian Precordillera, such as the Bermejo Basin (Cardozo and Jordan 2001) and the Central Andean foreland basin system of eastern Bolivia, northernmost Argentina, Paraguay and southwestern Brazil (Horton and DeCelles 1997).

Key processes in the foreland that affect sedimentation are the reactivation of crystalline basement uplifts, such as the Laramide structures in the Rocky Mountain area of North America (Beck et al. 1988) and the Sierras Pampeanas of Argentina (Jordan and Allmendinger 1986). Basement grabens in the foreland plate may be inverted during compression, such as the Birmingham Graben during the Lower Paleozoic Appalachian orogeny (Bayona and Thomas 2003), or the foreland plate may be faulted by the outer arc extensional stresses caused by flexure (Bradley and Kidd 1991). These are examples of important effects superimposed on the larger wavelength first-order signature of flexure.

8.6.2.5 Ocean trenches and accretionary basins

Ocean trenches are one of a series of sedimentary basin types found at convergent arc-related or ocean–continent

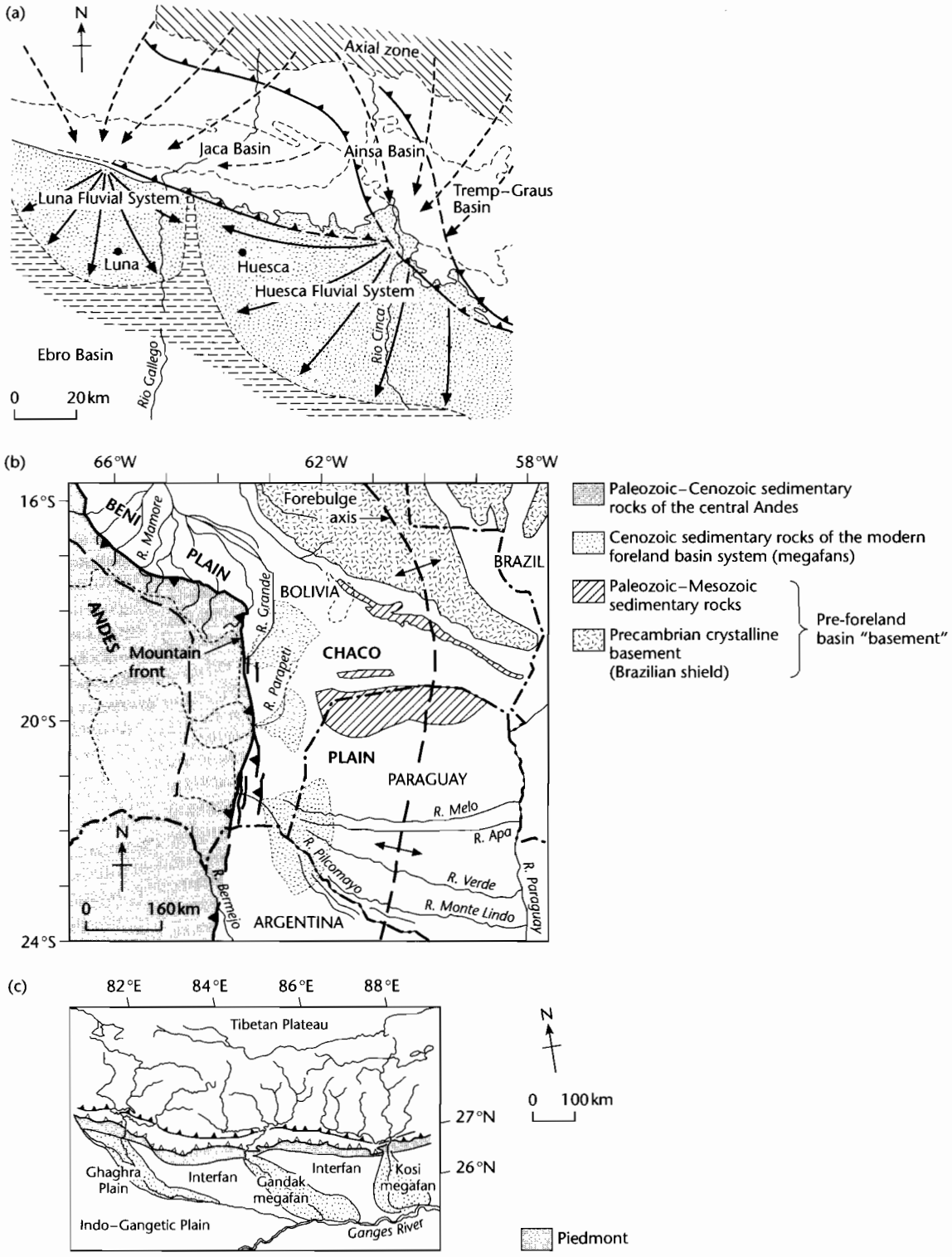

Fig. 8.59 Sediment dispersal patterns by rivers at mountain fronts. Large systems draining deep into the axial zones of orogenic belts break through the mountain front at re-entrants, producing large, low-gradient fans and megafans. Between the megafans are small, catchment–fan systems with local catchments. (a) Southern Pyrenees (Hirst and Nichols 1986), (b) Andes (Horton and DeCelles 1997), and (c) Himalayas (Gupta 1997). Note large variations in scale. (b), (c) Reproduced courtesy of Geological Society of America.

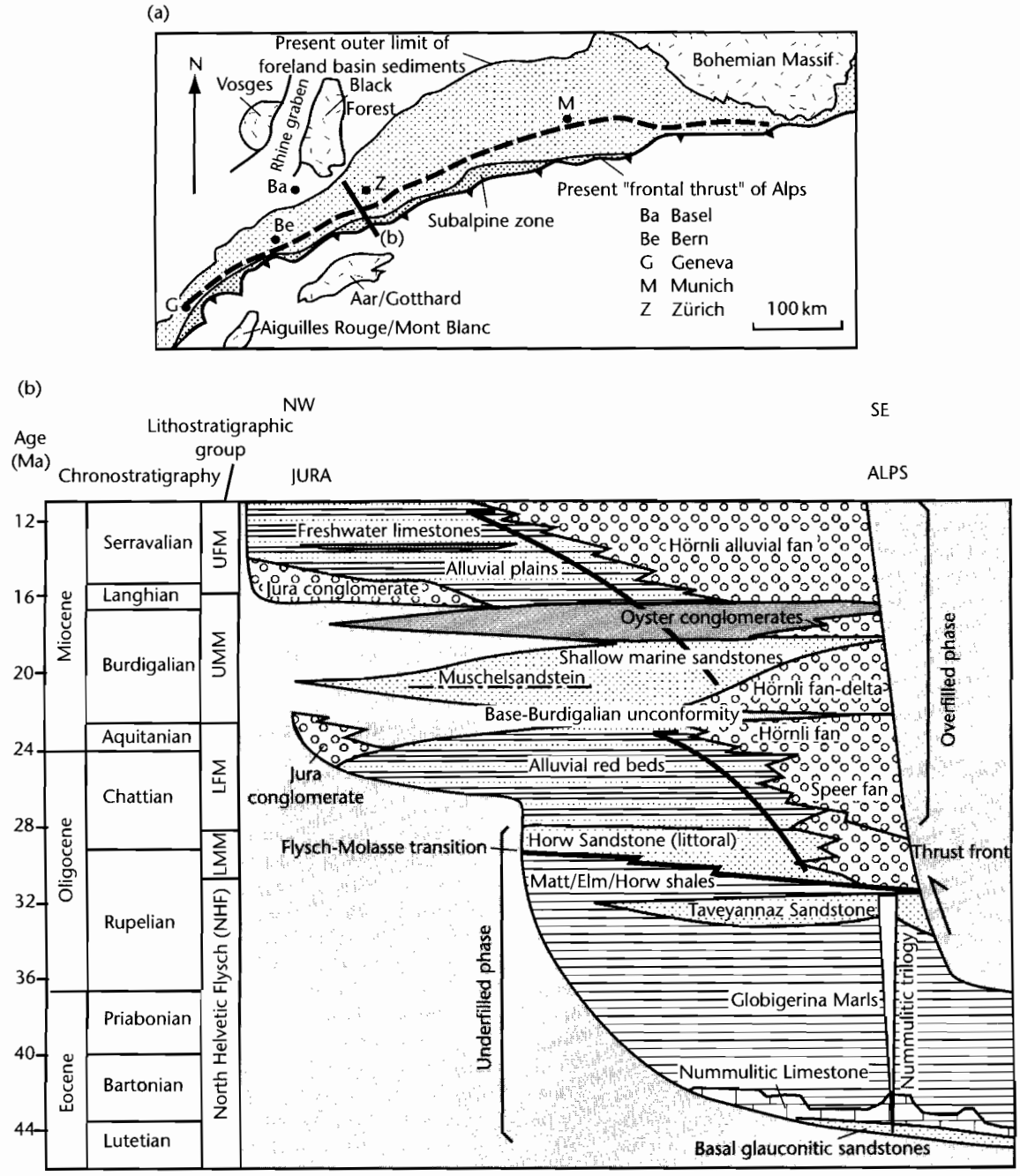

Fig. 8.60 The stratigraphy of the North Alpine Foreland Basin along a transect passing through Zürich, Switzerland (modified from Sinclair et al. 1991). The stratigraphy is made of a basal deepening-up sequence from shallow water Nummulitic Limestones to hemipelagic marls and turbidites derived from the Alpine orogen (the Nummulitic trilogy), followed by two grand shallowing-up and coarsening-up cycles. Coarse clastic wedges fringe the Alpine thrust front, whereas the feather-edge of the basin along the Jura margin was relatively passive, with the exception of some local pockets of conglomerate.

boundaries. Here we draw the distinction between: (i) *trenches* situated on the downbent oceanic lithosphere, (ii) *accretionary basins* perched on the accretionary subduction complex, (iii) *forearc basins* located between the arc and the subduction complex, and (iv) *backarc basins* found on the landward side of the arc (Fig. 8.55).

The association of *trench* and *accretionary basins* perched on the subduction complex of accreted slices of oceanic basement and cover is mechanically analogous to the foredeeps and thrust-sheet-top basins of continental collision zones. Although the mechanics may be similar between the two cases, the sedimentary fills are markedly different.

The longitudinal supply of sediment from the Bengal Fan in the north has produced marked differences in the nature of the trench and subduction complex around the Sunda arc. In Java, remote from the sediment source, the trench is 7 km deep and the accretionary subduction complex is under 1–3 km of water. Off northern Sumatra the trench is at 4 km depth and the subduction complex is partly emergent (Hamilton 1979). High sedimentation rates therefore appear to favor the growth of submarine fans or accretionary wedges completely across the trench, whereas sediment-starved margins have deep trenches with well-developed bathymetric profiles. Some active accretionary complexes can accumulate sediment in shelf and coastal environments, such as off the Alaskan arc, in the Makran, Pakistan, and Hawke Bay, New Zealand.

8.6.2.6 Forearc and backarc basins

Three types of sedimentary basin occur in the forearc region: (i) the accretionary basins located on subduction complexes mentioned in the previous section, (ii) intra-arc or intra-massif extensional basins, common where a broad forearc region has developed over continental crust, as in the Andes. These elongate basins typically follow volcanic lines or fundamental tectonic lineaments and are filled mainly with nonmarine fluviatile and lacustrine sediments dominated by volcanic constituents, and (iii) large basins located between the subduction complex and the magmatic arc, comprising "*residual*" basins with a basement of stretched continental crust or obducted oceanic crust, and "*constructed*" basins underlain by the landward portion of the subduction complex.

The oldest sediments of "residual" forearc basins are generally deep-water pelagic deposits, whereas those of "constructed" types may be shallower. Submarine fans build into the basins transversely from the magmatic arc. Intra-oceanic forearcs tend to be sediment-starved and remain deep marine, whereas sediment-nourished examples near major continental catchments may rapidly become shallow marine.

Depositional environments in *backarc basins* on oceanic crust are also deep marine, except along their margins where fluviatile, coastal, and shallow marine depositional environments may exist. Karig and Moore (1975) presented a model for the evolution of backarc basins based on the western Pacific examples. Initially, volcaniclastic wedges shed from the arc interfinger with a background of pelagic clays. As subsidence continues and outstrips sediment supply, the seafloor commonly descends below the *carbonate compensation depth* (CCD), so that the more evolved basin accumulates siliceous rather than calcareous clays. The adjacent continent may contribute clastic wedges into the landward edge of the basin.

Backarc extension is less common on continental crust because the arc commonly becomes compressional. However, some continental areas behind convergent ocean–continent boundaries are undergoing or have undergone widespread extension. The Basin and Range province of western USA is an example. The area has been substantially uplifted to a regional elevation of 2 to 3 km and half-graben and graben contain up to 3 km of nonmarine sediment. The Pannonian Basin, located to the south of the Carpathians (Burchfiel and Royden 1982), may also be due to backarc spreading.

8.6.3 Strike–slip basins

The tectonic style and evolutionary sequence of strike–slip (especially pull-apart) basins were discussed in Chapter 6. The sedimentary fills of strike–slip basins have a number of features in common (Miall 2000). Basin geometries are deep but relatively narrow, with high syndepositional relief causing conglomerates and breccias to be banked up against faulted basin margins. Sedimentation rates are rapid. Lateral facies changes are also rapid, so that marginal breccias may pass laterally directly into lacustrine mudstones. Fault movements cause syndepositional unconformities to form in individual basins and different stratigraphies to develop in closely adjacent basins, making correlation difficult. Basin sediments are commonly offset from their source, as may be proved by a mismatching between size of depositional system and drainage area, or between sediment petrography and hinterland geology. In modern basins there may be offsets of geomorphological features such as rivers, alluvial fans, or submarine canyons.

The best known intracontinental transform is the San Andreas system, and one of the best documented pull-

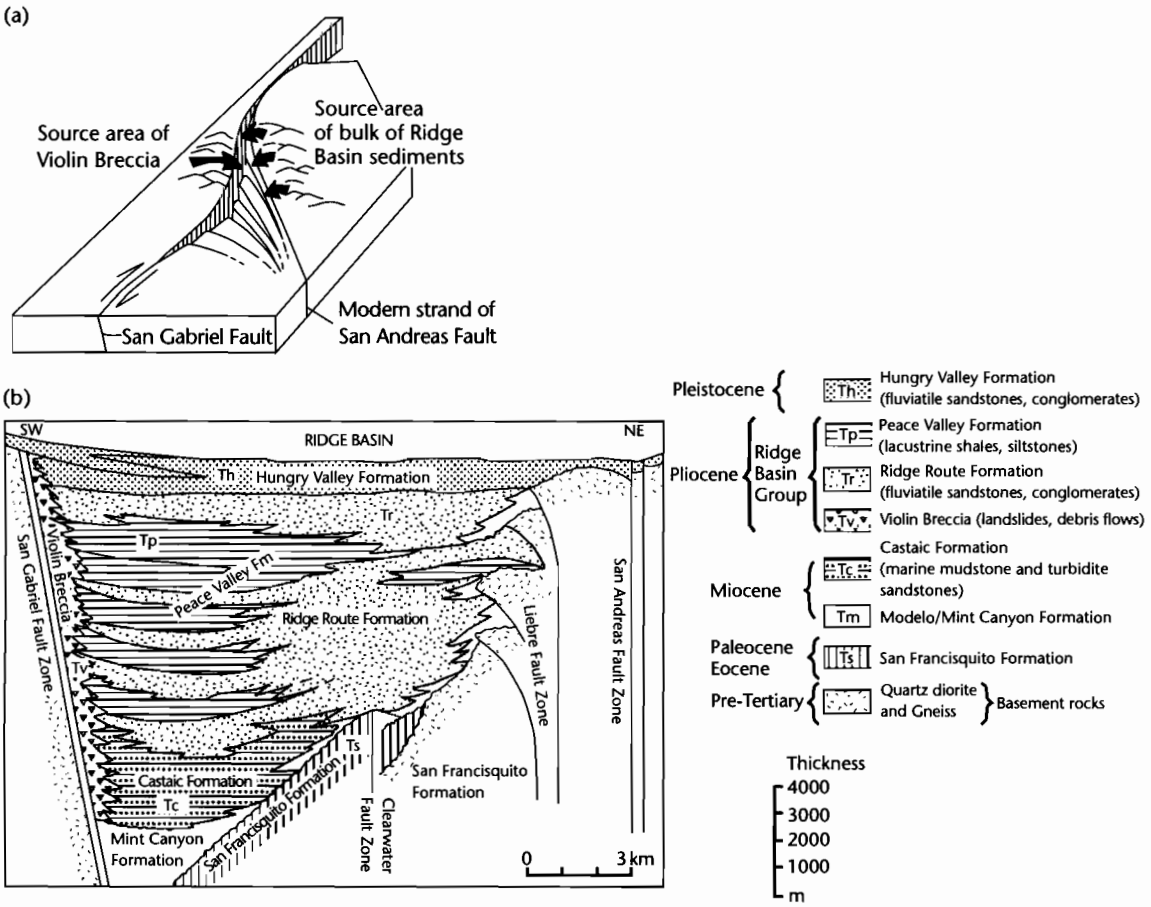

Fig. 8.61 Ridge Basin, California. (a) General tectonic and depositional setting for the Ridge Basin as a pull-apart on the releasing bend of the San Gabriel Fault (Crowell 1974); (b) Generalized cross-section showing the sedimentary facies and principal faults. The fine grained lacustrine depocenters (Peace Valley) and landslide-debris flow breccias (Violin Breccia) occur close to the San Gabriel Fault Zone (after Link and Osborne 1978; Crowell and Link 1982).

apart basins in this system is *Ridge Basin*, California. It shows many of the elements indicated above. The basin was initiated in the Miocene and continued to accumulate sediment during the Pliocene, after which it was uplifted. It contains over 13.5 km of sediment deposited at an estimated rate of 3 mm yr^{-1}, and is located between the San Andreas and San Gabriel Faults (Fig. 8.61). During the Late Miocene the San Gabriel Fault was a major active strand of the San Andreas system. The Ridge Basin formed to the east of a releasing bend in the fault. During the late Miocene–Pliocene over 60 km dextral strike–slip took place along the San Gabriel Fault, but in the Pleistocene slip was transferred to the San Andreas Fault along the northeastern flank of the basin.

The sedimentary fill of the basin (Crowell and Link 1982, Link 1982) is made up of a basal nonmarine unit (Mint Canyon) overlain by the 2.2 km thick, upper Miocene Castaic Formation, consisting of marine mudstones and turbidites. The Castaic Formation is overlain by the 9–11 km thick, mostly nonmarine Ridge Basin Group, with marine deposits in the lowermost 600 m. The Ridge Basin Group comprises marginal breccias along the active western fault scarp (Violin Breccia), central lacustrine deposits, chiefly mudstones (8 km), of the Peace Valley Formation, fluviatile clastic wedges of the Ridge Route Formation (9 km) along the eastern margin of the basin, and a basin-wide, final basin filling of alluvial sands and gravels (1.1 km) of the Hungry

Valley Formation. The marginal alluvial cones and talus of the Violin Breccia were derived from the SW and pass very rapidly (within 1.5 km) into lacustrine shales and siltstones of the Peace Valley Formation, or sandstones of the Ridge Route Formation. The thick clastic wedges of the Ridge Route Formation were shed from source areas to the NE of the basin, but the younger Hungry Valley Formation was derived from the N, NW, and W. This demonstrates the complexity of sourceland switching in strike–slip basins. Dextral strike–slip along the San Gabriel Fault displaced the source region for the Violin Breccia northwestwards with time. As a result, the successive alluvial fans that form the Violin Breccia become younger northwestward, and form an overlapping or shingled pattern. Within the axial part of the basin, sediments were transported southeastward down the axis of the basin concurrently with northwestward migration of the depocenter.

The Ridge Basin has been compared, in terms of its structural and sedimentological development, with the larger Hornelen Basin, Norway, and the smaller Little Sulphur Creek group of basins, southern California (Nilsen and McLaughlin 1985). Each basin is characterized by marginal fans located tight up against the active strike–slip fault, axial lacustrine facies, and streamflow-dominated fans along the opposite margin. These

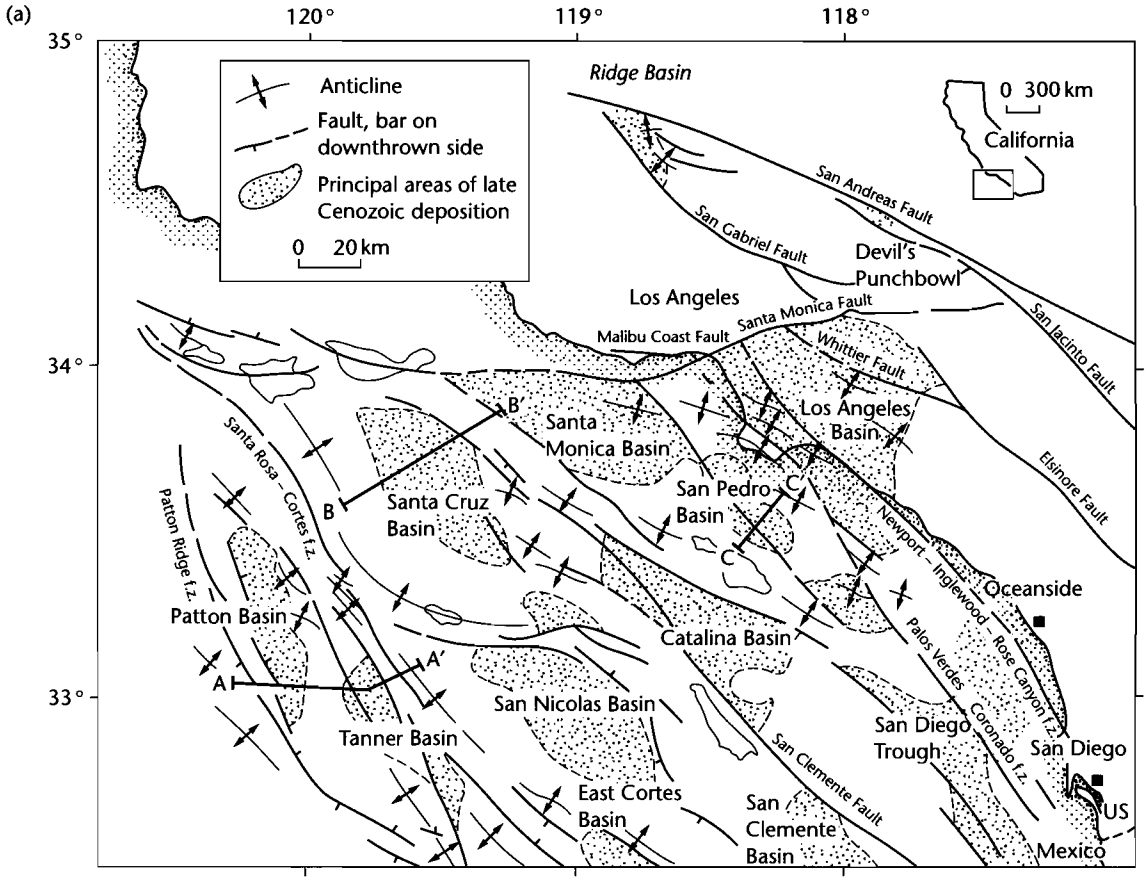

Fig. 8.62 Strike–slip basins of the California Borderland (Moore 1969; Junder 1976). (a) Map view; (b) Interpretations of seismic reflection profiles (Howell et al. 1980). Q, Pleistocene and Holocene sediments: Tp, middle and late Pliocene sediments; Tpm, Miocene and early Pliocene sediments; Tm, early to middle Miocene sediments; Tmo, cherty, calcareous and siliceous shale of upper Oligocene to middle Miocene; Tmv, Miocene volcanics; Kl-To, Upper Cretaceous to Oligocene sediments; TKJ, acoustic basement, probably equivalent to the Franciscan.

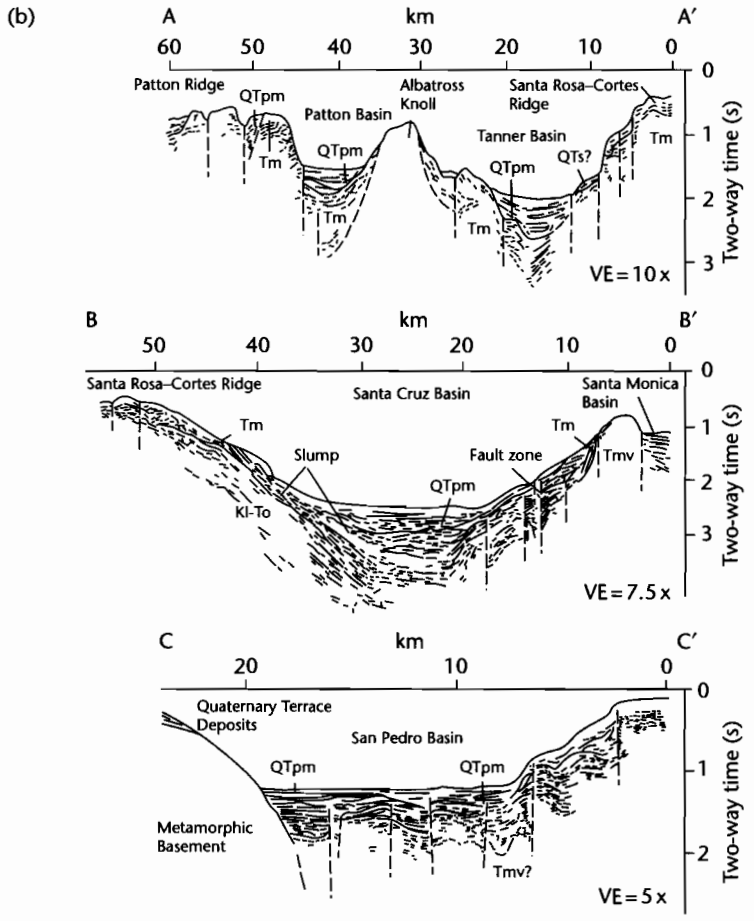

Fig. 8.62 *Continued*

streamflow-dominated fans contribute most of the sediment to the basin, sometimes filling the basin completely and spreading alluvial deposits across to the active fault scarp to interfinger with the talus fans. Rates of deformation, catchment, and fan development are commonly highly asymmetrical in basins of this type (Allen and Hovius 1998).

The present-day submarine equivalents of the Ridge Basin are found in the California Borderland Basins. This area, to the west of the San Andreas Fault, is underlain by an arc complex formed during subduction of the Pacific Plate in the Mesozoic to Early Cenozoic (Howell and Vedder 1981). A large number of small basins filled with submarine fans formed during the Paleogene, and Oligocene dextral strike–slip faulting fragmented the region into *en echelon* ridges and rhomboidal basins (Fig. 8.62). Sedimentation is dominated by turbidites fed from the nearby American coast into a background environment of fall-out of fine-grained terrigenous and pelagic material. The region has several well-studied deep sea fans (e.g., La Jolla, Navy) characterized by important submarine slides (e.g., Sur Submarine slide on Monterey fan, described by Normark and Gutmacher 1988). Sedimentation rates increase towards the coast, so that the Los Angeles and Ventura Basins located close to the continental source contain as much as 8 km of Neogene sediment, whereas the more offshore basins such as the Tanner and Patton Basins (Fig. 8.62) have much reduced sedimentary thicknesses (Howell et al. 1980).

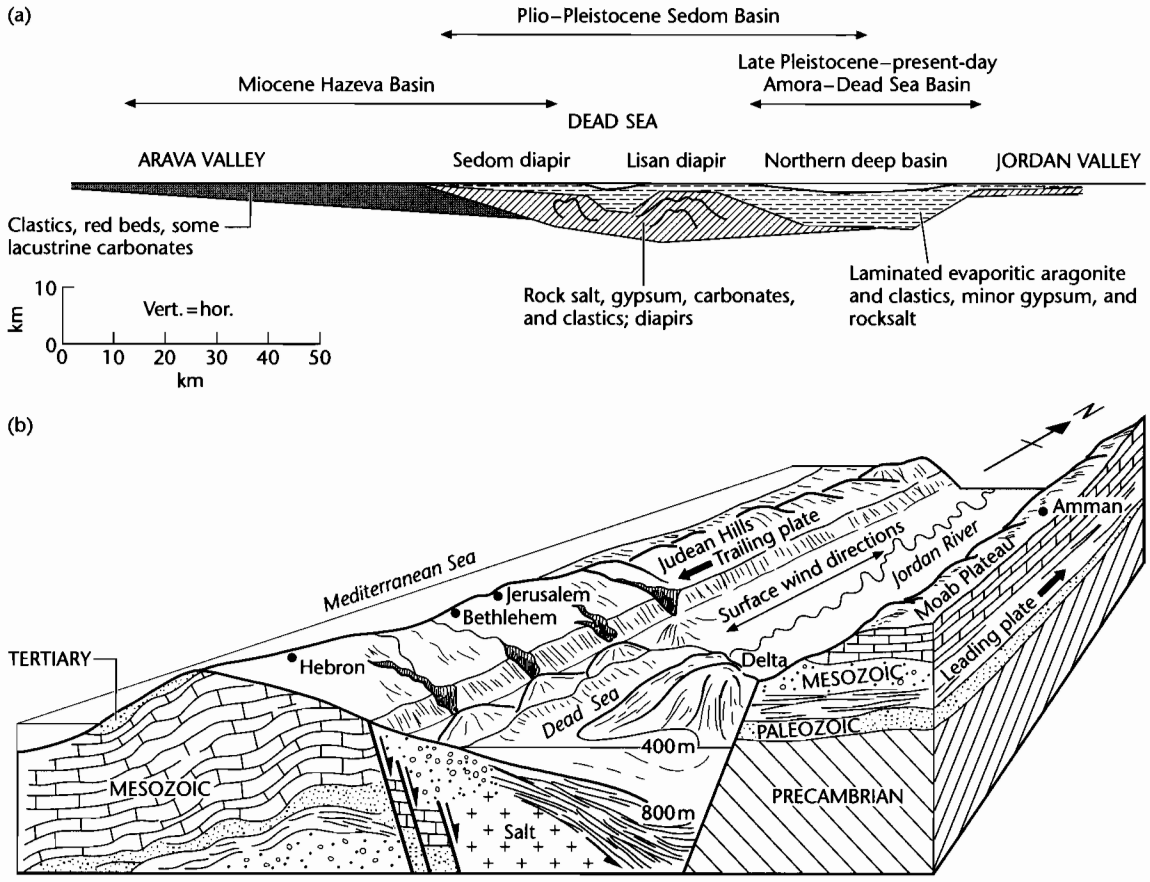

Fig. 8.63 Cross-section (a) and 3-D view (b) of the Dead Sea–Arava depression. (a) shows the northward migration of the basin depocenters. Early Miocene (25–14 Ma) strike–slip of about 60–65 km opened up the Arava Basin, which was filled with about 2 km of red beds during a pause in the strike–slip displacement. Later movement in the last 4.5 Myr has allowed the deposition of >4 km of marine to lacustrine rock salt of the Sedom Formation, followed by 3.5 km of lacustrine evaporitic carbonates and clastics (after Zak and Freund 1981); (b) Today, sediment enters the northern Basin *via* high discharge ephemeral streams feeding fan deltas along the semi-arid western edge of the basin (Judean Hills), and the perennial, axial-flowing Jordan River. The Jordan has a drainage area in a humid region, and deposits a fine-grained delta at its mouth. Autochthonous supply to the lake is of aragonite and gypsum precipitates (Manspeizer 1985).

The sedimentation in a classic pull-apart in an arid climate is well illustrated by the Dead Sea. Movement along the Dead Sea Fault commenced in the Miocene in response to the opening of the Red Sea. It has continued to move up to the present day. The basin contains over 10 km of fluvial clastics, lacustrine limestones, and evaporites. Like the Ridge Basin, depocenters have moved considerably, producing a highly diachronous fill. The Miocene Hazeva Formation consists of continental clastics and some lacustrine carbonates and is found in the Arava Valley in the south. The Pliocene–lower Pleistocene Sedom Formation consists mainly of lacustrine salts, gypsum, carbonates, and some clastics and occurs in the central section. The Pleistocene to Recent Amora and younger formations consist of laminated evaporitic (gypsum) and aragonite sediments which are accumulating today in the modern Dead Sea in the northern sector of the basin (Fig. 8.63) (Zak and Freund 1981).